CMS-SUS-13-011

Search for top-squark pair production in the single-lepton final state in pp collisions at $\sqrt{s} = 8$ TeV

The CMS Collaboration[*]

Abstract

This paper presents a search for the pair production of top squarks in events with a single isolated electron or muon, jets, large missing transverse momentum, and large transverse mass. The data sample corresponds to an integrated luminosity of $19.5\,\text{fb}^{-1}$ of pp collisions collected in 2012 by the CMS experiment at the LHC at a center-of-mass energy of $\sqrt{s} = 8$ TeV. No significant excess in data is observed above the expectation from standard model processes. The results are interpreted in the context of supersymmetric models with pair production of top squarks that decay either to a top quark and a neutralino or to a bottom quark and a chargino. For small mass values of the lightest supersymmetric particle, top-squark mass values up to around 650 GeV are excluded.

*See Appendix C for the list of collaboration members

1 Introduction

The standard model (SM) has been extremely successful at describing particle physics phenomena. However, it suffers from such shortcomings as the hierarchy problem, where fine-tuned cancellations of large quantum corrections are required in order for the Higgs boson to have a mass at the electroweak symmetry breaking scale of order $100\,\text{GeV}$ [1–6]. Supersymmetry (SUSY) is a popular extension of the SM that postulates the existence of a superpartner for every SM particle, with the same quantum numbers but differing by one half-unit of spin. SUSY potentially provides a "natural", i.e., not fine-tuned, solution to the hierarchy problem through the cancellations of the quadratic divergences of the top-quark and top-squark loops. In addition, it provides a connection to cosmology, with the lightest supersymmetric particle (LSP), if neutral and stable, serving as a dark matter candidate in R-parity conserving SUSY models.

This paper describes a search for the pair production of top squarks using the full dataset collected at $\sqrt{s} = 8\,\text{TeV}$ by the Compact Muon Solenoid (CMS) experiment [7] at the Large Hadron Collider (LHC) during 2012, corresponding to an integrated luminosity of $19.5\,\text{fb}^{-1}$. This search is motivated by the consideration that relatively light top squarks, with masses below around $1\,\text{TeV}$, are necessary if SUSY is to be the natural solution to the hierarchy problem [8–12]. These constraints are especially relevant given the recent discovery of a particle that closely resembles a Higgs boson, with a mass of $\sim 125\,\text{GeV}$ [13–15]. Searches for top-squark pair production have also been performed by the ATLAS Collaboration at the LHC in several final states [16–20], and by the CDF [21] and D0 [22] Collaborations at the Tevatron.

The search presented here focuses on two decay modes of the top squark ($\tilde{t}$): $\tilde{t} \to t\tilde{\chi}_1^0$ and $\tilde{t} \to b\tilde{\chi}^+$. These modes are expected to have large branching fractions if kinematically allowed. Here t and b are the top and bottom quarks, and the neutralinos ($\tilde{\chi}^0$) and charginos ($\tilde{\chi}^\pm$) are the mass eigenstates formed by the linear combination of the gauginos and higgsinos, which are the fermionic superpartners of the gauge and Higgs bosons, respectively. The charginos are unstable and may subsequently decay into neutralinos and W bosons, leading to the following processes of interest: $pp \to \tilde{t}\tilde{t}^* \to t\bar{t}\tilde{\chi}_1^0\tilde{\chi}_1^0 \to b\bar{b}W^+W^-\tilde{\chi}_1^0\tilde{\chi}_1^0$ and $pp \to \tilde{t}\tilde{t}^* \to b\bar{b}\tilde{\chi}_1^+\tilde{\chi}_1^- \to b\bar{b}W^+W^-\tilde{\chi}_1^0\tilde{\chi}_1^0$, as displayed in Fig. 1. The lightest neutralino $\tilde{\chi}_1^0$ is considered to be the stable LSP, which escapes without detection.

The analysis is based on events where one of the W bosons decays leptonically and the other hadronically. This results in one isolated lepton and four jets, two of which originate from b quarks. The two neutralinos and the neutrino from the W decay can result in large missing transverse momentum (E_T^{miss}).
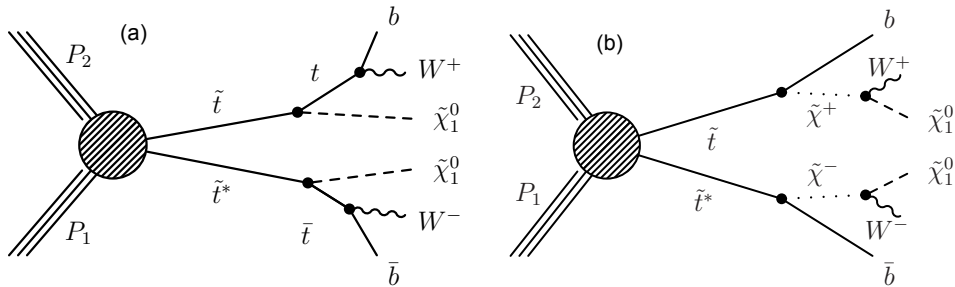

Figure 1: Diagram for top-squark pair production for (a) the $\tilde{t} \to t\tilde{\chi}_1^0 \to bW\tilde{\chi}_1^0$ decay mode and (b) the $\tilde{t} \to b\tilde{\chi}^+ \to bW\tilde{\chi}_1^0$ decay mode.

The largest backgrounds in this search arise from events with a top-antitop ($t\bar{t}$) quark pair

where one top quark decays hadronically and the other leptonically, and from events with a W boson produced in association with jets (W + jets). These backgrounds, like the signal, contain a single leptonically decaying W boson. The transverse mass, defined as $M_T \equiv \sqrt{2E_T^{miss}p_T^\ell(1 - \cos(\Delta\phi))}$, where p_T^ℓ is the transverse momentum of the lepton and $\Delta\phi$ is the difference in azimuthal angles between the lepton and E_T^{miss} directions, has a kinematic endpoint $M_T < M_W$ for these backgrounds, where M_W is the W boson mass. For signal events, the presence of LSPs in the final state allows M_T to exceed M_W. Hence we search for an excess of events with large M_T. The dominant background with large M_T arises from the "dilepton $t\bar{t}$" channel, i.e., $t\bar{t}$ events where both W bosons decay leptonically but with one of the leptons not identified. In these events the presence of two neutrinos can lead to large values of E_T^{miss} and M_T.

2 The CMS detector

The central feature of the CMS apparatus is a superconducting solenoid, 13 m in length and 6 m in diameter, which provides an axial magnetic field of 3.8 T. Within the field volume are several particle detection systems. Charged-particle trajectories are measured with silicon pixel and strip trackers, covering $0 \leq \phi < 2\pi$ in azimuth and $|\eta| < 2.5$ in pseudorapidity, where $\eta \equiv -\ln[\tan(\theta/2)]$ and θ is the polar angle of the trajectory of the particle with respect to the counterclockwise proton beam direction. A lead-tungstate crystal electromagnetic calorimeter and a brass/scintillator hadron calorimeter surround the tracking volume, providing energy measurements of electrons, photons, and hadronic jets. Muons are identified and measured in gas-ionization detectors embedded in the steel flux return yoke of the solenoid. The CMS detector is nearly hermetic, allowing momentum balance measurements in the plane transverse to the beam direction. A two-tier trigger system selects pp collision events of interest for use in physics analyses. A more detailed description of the CMS detector can be found elsewhere [7].

3 Signal and background Monte Carlo simulation

Simulated samples of SM processes are generated using the POWHEG [23], MC@NLO [24, 25], and MADGRAPH 5.1.3.30 [26] Monte Carlo (MC) event generator programs with the CT10 [27] (POWHEG), CTEQ6M [28] (MC@NLO), and CTEQ6L1 [28] (MADGRAPH) parton distribution functions. The reference sample for $t\bar{t}$ events is generated with POWHEG, while the MADGRAPH and MC@NLO generators are used for crosschecks and validations. All SM processes are normalized to cross section calculations valid to next-to-next-to-leading order (NNLO) [29] or approximate NNLO [30] when available, and otherwise to next-to-leading order (NLO) [24, 25, 31–34].

For the signal events, the production of top-squark pairs is generated with MADGRAPH, including up to two additional partons at the matrix element level. The decays of the top squarks are generated with PYTHIA [35] assuming 100% branching fraction for either $\tilde{t} \to t\tilde{\chi}_1^0$ or $\tilde{t} \to b\tilde{\chi}^+$. A grid of signal events is generated as a function of the top-squark and neutralino masses in 25 GeV steps. We also consider scenarios with off-shell top quarks (for $\tilde{t} \to t\tilde{\chi}_1^0$) and off-shell W bosons (for $\tilde{t} \to b\tilde{\chi}^+$ followed by $\tilde{\chi}_1^+ \to W^+\tilde{\chi}_1^0$). For the $\tilde{t} \to b\tilde{\chi}^+$ decay mode, the chargino mass is specified by a third parameter x defined as $m_{\tilde{\chi}_1^\pm} = x \cdot m_{\tilde{t}} + (1 - x) \cdot m_{\tilde{\chi}_1^0}$. We consider three mass spectra, namely $x = 0.25, 0.50,$ and 0.75. The lowest top squark mass that we consider is $m_{\tilde{t}} = 100$ GeV for $\tilde{t} \to t\tilde{\chi}_1^0$, and $m_{\tilde{t}} = 200$ (225, 150) GeV for $\tilde{t} \to b\tilde{\chi}^+$ with $x = 0.25$ (0.50, 0.75).

The polarizations of the final- and intermediate-state particles (top quarks in the $\widetilde{t} \to t\widetilde{\chi}_1^0$ scenario, and charginos and W bosons in the $\widetilde{t} \to b\widetilde{\chi}^+$ case) are model dependent and are nontrivial functions of the top-squark, chargino, and neutralino mixing matrices [36, 37]. The SUSY MC events are generated without polarization. The effect of this choice on the final result is discussed in Section 9. Expected signal event rates are normalized to cross sections calculated at NLO in the strong coupling constant, including the resummation of soft gluon emission at next-to-leading-logarithmic accuracy (NLO+NLL) [38–43].

For both signal and background events, multiple proton-proton interactions in the same or nearby bunch crossings (pileup) are simulated using PYTHIA and superimposed on the hard collision. The simulation of the detector response to SUSY signal events is performed using the CMS fast simulation package [44], whereas almost all SM samples are simulated using a GEANT4-based [45] model of the CMS detector. The exceptions are the MADGRAPH $t\bar{t}$ samples used to study the sensitivity of estimated backgrounds to the details of the generator settings; these samples are processed with the fast simulation. The two simulation methods provide consistent results for the acceptances of processes of interest to this analysis. The simulated events are reconstructed and analyzed with the same software used to process the data.

4 Event selection

4.1 Object definition and event preselection

The data used for this search were collected using high transverse momentum (p_T), isolated, single-electron and single-muon triggers with p_T thresholds of 27 and 24 GeV, respectively. The electron (muon) trigger efficiency, as measured with a sample of $Z \to \ell\ell$ events, varies between 85% and 97% (80% and 95%), depending on the η and p_T of the leptons. Data collected with high-p_T double-lepton triggers (ee, eμ, or $\mu\mu$, with p_T thresholds of 17 GeV for one lepton and 8 GeV for the other) are used for studies of dilepton control regions.

Events are required to have an electron (muon) with $p_T > 30\,(25)$ GeV. Electrons are required to lie in the barrel region of the electromagnetic calorimeter ($|\eta| < 1.4442$), while muons are considered up to $|\eta| = 2.1$. Electron candidates are reconstructed starting from a cluster of energy deposits in the electromagnetic calorimeter. The cluster is then matched to a reconstructed track. The electron selection is based on the shower shape, track-cluster matching, and consistency between the cluster energy and the track momentum [46]. Muon candidates are reconstructed by performing a global fit that requires consistent hit patterns in the tracker and the muon system [47].

The particle flow (PF) method [48] is used to reconstruct final-state particles. Leptons are required to be isolated from other activity in the event. A measure of lepton isolation is the scalar sum (p_T^{sum}) of the p_T of all PF particles, excluding the lepton itself, within a cone of radius $\Delta R \equiv \sqrt{(\Delta\eta)^2 + (\Delta\phi)^2} = 0.3$, where $\Delta\eta\,(\Delta\phi)$ is the difference in $\eta\,(\phi)$ between the lepton and the PF particle at the primary interaction vertex. The average contribution of particles from pileup interactions is estimated and subtracted from the p_T^{sum} quantity. The isolation requirement is $p_T^{\mathrm{sum}} < \min(5\,\mathrm{GeV}, 0.15 \cdot p_T^\ell)$. Typical lepton identification and isolation efficiencies, measured in samples of $Z \to \ell\ell$ events, are 84% for electrons and 91% for muons, with variations at the level of a few percent depending on p_T and η.

To reduce the background from $t\bar{t}$ events in which both W bosons decay leptonically (denoted as $t\bar{t} \to \ell\ell$ in the following), events are rejected if they contain evidence for an additional lepton. Specifically, we reject events with a second isolated lepton of $p_T > 5$ GeV, identified

with requirements that are considerably looser than for the primary lepton. We also reject events with an isolated track of $p_T > 10\,\text{GeV}$ with opposite sign with respect to the primary lepton, as well as events with a jet of $p_T > 20\,\text{GeV}$ consistent with the hadronic decay of a τ lepton [49]. The isolation algorithm used at this stage differs slightly from the one used in the selection of primary leptons: the cone has radius $\Delta R = 0.4$, the p_T^{sum} variable is constructed using charged PF particles only, and the isolation requirement is $p_T^{\text{sum}} < \alpha \cdot p_T$, where p_T is the transverse momentum of the track (lepton) and $\alpha = 0.1\,(0.2)$, for tracks (leptons).

The PF particles are clustered to form jets using the anti-k_T clustering algorithm [50] with a distance parameter of 0.5, as implemented in the FASTJET package [51, 52]. The contribution to the jet energy from pileup is estimated on an event-by-event basis using the jet area method described in Ref. [53], and is subtracted from the overall jet p_T. Jets from pileup interactions are suppressed using a multivariate discriminant based on the multiplicity of objects clustered in the jet, the topology of the jet shape, and the impact parameters of the charged tracks with respect to the primary interaction vertex. The jets must be separated from the lepton by $\Delta R > 0.4$ in order to resolve overlaps.

Selected events are required to contain at least four jets with $p_T > 30\,\text{GeV}$ and $|\eta| < 2.4$. At least one of these jets must be consistent with containing the decay of a heavy-flavor hadron, as identified using the medium operating point of the combined secondary vertex bottom-quark (b-quark) tagging algorithm (CSVM) [54]. We refer to such jets as "b-tagged jets". The efficiency of this algorithm for bottom-quark jets in the p_T range 30–400 GeV varies between approximately 60 and 75% for $|\eta| < 2.4$. The nominal misidentification rate for light-quark or gluon jets is 1% [54].

The missing transverse momentum is defined as the magnitude of the vector sum of the transverse momenta of all PF particles over the full calorimeter coverage ($|\eta| < 5$). The E_T^{miss} vector is the negative of that same vector sum. The calibrations that are applied to the energy measurements of jets are propagated consistently as a correction to the E_T^{miss} obtained from PF particles. We require $E_T^{\text{miss}} > 100\,\text{GeV}$.

To summarize, events are required to contain one isolated lepton (e or μ), no additional isolated track or hadronic τ-lepton candidate, at least four jets with at least one b-tagged jet, and $E_T^{\text{miss}} > 100\,\text{GeV}$; this is referred to below as the "event preselection". Signal regions are defined demanding $M_T > 120\,\text{GeV}$. This requirement provides large suppression of the SM backgrounds while retaining high signal efficiency. Requirements on several kinematic quantities or on the output of boosted decision tree (BDT) multivariate discriminants are also used to define the signal regions, as described below.

4.2   Kinematic quantities

To reduce the dominant $t\bar{t} \to \ell\ell$ background, we make use of the quantity M_{T2}^W, defined as the minimum "mother" particle mass compatible with all the transverse momenta and mass-shell constraints [55]. This variable is a variant of the M_{T2} observable [56–58], and is designed specifically to suppress the $t\bar{t} \to \ell\ell$ background with one undetected lepton in the top squark search. By construction, for the dilepton $t\bar{t}$ background without mismeasurement effects, M_{T2}^W has an endpoint at the top-quark mass. The M_{T2}^W calculation relies on the correct identification of the b-quark jets and the correct pairing of the b-quark jets with the leptons. The M_{T2}^W value in the event is defined as the minimum of the M_{T2}^W values calculated from all possible combinations of b-quark jets and the lepton. For events with only one b-tagged jet, the combinations are performed using each of the three remaining highest p_T jets as the possible second b-quark jet.

In the $\widetilde{t} \to t\widetilde{\chi}_1^0$ search, the dilepton $t\bar{t}$ background is suppressed by requiring that three of the jets in the event be consistent with the $t \to bW \to bq\bar{q}$ decay chain. For each triplet of jets in the event we construct a hadronic top χ^2 as:

$$\chi^2 = \frac{(M_{j_1 j_2 j_3} - M_{\text{top}})^2}{\sigma_{j_1 j_2 j_3}^2} + \frac{(M_{j_1 j_2} - M_{\text{W}})^2}{\sigma_{j_1 j_2}^2}. \tag{1}$$

Here $M_{j_1 j_2 j_3}$ is the mass of the three-jet system, $M_{j_1 j_2}$ is the mass of two of the jets posited to originate from W boson decay, and $\sigma_{j_1 j_2 j_3}$ and $\sigma_{j_1 j_2}$ are the uncertainties on these masses calculated from the jet energy resolutions [59]. The three-jet mass $M_{j_1 j_2 j_3}$ is computed after requiring $M_{j_1 j_2} = M_{\text{W}}$ using a constrained kinematic fit, while $M_{j_1 j_2}$ in Eqn. 1 is the two-jet mass before the fit. Finally, $M_{\text{top}} = 173.5\,\text{GeV}$ ($M_{\text{W}} = 80.4\,\text{GeV}$) is the mass of the top quark (W boson) [60]. The three jets are required to have $p_{\text{T}} > 30\,\text{GeV}$ and $|\eta| < 2.4$ and to be among the six leading selected jets. The jet assignments are made consistently with the b-tagging information, i.e., j_3 must be b-tagged if there are at least two b-tagged jets and j_1 and j_2 cannot be b-tagged unless there are at least three b-tagged jets in the event. The minimum hadronic top χ^2 amongst all possible jet combinations is used as a discriminant on an event-by-event basis.

Two topological variables are used in the selection of signal candidates. The first is the minimum $\Delta\phi$ value between the $E_{\text{T}}^{\text{miss}}$ vector and either of the two highest p_{T} jets, referred to below as "min $\Delta\phi$". Background $t\bar{t}$ events tend to have high-p_{T} top quarks, and thus objects in these events tend to be collinear in the transverse plane, resulting in smaller values of $\Delta\phi$ than is typical for signal events. The second variable is $H_{\text{T}}^{\text{ratio}}$, defined as the fraction of the total scalar sum of the jet transverse energies (H_{T}) with $p_{\text{T}} > 30\,\text{GeV}$ and $|\eta| < 2.4$ that lies in the same hemisphere as the $E_{\text{T}}^{\text{miss}}$ vector. This quantity tends to be smaller for signal than for background events, because in signal events the visible particles recoil against the LSPs, resulting on average in events with more energy in the opposite hemisphere to the $E_{\text{T}}^{\text{miss}}$.

In the $\widetilde{t} \to b\widetilde{\chi}^+$ decay mode, the bottom quarks arise from the decay of the top squark, while in background events they originate from the decay of the top quark. As a result, in most of the signal parameter space the p_{T} spectrum of the bottom quarks is harder for signal than for background events. Conversely, in the $\widetilde{t} \to t\widetilde{\chi}_1^0$ decay mode, if the top quark is off-shell, the p_{T} spectrum of the bottom quarks is softer for signal than for the background. The p_{T} value of the highest-p_{T} b-tagged jet is therefore a useful discriminant. An additional, related, discriminating variable is the ΔR separation between this jet and the lepton. Finally, the p_{T} spectrum of the lepton can be used to discriminate between on-shell and off-shell leptonic W decays, which occur in the $\widetilde{t} \to b\widetilde{\chi}^+$ mode when the mass splitting between the chargino and the LSP is smaller than the W boson mass.

The distributions after the preselection of $E_{\text{T}}^{\text{miss}}$, M_{T}, and the kinematic quantities described above, are shown in Fig. 2. These quantities are seen to be in agreement with the simulation of the SM background processes that will be discussed in more detail in Section 5.

4.3   Signal region definition

Two approaches are pursued to define the signal regions (SRs): a "cut-based" approach based on sequential selections on individual variables, and a BDT multivariate approach implemented via the TMVA package [61]. In both methods, we apply the preselection requirements of Section 4.1. The cut-based signal regions are defined by adding requirements on individual kinematic variables. In contrast, the BDT combines the kinematic variables into a single discriminant, and the BDT SRs are defined by requirements on this discriminant. The BDT approach
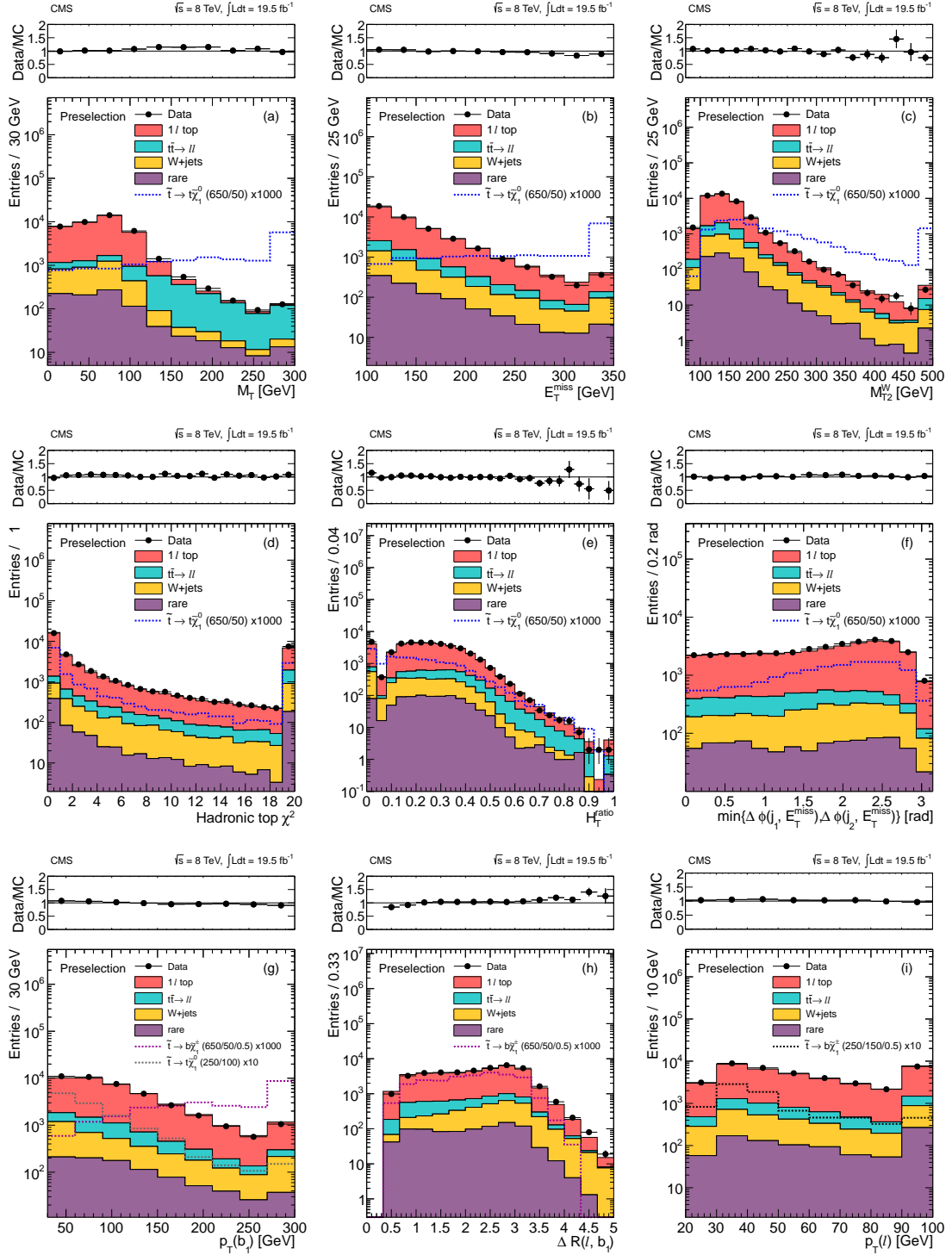
Figure 2: Comparison of data with MC simulation for the distributions of (a) M_T, (b) E_T^{miss}, (c) M_{T2}^W, (d) hadronic top χ^2, (e) H_T^{ratio}, (f) minimum $\Delta\phi$ between the E_T^{miss} vector and the two leading jets, (g) p_T of the leading b-tagged jet, (h) ΔR between the leading b-tagged jet and the lepton, and (i) lepton p_T, after the preselection. For the plots (a)-(f), distributions for the $\tilde{t} \rightarrow t\tilde{\chi}_1^0$ model with $m_{\tilde{t}} = 650\,\text{GeV}$ and $m_{\tilde{\chi}_1^0} = 50\,\text{GeV}$, scaled by a factor of 1000, are overlaid. We also show distributions of $\tilde{t} \rightarrow t\tilde{\chi}_1^0$ with $m_{\tilde{t}} = 250\,\text{GeV}$ and $m_{\tilde{\chi}_1^0} = 100\,\text{GeV}$ for (g), scaled by 10, and of $\tilde{t} \rightarrow b\tilde{\chi}^+$ with $m_{\tilde{t}} = 650\,\text{GeV}$, $m_{\tilde{\chi}_1^0} = 50\,\text{GeV}$, and $x = 0.5$ for (h) and (i), scaled by 1000, as well as of $m_{\tilde{t}} = 250\,\text{GeV}$, $m_{\tilde{\chi}_1^0} = 150\,\text{GeV}$, and $x = 0.5$ for (i), scaled by 10. In all distributions the last bin contains the overflow.

improves the expected sensitivity of the search by up to 40% with respect to the cut-based approach, at the cost of additional complexity. The primary result of our search is obtained with the BDT, while the cut-based analysis serves as a crosscheck. Table 1 lists the variables used in the training of the BDTs (Section 4.3.1) and summarizes the requirements for the cut-based SRs (Section 4.3.2).

Table 1: Summary of the variables used as inputs for the BDTs and of the kinematic requirements in the cut-based analysis. All signal regions include the requirement $M_T > 120\,\text{GeV}$. For the $\tilde{t} \to t\tilde{\chi}_1^0$ BDT trained in the region where the top quark is off-shell, the hadronic top χ^2 is not included and the leading b-tagged jet p_T is included. The lepton p_T is used only in the training of the $\tilde{t} \to b\tilde{\chi}^+$ BDT in the case where the W boson is off-shell.

| | $\tilde{t} \to t\tilde{\chi}_1^0$ | | | $\tilde{t} \to b\tilde{\chi}^+$ | | |
| | | Cut-based | | | Cut-based | |
Selection	BDT	Low ΔM	High ΔM	BDT	Low ΔM	High ΔM
E_T^{miss} (GeV)	yes	$> 150, 200,$ $250, 300$	$> 150, 200,$ $250, 300$	yes	$> 100, 150,$ $200, 250$	$> 100, 150,$ $200, 250$
M_{T2}^W (GeV)	yes		>200	yes		>200
min $\Delta\phi$	yes	>0.8	>0.8	yes	>0.8	>0.8
H_T^{ratio}	yes			yes		
Hadronic top χ^2	(on-shell top)	<5	<5			
Leading b-tagged jet p_T (GeV)	(off-shell top)			yes		>100
$\Delta R(\ell,\text{leading b-tagged jet})$				yes		
Lepton p_T (GeV)				(off shell W)		

4.3.1   BDT signal regions

The BDTs are trained on samples of MC signal and background events satisfying the preselection requirements and with $M_T > 120\,\text{GeV}$. The BDTs are trained with MADGRAPH samples for $\tilde{t} \to t\tilde{\chi}_1^0$ and a mixture of MADGRAPH and PYTHIA samples for $\tilde{t} \to b\tilde{\chi}^+$. The choice of generators has little impact on the final result. The background MC sample contains all the expected SM processes.

Separate BDTs are trained for the $\tilde{t} \to t\tilde{\chi}_1^0$ and $\tilde{t} \to b\tilde{\chi}^+$ decay modes and for different regions of parameter space. In what follows we refer to the different BDTs as BDTn, where n is the region number defined in Fig. 3. In general, for a given BDT, the optimal requirement does not depend strongly on the point in parameter space within each region. Thus, for almost all regions a single BDT requirement is sufficient, and each such requirement defines a BDT signal region. The exceptions are BDT1 for the $\tilde{t} \to t\tilde{\chi}_1^0$ signal model and BDT2 for the $\tilde{t} \to b\tilde{\chi}^+$ signal model with parameter $x = 0.5$; in these regions we choose two BDT operating points, referred to as "tight" and "loose".

BDT distributions after the preselection are shown in Fig. 4 for four of the 16 BDTs (two tight and two loose BDTs). The data are in agreement with the MC simulation of SM processes.

4.3.2   Cut-based signal regions

For the $\tilde{t} \to t\tilde{\chi}_1^0$ model, two types of signal regions are distinguished: those targeting "small ΔM" and those targeting "large ΔM", where $\Delta M \equiv m_{\tilde{t}} - m_{\tilde{\chi}^0}$. Both categories include the requirement that the azimuthal angular difference between the two leading jets and the E_T^{miss} vector exceed 0.8 radians, in addition to the requirement that the value of the hadronic top χ^2 be less than 5. The $M_{T2}^W > 200\,\text{GeV}$ requirement is applied only for the large ΔM signal regions. Within each set, the SRs are distinguished by four successively tighter E_T^{miss} requirements: $E_T^{\text{miss}} > 150, 200, 250,$ and $300\,\text{GeV}$.

For the $\tilde{t} \to b\tilde{\chi}^+$ model, the same approach is followed as for $\tilde{t} \to t\tilde{\chi}_1^0$ by defining two sets of signal regions, one for small ΔM and one for high ΔM, where ΔM here is the mass difference
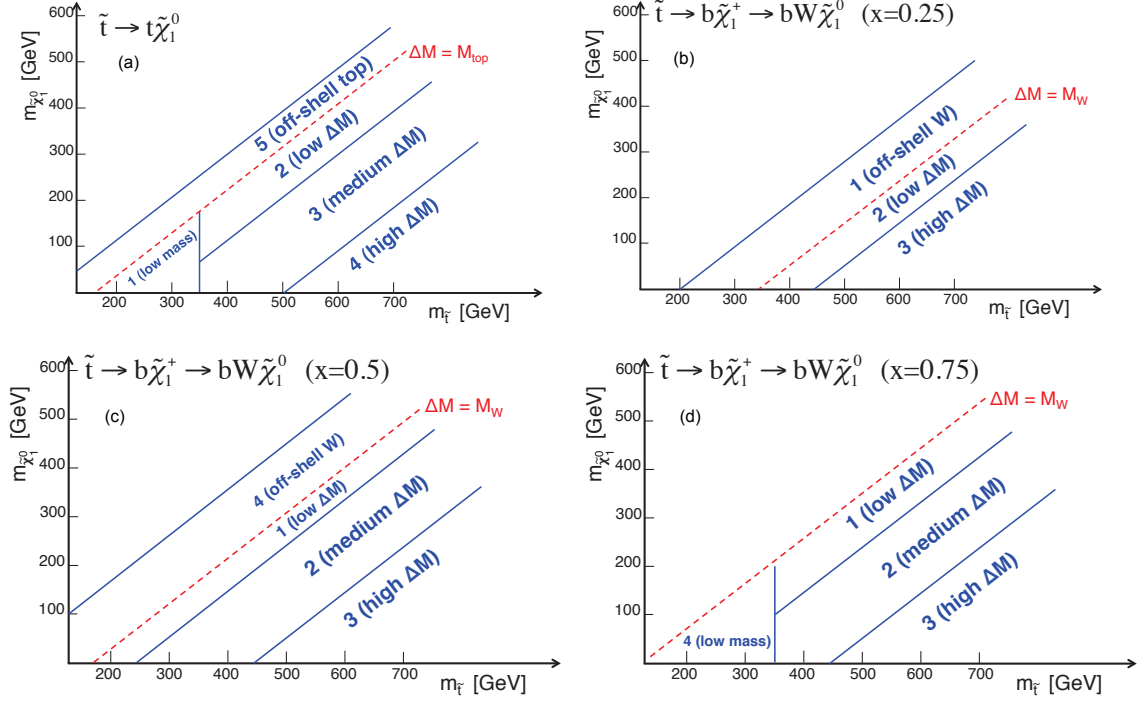
Figure 3:   The regions used to train the BDTs, in the $m_{\widetilde{\chi}_1^0}$ vs. $m_{\widetilde{t}}$ parameter space, for (a) the $\widetilde{t} \to t\widetilde{\chi}_1^0$ scenario, and for (b) the $\widetilde{t} \to b\widetilde{\chi}^+$ $x = 0.25$, (c) 0.5, and (d) 0.75 scenarios. The dashed lines correspond to $\Delta M \equiv m_{\widetilde{t}} - m_{\widetilde{\chi}_1^0} = M_{\text{top}}$ for $\widetilde{t} \to t\widetilde{\chi}_1^0$, and $\Delta M \equiv m_{\chi_1^+} - m_{\widetilde{\chi}_1^0} = M_W$ for $\widetilde{t} \to b\widetilde{\chi}^+$.

between the chargino and the LSP. Just as in the $\widetilde{t} \to t\widetilde{\chi}_1^0$ case, SRs are distinguished by increasingly tighter requirements on E_T^{miss}. Since in the case of $\widetilde{t} \to b\widetilde{\chi}^+$ the signal has no top quark in its decay products, the requirement on the hadronic top χ^2 is not used. The large ΔM selection includes the M_{T2}^W requirement, as well as the requirement that the leading b-tagged jet have p_T larger than 100 GeV.

4.3.3   Signal regions summary

To summarize, this search uses two complementary approaches: one a cut-based approach and the other a BDT multivariate method. Correspondingly, there are two distinct sets of signal regions. In the BDT case, the SRs are defined by requirements on the BDT outputs. The BDT SRs provide the primary result, since the BDT method has better expected sensitivity. There are a total of 16 cut-based SRs (eight each for the $\widetilde{t} \to t\widetilde{\chi}_1^0$ and $\widetilde{t} \to b\widetilde{\chi}^+$ cases) and 18 BDT SRs (six for the $\widetilde{t} \to t\widetilde{\chi}_1^0$ mode and 12 for the $\widetilde{t} \to b\widetilde{\chi}^+$ mode). The expected number of background events in the SRs varies between approximately 4 and 1600 (see Section 8).

5   Background estimation methodology

The SM background is divided into four categories that are evaluated separately. The largest background contribution after full selection is $t\bar{t}$ production in which both W bosons decay leptonically ($t\bar{t} \to \ell\ell$), but one of the leptons is not identified. The second largest background consists of $t\bar{t}$ production in which one W boson decays leptonically and the other hadronically ($t\bar{t} \to \ell + \text{jets}$), as well as single-top-quark production in the s- and t-channels: These are

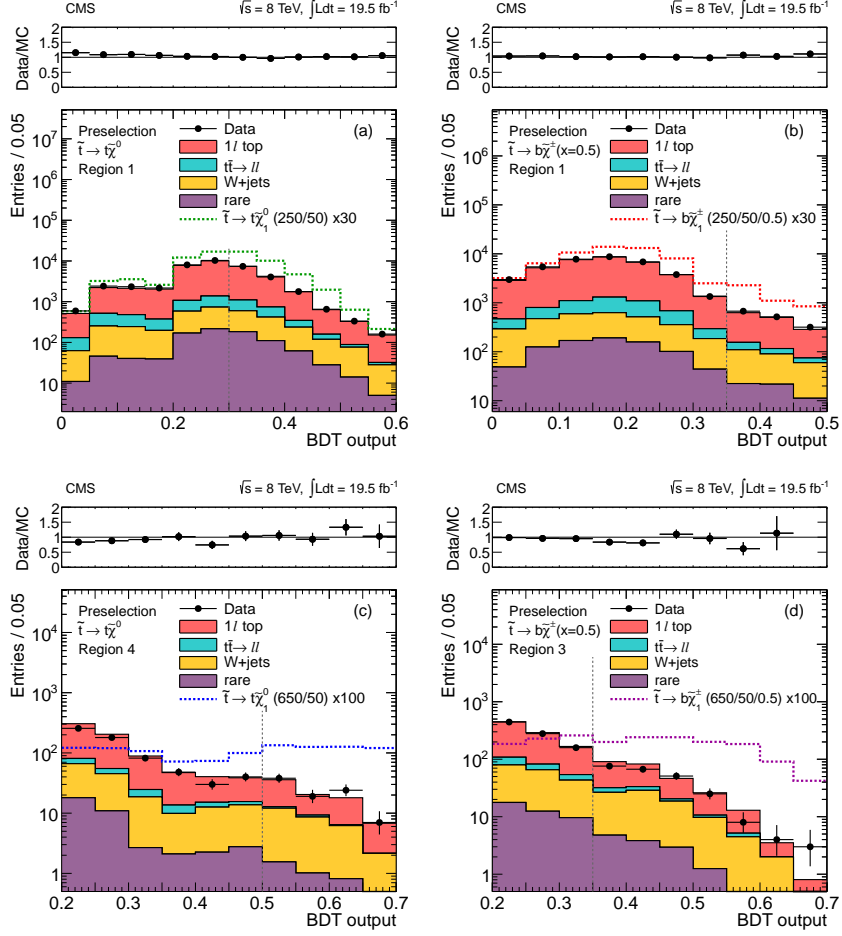Figure 4: Comparison of data and MC simulation for sample BDT outputs. (a) $\tilde{t} \to t\tilde{\chi}_1^0$ scenario in training region 1; (b) $\tilde{t} \to b\tilde{\chi}^+$ scenario with $x = 0.5$ in training region 1; (c) $\tilde{t} \to t\tilde{\chi}_1^0$ scenario in training region 4; (d) $\tilde{t} \to b\tilde{\chi}^+$ scenario with $x = 0.5$ in training region 3. Only the event preselection is applied, and in all cases the last bin contains the overflow. Events in the signal regions are further selected by requiring $M_T > 120$ GeV and by applying BDT requirements as indicated by the vertical dashed lines. We also overlay expectations for possible signals with $m_{\tilde{t}} = 250$ GeV and $m_{\tilde{\chi}_1^0} = 50$ GeV (panels (a) and (b)) and $m_{\tilde{t}} = 650$ GeV and $m_{\tilde{\chi}_1^0} = 50$ GeV (panels (c) and (d)). For display purposes, these are scaled up by factors of 30 and 100 respectively.

collectively referred to as "single-lepton-top-quark" processes. The third largest background consists of a variety of SM processes with small cross sections, including $t\bar{t}$ events produced in association with a vector boson ($t\bar{t}W$, $t\bar{t}Z$, $t\bar{t}\gamma$), processes with two (WW, WZ, ZZ) and three (WWW, WWZ, WZZ, ZZZ) electroweak vector bosons, and single-top-quark production in the tW-channel. These processes are collectively referred to as the "rare" processes. The fourth and final background contribution is from the production of W bosons with jets (W + jets). The multijet contribution to the background is negligible in the signal regions due to the requirement of a high-p_T isolated lepton, large M_T, large E_T^{miss}, and a b-tagged jet. Here, "multijet" refers to events composed entirely of jets, without a lepton, W or Z boson, or top quark.

Backgrounds are estimated from MC simulations, with small corrections (see below). The simulation is validated in control regions (CRs) designed to enrich the data sample in specific

sources of background while maintaining kinematic properties that are similar to those in the signal regions (see Section 6). In the CRs the kinematic variables used in the cut-based and BDT selections are examined to verify that they are properly modeled. A key distribution in each CR is that of M_T after the cut-based or BDT selection requirements, since $M_T > 120\,\text{GeV}$ is the final criterion that defines each signal region. The data/MC comparison of the number of events with $M_T > 120\,\text{GeV}$ is then a direct test of the ability of the method to correctly predict the SM background in the signal regions.

The CR studies are designed to extract data/MC scale factors to be applied to the MC predictions for the background in the signal regions. We find that the only scale factor required is related to an underestimation of the M_T tail for single-lepton-top-quark and W + jets events, as discussed in more detail in Section 6.
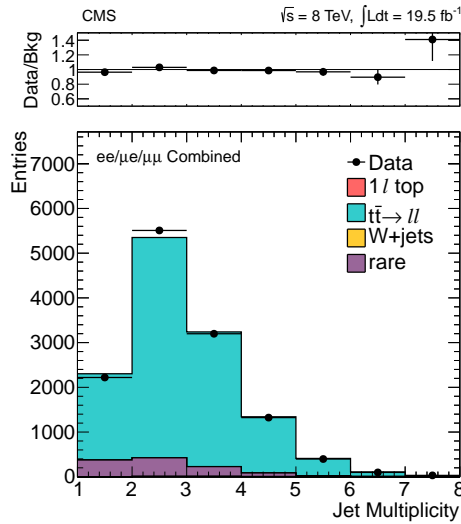

Figure 5: Comparison of the jet multiplicity distributions in data and MC simulation in the sample dominated by $t\bar{t} \to \ell\ell$ events.

The selection of signal events requires at least four hadronic jets. As mentioned above, the dominant background consists of $t\bar{t} \to \ell\ell$ events with one unidentified lepton. These events satisfy the signal region selection only if there are two additional jets from initial- or final-state radiation (ISR/FSR) or if there is one such jet in conjunction with a second lepton identified as a jet (e.g., in the case of hadronic τ-lepton decays). To validate the modeling of ISR/FSR, a data control sample of $t\bar{t} \to \ell\ell$ events is defined by requiring the presence of exactly two opposite-sign leptons (electrons or muons) in events satisfying dilepton triggers. To suppress the Z + jets background that is present in this control sample, same-flavor (ee or $\mu\mu$) events with an invariant mass in the range $76 < m_{\ell\ell} < 106\,\text{GeV}$ are rejected, the presence of at least one b-tagged jet is required, and minimum requirements are imposed on E_T^{miss}. We then compare the distribution of the number of jets in data and MC simulation, as displayed in Fig. 5. The fraction of $t\bar{t} \to \ell\ell$ events with three or more jets is found to be in agreement with the expectation from the MC simulation within a 3% statistical uncertainty.

To minimize systematic uncertainties associated with the $t\bar{t}$ production cross section, integrated luminosity, lepton efficiency, and jet energy scale, the $t\bar{t}$ MC backgrounds at high M_T are always normalized to the number of events in data in the transverse-mass peak region, defined as $50 < M_T < 80\,\text{GeV}$, after subtracting the contribution from rare backgrounds. We refer to this normalization factor as the "tail-to-peak ratio". Background contributions from rare

processes are taken directly from the simulated samples. Their rates are normalized using the corresponding NLO cross sections.

6 Control region studies

Three CRs are used in this analysis. A sample dominated by $t\bar{t} \to \ell\ell$ events is obtained by requiring the presence of two leptons (CR-2ℓ). A sample dominated by a mixture of $t\bar{t} \to \ell +$ jets and $t\bar{t} \to \ell\ell$ events is obtained by requiring the presence of a lepton and one isolated track or hadronic τ-lepton candidate (CR-ℓt). A sample dominated by W + jets events is obtained by vetoing events with b-tagged jets (CR-0b).

In all CRs, we apply the various SR selections and compare data and MC yields with $M_T > 120\,$GeV after normalizing the M_T distribution to the transverse-mass peak region as described in Section 5. In the case of CR-2ℓ, the definition of M_T is ambiguous because there are two identified leptons; we take the M_T value constructed from the leading lepton and the E_T^{miss} vector.

The BDT output distribution trained in $\tilde{t} \to t\tilde{\chi}_1^0$ region 1 (BDT1) is shown in Fig. 6 for the three control regions. The M_T distribution after the BDT signal region requirement is also displayed (in the case of CR-0b this is corrected using the scale factor discussed below). Similar levels of agreement between data and MC simulation are found for the other SR-like selections.

For CR-2ℓ and CR-ℓt, the number of data events with $M_T > 120\,$GeV is consistent with the MC prediction. The level of agreement is used to assess a systematic uncertainty for the $t\bar{t} \to \ell\ell$ background prediction. The uncertainty ranges from 5% for the loosest signal regions to 70% for the tightest signal regions, reflecting the limited statistical precision of the control samples after applying the M_T and BDT requirements. The fraction of events in CR-2ℓ and CR-ℓt with $M_T > 120\,$GeV that could be from stop pair production varies between approximately 1% and 20%, depending on the CR and the masses of the top squark and the LSP. This contribution is always much smaller than the statistical uncertainty on the data event counts.

In the case of CR-0b, the transverse-mass distribution of events exhibits a small excess at high M_T with respect to the MC prediction. This discrepancy, illustrated in Fig. 7 using the high-statistics samples of the preselection level, is attributed to imperfect modeling of the tails of the E_T^{miss} resolution in W + jets events. The data/MC agreement in the CR-0b M_T tail can be restored by rescaling the W + jets contribution by a factor of 1.2 ± 0.3, as seen for example in Fig. 6, bottom right. We find that this factor is insensitive to the details of the selection of the kinematic variables in Table 1 for the CR-0b event sample.

The observation that the simulation underestimates the M_T tail in the W + jets sample suggests that a similar effect should exist in the single-lepton-top-quark background. However, the M_T tail is more populated for the W + jets background than for the single-lepton-top-quark background, due to a significant contribution from very off-shell W bosons. This contribution is much less pronounced for the single-lepton-top-quark background because, ignoring the top-quark width, the lepton-neutrino mass $M_{\ell\nu}$ cannot exceed the difference between the top- and bottom-quark masses, $M_{\ell\nu} < M_{\mathrm{top}} - M_{\mathrm{b}}$. This bound can be violated only if both the top quark and W boson from top quark decays are off-shell. For this reason the scale factor of 1.2 ± 0.3 measured in W + jets events cannot be simply applied to the single-lepton-top-quark simulated sample. The scale factor is larger in the single-lepton-top-quark sample because the fraction of events that have $M_T > 120\,$GeV due to E_T^{miss} mismeasurement is larger than in the W + jets sample.
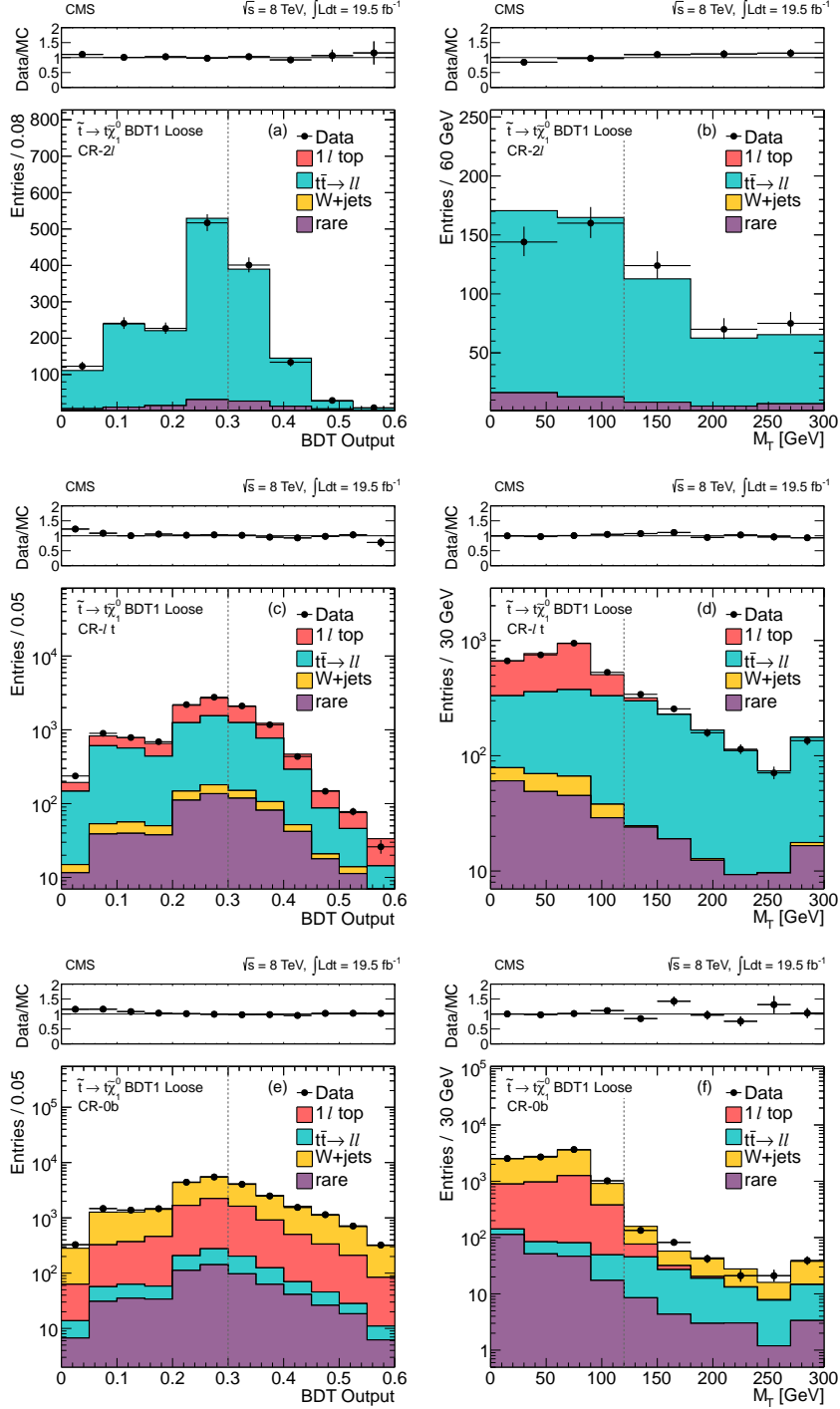
Figure 6: Comparison of data and MC simulation for the distributions of M_T and BDT output for the control regions associated with the BDT trained in region 1 for the $\widetilde{t} \rightarrow t\widetilde{\chi}_1^0$ scenario. The M_T distributions are shown after the "BDT1 loose" requirement indicated by vertical dashed lines on the BDT output plots. (a)-(b): CR-2ℓ; (c)-(d): CR-ℓt; (e)-(f): CR-0b. The vertical dashed lines in the M_T plots correspond to the $M_T > 120\,\mathrm{GeV}$ selection requirement. For CR-0b, the scale factors are applied to the MC distribution in the M_T tail. The last bin in all distributions contains the overflow.
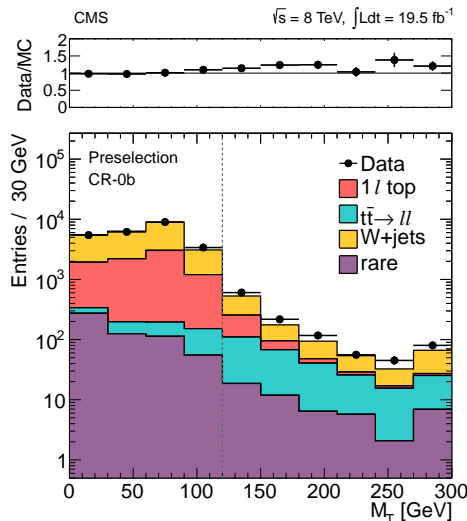
Figure 7: Comparison of data and MC simulation for the M_T distribution in the CR-0b control region, after the preselection. The M_T tail is underestimated by the simulation. A scale factor derived from this control region is used to correct the predictions of the W + jets and single-lepton-top-quark backgrounds. The last bin of the distribution includes the overflow.

Following the arguments given above, a lower bound on the data tail-to-peak ratio for the single-lepton-top-quark sample (R_{top}) can be obtained by scaling the MC value of R_{top} by the W + jets scale factor (1.2 ± 0.3). Conversely, an upper bound for R_{top} is $R_{top} = R_{W+jets}$, where R_{W+jets} is the tail-to-peak ratio for W + jets in the data, i.e., its MC value scaled up by 1.2 ± 0.3. This is an overestimate of the true value of R_{top} because, as mentioned above, the M_T tail is more populated for the W + jets sample than for the one-lepton-top sample. Since the true value of R_{top} lies between these two extremes, we take the average of the upper and lower bounds. The resulting scale factor for R_{top} with respect to its uncorrected MC result lies between 1.5 and 2, depending on the signal region. The associated uncertainty includes the statistical uncertainty in the data/MC scale factor from CR-0b, and half the difference between these upper and lower bounds.

7 Systematic uncertainties of the background prediction

All backgrounds except for the rare contribution are normalized to data in the M_T-peak region, so the statistical uncertainties of the data and MC yields in the M_T-peak region contribute to the uncertainty of the background predictions in the high-M_T signal regions. This normalization is repeated after varying the W + jets background yield in the M_T-peak region by $\pm 50\%$ to estimate the associated systematic uncertainty.

For the $t\bar{t} \to \ell\ell$ background, the dominant uncertainty is assessed by comparing the data and MC yields in the high-M_T regions of the CR-2ℓ and CR-ℓt samples after applying the kinematic requirements for the corresponding signal region. This uncertainty varies between 5% and 70%. The uncertainty for the modeling of additional jets from radiation in $t\bar{t} \to \ell\ell$ events results in a 3% uncertainty on the dilepton background. The uncertainty from the limited number of events in the $t\bar{t} \to \ell\ell$ MC sample also contributes, particularly in the tight signal regions.

An additional uncertainty is associated with the efficiency to identify a second lepton (e, μ, or one-prong hadronic τ-lepton decay) as an isolated track. We verify that the simulation re-

produces the efficiency of the isolated track requirement through studies of $Z \to \ell\ell$ events in data, and we assign a systematic uncertainty of 6%. An uncertainty of 7%, based on studies of the efficiency for τ-lepton identification in data and simulation, is applied to events with a hadronic τ-lepton in the hadronic τ-lepton veto acceptance. We also verify the stability of the $t\bar{t} \to \ell\ell$ MC background prediction by comparing the results of the nominal POWHEG sample with those obtained using MADGRAPH and MC@NLO, by varying the MADGRAPH scale parameters for renormalization and factorization, as well as the scale for the matrix element and parton shower matching, up and down by a factor of two, and by varying the top-quark mass in the range 178.5 to 166.5 GeV. Since the resulting background predictions are consistent within the systematic uncertainties discussed above, we do not assess an additional uncertainty from the $t\bar{t}$ MC stability tests.

The uncertainty of the W + jets background prediction is dominated by the uncertainty from the tail-to-peak ratio, as determined from data/MC comparisons in the CR-0b control region. The main uncertainty for the single-lepton-top-quark background arises from the difference in the tail-to-peak ratios for W + jets and single-lepton-top-quark events.

Table 2: The bottom row of this table shows the relative uncertainty (in percent) of the total background predictions for the $\widetilde{t} \to t\widetilde{\chi}_1^0$ BDT signal regions. The breakdown of this total uncertainty in terms of its individual components is also shown.

| | $\widetilde{t} \to t\widetilde{\chi}_1^0$ | | | | | |
Sample	BDT1–Loose	BDT1–Tight	BDT2	BDT3	BDT4	BDT5
M_T-peak data and MC (stat)	1.0	2.1	2.7	5.3	8.7	3.0
$t\bar{t} \to \ell\ell$ N_{jets} modeling	1.7	1.6	1.6	1.1	0.4	1.7
$t\bar{t} \to \ell\ell$ (CR-ℓt and CR-2ℓ tests)	4.0	8.2	11.0	12.5	7.2	13.8
2nd lepton veto	1.5	1.4	1.4	0.9	0.3	1.4
$t\bar{t} \to \ell\ell$ (stat.)	1.1	2.8	3.4	7.0	7.4	3.3
W+jets cross section	1.6	2.2	2.8	1.7	2.7	2.2
W+jets (stat.)	1.1	1.9	2.0	4.6	10.8	5.2
W+jets SF uncertainty	8.3	7.7	6.8	8.1	9.7	8.6
$1 - \ell$ top (stat.)	0.4	0.8	0.8	1.4	4.4	1.2
$1 - \ell$ top tail-to-peak ratio	9.0	11.4	12.4	19.6	28.5	9.1
Rare processes cross section	1.8	3.0	4.0	8.1	15.7	0.7
Total	13.4	17.1	19.3	27.8	38.4	20.2

The main contributors to the rare SM backgrounds are $pp \to t\bar{t}Z$ and $pp \to t\bar{t}W$; these processes have not yet been measured accurately. As mentioned in Section 3, we normalize their rates to the respective NLO cross-section calculations [31, 32]. We assign an overall conservative uncertainty of 50% to account for missing higher order terms, as well as possible mismodeling of their kinematical properties (see for example the discussion of Ref. [31]).

The systematic uncertainties for the $\widetilde{t} \to t\widetilde{\chi}_1^0$ BDT analysis are summarized in Table 2. The uncertainties for all other signal regions are presented in Appendix A.1.

8   Results

A summary of the background expectations and the corresponding data counts for each signal region is shown in Table 3 for the $\widetilde{t} \to t\widetilde{\chi}_1^0$ BDT analysis, Table 4 for the $\widetilde{t} \to t\widetilde{\chi}_1^0$ cut-based analysis, Table 5 for the $\widetilde{t} \to b\widetilde{\chi}^+$ BDT analysis, and Table 6 for the $\widetilde{t} \to b\widetilde{\chi}^+$ cut-based analysis. Figure 8 presents a comparison of data with MC simulation for the M_T and BDT-output distributions of events that satisfy a loose and a tight $\widetilde{t} \to t\widetilde{\chi}_1^0$ BDT signal-region requirement. Equivalent plots for $\widetilde{t} \to b\widetilde{\chi}^+$ are shown in Fig. 9. The M_T and BDT output distributions for the other signal regions are presented in Appendix A.2.

Table 3: The result of the $\widetilde{t} \to t\widetilde{\chi}_1^0$ BDT analysis. For each signal region the individual background contributions, total background, and observed yields are indicated. The uncertainty includes both the statistical and systematic components. The expected yields for two example signal models are also indicated (statistical uncertainties only). The first and second numbers in parentheses indicate the top-squark and neutralino masses, respectively, in GeV.

	$\widetilde{t} \to t\widetilde{\chi}_1^0$					
Sample	BDT1–Loose	BDT1–Tight	BDT2	BDT3	BDT4	BDT5
$t\bar{t} \to \ell\ell$	438 ± 37	68 ± 11	46 ± 10	5 ± 2	0.3 ± 0.3	48 ± 13
1ℓ top	251 ± 93	37 ± 17	22 ± 12	4 ± 3	0.8 ± 0.9	30 ± 12
$W + $ jets	27 ± 7	7 ± 2	6 ± 2	2 ± 1	0.8 ± 0.3	5 ± 2
Rare	47 ± 23	11 ± 6	10 ± 5	3 ± 1	1.0 ± 0.5	4 ± 2
Total	763 ± 102	124 ± 21	85 ± 16	13 ± 4	2.9 ± 1.1	87 ± 18
Data	728	104	56	8	2	76
$\widetilde{t} \to t\widetilde{\chi}_1^0$ (250/50)	285 ± 8.5	50 ± 3.5	28 ± 2.6	4.4 ± 1.0	0.3 ± 0.3	34 ± 2.9
$\widetilde{t} \to t\widetilde{\chi}_1^0$ (650/50)	12 ± 0.2	7.2 ± 0.2	9.8 ± 0.2	6.5 ± 0.2	4.3 ± 0.1	2.9 ± 0.1

The observed and predicted yields agree in all signal regions within about 1.0–1.5 standard deviations. Therefore, we observe no evidence for top-squark pair production. We note that there is a tendency for the background predictions to lie somewhat above the observed yields; however, the yields and background predictions in different signal regions are correlated, both for the BDT and cut-based analysis. The interpretation of the results in the context of models of top-squark pair production is presented in Section 9.

Table 4: The result of the $\widetilde{t} \to t\widetilde{\chi}_1^0$ cut-based analysis. For each signal region the individual background contributions, total background, and observed yields are indicated. The uncertainty includes both the statistical and systematic components. The expected yields for two example signal models are also indicated (statistical uncertainties only). The first and second numbers in parentheses indicate the top-squark and neutralino masses, respectively, in GeV.

Sample	$E_T^{\text{miss}} > 150\,\text{GeV}$	$E_T^{\text{miss}} > 200\,\text{GeV}$	$E_T^{\text{miss}} > 250\,\text{GeV}$	$E_T^{\text{miss}} > 300\,\text{GeV}$
	Low ΔM Selection			
$t\bar{t} \to \ell\ell$	131 ± 15	42 ± 7	17 ± 5	5.6 ± 2.5
1ℓ top	94 ± 47	30 ± 19	9 ± 6	3.1 ± 2.4
$W + $ jets	10 ± 3	5 ± 1	2 ± 1	1.0 ± 0.4
Rare	16 ± 8	7 ± 4	4 ± 2	1.8 ± 0.9
Total	251 ± 50	83 ± 21	31 ± 8	11.5 ± 3.6
Data	227	69	21	9
$\widetilde{t} \to t\widetilde{\chi}_1^0$ (250/50)	108 ± 3.7	32 ± 2.0	12 ± 1.2	5.2 ± 0.8
$\widetilde{t} \to t\widetilde{\chi}_1^0$ (650/50)	8.0 ± 0.1	7.2 ± 0.1	6.2 ± 0.1	4.9 ± 0.1
	High ΔM Selection			
$t\bar{t} \to \ell\ell$	8 ± 2	5 ± 2	3.2 ± 1.4	1.4 ± 0.9
1ℓ top	13 ± 6	6 ± 4	3.0 ± 2.2	1.4 ± 1.0
$W + $ jets	4 ± 1	2 ± 1	1.5 ± 0.5	0.9 ± 0.3
Rare	4 ± 2	3 ± 1	1.8 ± 0.9	1.0 ± 0.5
Total	29 ± 7	17 ± 5	9.5 ± 2.8	4.7 ± 1.4
Data	23	11	3	2
$\widetilde{t} \to t\widetilde{\chi}_1^0$ (250/50)	10 ± 1.1	4.6 ± 0.8	2.3 ± 0.5	1.4 ± 0.4
$\widetilde{t} \to t\widetilde{\chi}_1^0$ (650/50)	4.9 ± 0.1	4.7 ± 0.1	4.3 ± 0.1	3.7 ± 0.1

9 Interpretation

The results of the search are interpreted in the context of models of top-squark pair production. As discussed in Section 3, we separately consider two possible decay modes of the top squark,
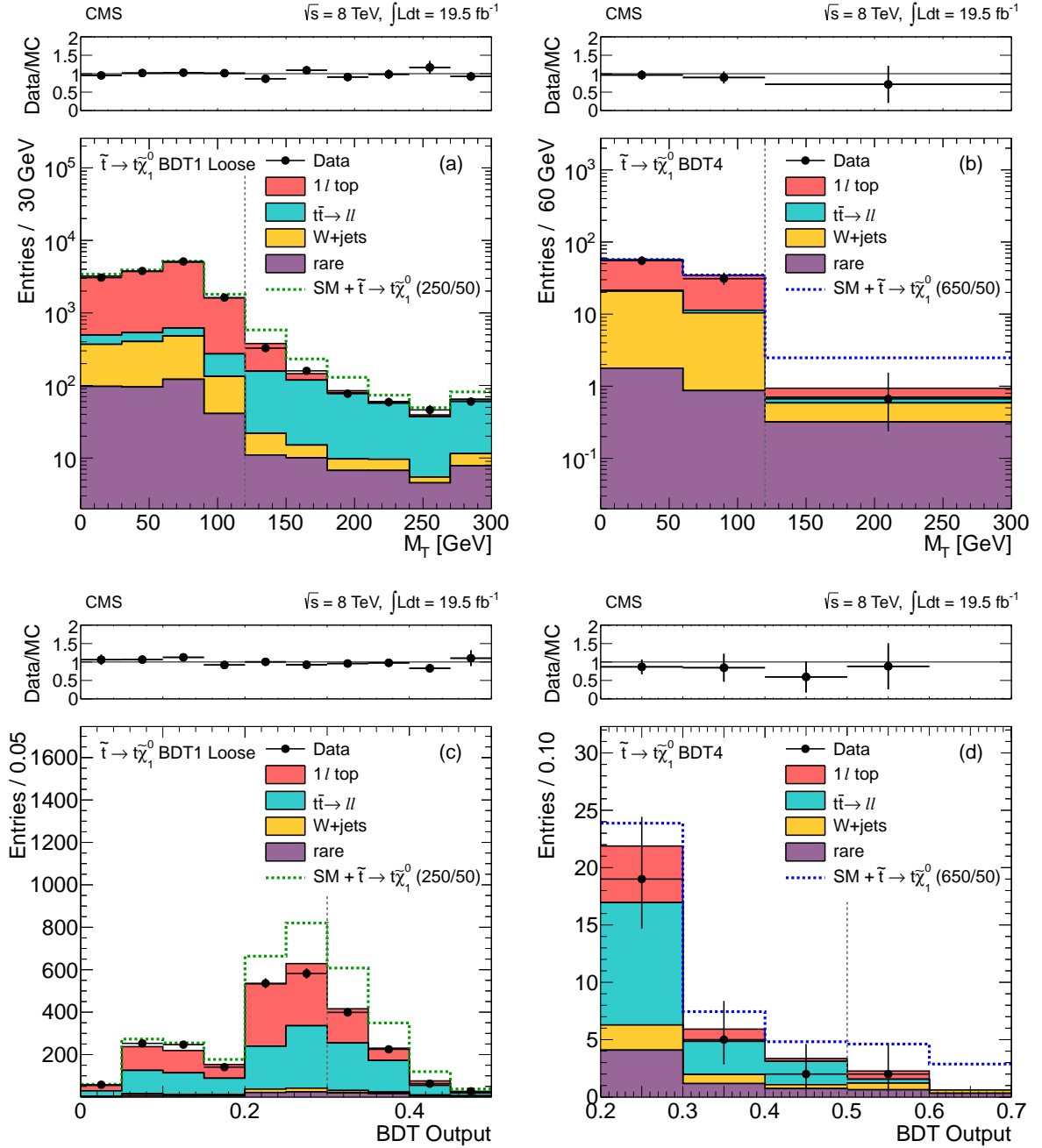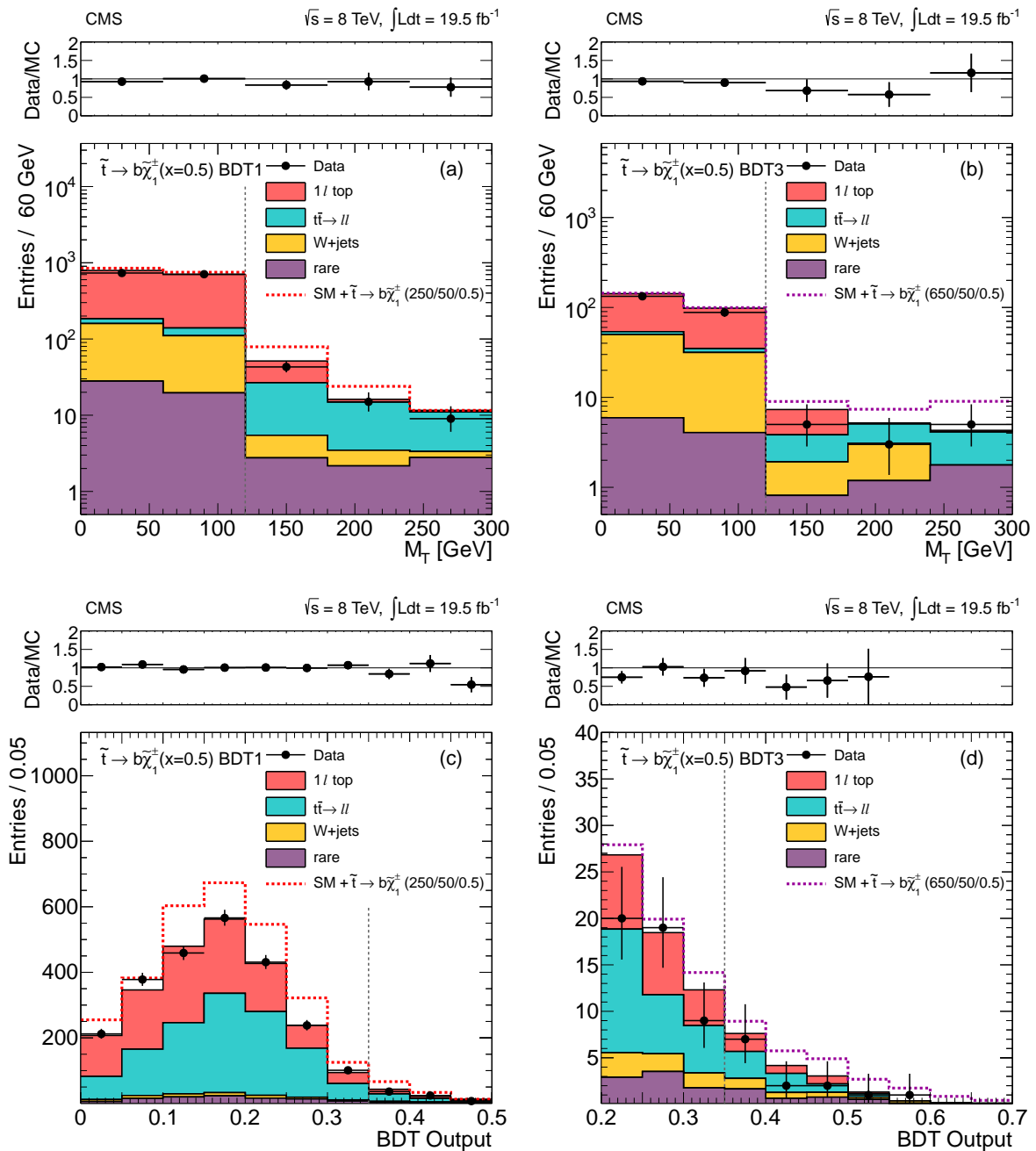
Figure 8: Comparison of data and MC simulation for the distributions of BDT output and M_T corresponding to the tightest and loosest signal region selections in the $\tilde{t} \to t\tilde{\chi}_1^0$ scenario. The M_T distributions are shown after the requirement on the BDT output, and the BDT output distributions are shown after the $M_T > 120$ GeV requirement (these requirements are also indicated by vertical dashed lines on the respective distributions). (a) M_T after the loose cut on the BDT1 output; (b) M_T after the cut on the BDT4 output; (c) BDT1 output after the M_T cut; (d) BDT4 output after the M_T cut. Expected signal distributions for $m_{\tilde{\chi}_1^0} = 50$ GeV and $m_{\tilde{t}} = 250$ GeV or 650 GeV are also overlayed, as indicated in the figures. In plot (b), the bin to the right of the vertical line contains all events with $M_T > 120$ GeV, and has been scaled by a factor of 1/3 to indicate the number of events per 60 GeV. In all distributions the last bin contains the overflow.

Figure 9: Comparison of data and MC simulation for the distributions of BDT output and M_T corresponding to the tightest and loosest signal region selections in the $x = 0.5$ $\widetilde{t} \to b\widetilde{\chi}^+$ scenario with an on-shell W boson. The M_T distributions are shown after the requirement on the BDT output, and the BDT output distributions are shown after the $M_T > 120\,\text{GeV}$ requirement (these requirements are also indicated by vertical dashed lines on the respective distributions). (a) M_T after the cut on the BDT1 output; (b) M_T after the cut on the BDT3 output; (c) BDT1 output after the M_T cut; (d) BDT3 output after the M_T cut. Expected signal distributions for $x = 0.5$ with $m_{\widetilde{\chi}^0_1} = 50\,\text{GeV}$ and $m_{\widetilde{t}} = 250\,\text{GeV}$ or $650\,\text{GeV}$ are also overlayed, as indicated in the figures. In all distributions the last bin contains the overflow.

Table 5: The result of the $\widetilde{t} \to b\widetilde{\chi}^{+}$ BDT analysis. For each signal region the individual background contributions, total background, and observed yields are indicated. The uncertainty includes both the statistical and systematic components. The expected yields for several example signal models are also indicated (statistical uncertainties only). The first number in parentheses indicates the top-squark mass, the second the gluino mass, and the third the chargino mass parameter x. The units of the two mass values are GeV.

$\widetilde{t} \to b\widetilde{\chi}^{+}$ $x = 0.25$

Sample	BDT1	BDT2	BDT3
$t\bar{t} \to \ell\ell$	18 ± 4	2.2 ± 1.3	1.2 ± 1.0
1ℓ top	10 ± 5	4.0 ± 1.8	1.5 ± 0.8
$W + $ jets	3 ± 1	2.0 ± 0.7	0.7 ± 0.3
Rare	4 ± 2	1.6 ± 0.8	1.0 ± 0.5
Total	35 ± 6	9.8 ± 2.4	4.4 ± 1.4
Data	29	7	2
$\widetilde{t} \to b\widetilde{\chi}^{+}$ (450/50/0.25)	19 ± 2.9	11 ± 2.2	5.2 ± 1.5
$\widetilde{t} \to b\widetilde{\chi}^{+}$ (600/100/0.25)	8.8 ± 0.8	7.5 ± 0.8	5.6 ± 0.7

$\widetilde{t} \to b\widetilde{\chi}^{+}$ $x = 0.5$

Sample	BDT1	BDT2–Loose	BDT2–Tight	BDT3	BDT4
$t\bar{t} \to \ell\ell$	40 ± 5	21 ± 4	4 ± 2	6 ± 2	100 ± 16
1ℓ top	24 ± 10	15 ± 7	4 ± 3	4 ± 2	33 ± 12
$W + $ jets	5 ± 1	5 ± 1	2 ± 1	3 ± 1	5 ± 1
Rare	8 ± 4	8 ± 4	3 ± 1	4 ± 2	8 ± 4
Total	77 ± 12	50 ± 9	13 ± 4	17 ± 4	146 ± 21
Data	67	35	12	13	143
$\widetilde{t} \to b\widetilde{\chi}^{+}$ (250/50/0.5)	45 ± 7.6	24 ± 5.2	5.7 ± 2.4	5.2 ± 2.6	55 ± 8.1
$\widetilde{t} \to b\widetilde{\chi}^{+}$ (650/50/0.5)	3.5 ± 0.4	9.5 ± 0.7	5.6 ± 0.5	8.3 ± 0.6	3.2 ± 0.4

$\widetilde{t} \to b\widetilde{\chi}^{+}$ $x = 0.75$

Sample	BDT1	BDT2	BDT3	BDT4
$t\bar{t} \to \ell\ell$	37 ± 5	9 ± 2	3.1 ± 1.3	248 ± 22
1ℓ top	17 ± 9	6 ± 5	1.6 ± 1.6	188 ± 70
$W + $ jets	4 ± 1	4 ± 1	1.6 ± 0.6	22 ± 6
Rare	4 ± 2	4 ± 2	1.8 ± 0.9	20 ± 10
Total	61 ± 10	22 ± 6	8.1 ± 2.3	478 ± 74
Data	50	13	5	440
$\widetilde{t} \to b\widetilde{\chi}^{+}$ (250/50/0.75)	115 ± 13	21 ± 5.6	8.0 ± 3.7	518 ± 28
$\widetilde{t} \to b\widetilde{\chi}^{+}$ (650/50/0.75)	3.9 ± 0.4	8.4 ± 0.6	6.8 ± 0.6	5.5 ± 0.5

$\widetilde{t} \to t\widetilde{\chi}_1^0$ and $\widetilde{t} \to b\widetilde{\chi}^{+} \to bW\widetilde{\chi}_1^0$, each with 100% branching fraction. Using the results of Section 8, we compute 95% confidence level (CL) cross section upper limits for top-squark pair production in the $m_{\widetilde{\chi}_1^0}$ vs. $m_{\widetilde{t}}$ parameter space. Then, based on the expected $pp \to \widetilde{t}\widetilde{t}^{*}$ production rate, these cross section limits are used to exclude regions of SUSY parameter space. For the $\widetilde{t} \to b\widetilde{\chi}^{+}$ scenario, the mass of the intermediate $\widetilde{\chi}_1^{\pm}$ is specified by the parameter x defined in Section 3.

In setting limits, we account for the following sources of systematic uncertainty associated with the signal event acceptance and efficiency. The uncertainty of the integrated luminosity determination is 4.4% [62]. Samples of $Z \to \ell\ell$ events are used to measure the lepton efficiencies, and the corresponding uncertainties are propagated to the signal event acceptance and efficiency. These uncertainties are 3% for the trigger efficiency and a combined 5% for the lepton identification and isolation efficiency, where we also account for additional uncertainties in the modeling of the lepton isolation due to the differences in the hadronic activity in $Z \to \ell\ell$ and SUSY events. The uncertainty of the efficiency to tag bottom-quark jets results in an uncertainty for the acceptance that depends on model details but is typically less than 1%. The energy scale

Table 6: The result of the $\widetilde{t} \to b\widetilde{\chi}^+$ cut-based analysis. For each signal region the individual background contributions, total background, and observed yields are indicated. The uncertainty includes both the statistical and systematic components. The expected yields for several sample signal models are also indicated (statistical uncertainties only). The first number in parentheses indicates the top-squark mass, the second the gluino mass, and the third the chargino mass parameter x. The units of the two mass values are GeV.

Sample	$E_{\mathrm{T}}^{\mathrm{miss}} > 100\,\mathrm{GeV}$	$E_{\mathrm{T}}^{\mathrm{miss}} > 150\,\mathrm{GeV}$	$E_{\mathrm{T}}^{\mathrm{miss}} > 200\,\mathrm{GeV}$	$E_{\mathrm{T}}^{\mathrm{miss}} > 250\,\mathrm{GeV}$
Low ΔM Selection				
$t\bar{t} \to \ell\ell$	875 ± 57	339 ± 23	116 ± 14	40 ± 9
1ℓ top	658 ± 192	145 ± 70	41 ± 24	14 ± 9
$W + \mathrm{jets}$	59 ± 15	21 ± 5	8 ± 2	4 ± 1
Rare	70 ± 35	33 ± 17	16 ± 8	8 ± 4
Total	1662 ± 203	537 ± 75	180 ± 28	66 ± 13
Data	1624	487	151	52
$\widetilde{t} \to b\widetilde{\chi}^+$ (450/50/0.25)	47 ± 3.3	33 ± 2.7	19 ± 2.0	8.7 ± 1.4
$\widetilde{t} \to b\widetilde{\chi}^+$ (600/100/0.25)	15 ± 0.7	13 ± 0.7	11 ± 0.6	7.9 ± 0.5
$\widetilde{t} \to b\widetilde{\chi}^+$ (250/50/0.5)	419 ± 17	157 ± 9.9	52 ± 5.4	21 ± 3.4
$\widetilde{t} \to b\widetilde{\chi}^+$ (650/50/0.5)	14 ± 0.6	13 ± 0.5	11 ± 0.5	8.4 ± 0.4
$\widetilde{t} \to b\widetilde{\chi}^+$ (250/50/0.75)	854 ± 26	399 ± 18	144 ± 10	56 ± 6.4
$\widetilde{t} \to b\widetilde{\chi}^+$ (650/50/0.75)	17 ± 0.7	16 ± 0.6	13 ± 0.6	11 ± 0.5
High ΔM Selection				
$t\bar{t} \to \ell\ell$	25 ± 5	12 ± 3	7 ± 2	2.9 ± 1.5
1ℓ top	35 ± 10	15 ± 6	6 ± 3	2.7 ± 1.8
$W + \mathrm{jets}$	9 ± 2	5 ± 1	2 ± 1	1.8 ± 0.6
Rare	9 ± 5	7 ± 3	4 ± 2	2.4 ± 1.2
Total	79 ± 12	38 ± 7	19 ± 5	9.9 ± 2.7
Data	90	39	18	5
$\widetilde{t} \to b\widetilde{\chi}^+$ (450/50/0.25)	30 ± 2.7	23 ± 2.3	15 ± 1.8	7.3 ± 1.3
$\widetilde{t} \to b\widetilde{\chi}^+$ (600/100/0.25)	11 ± 0.6	9.7 ± 0.6	8.4 ± 0.6	6.1 ± 0.5
$\widetilde{t} \to b\widetilde{\chi}^+$ (250/50/0.5)	37 ± 4.8	23 ± 3.8	11 ± 2.6	5.0 ± 1.7
$\widetilde{t} \to b\widetilde{\chi}^+$ (650/50/0.5)	11 ± 0.5	9.8 ± 0.5	8.6 ± 0.4	6.7 ± 0.4
$\widetilde{t} \to b\widetilde{\chi}^+$ (250/50/0.75)	32 ± 5.2	23 ± 4.4	11 ± 2.9	3.6 ± 1.4
$\widetilde{t} \to b\widetilde{\chi}^+$ (650/50/0.75)	9.2 ± 0.5	8.4 ± 0.5	7.5 ± 0.4	6.3 ± 0.4

of hadronic jets is known to 1–4%, depending on η and p_{T}, yielding an uncertainty of 3–15% for the signal event selection efficiency. The larger uncertainties correspond to models for which the difference between the masses of the top squark and LSP is small.

The experimental acceptance for signal events depends on the level of ISR activity, especially in the small ΔM region where an initial-state boost may be required for an event to satisfy the selection requirements, including those on $E_{\mathrm{T}}^{\mathrm{miss}}$, M_{T}, and the number of reconstructed jets. The modeling of ISR in MADGRAPH is investigated by comparing the predicted and measured p_{T} spectra of the system recoiling against the ISR jets in $Z + \mathrm{jets}$, $t\bar{t}$, and WZ events. Good agreement is observed at lower p_{T}, while the simulation is found to over predict the data by about 10% at a p_{T} value of 150 GeV, rising to 20% for $p_{\mathrm{T}} > 250$ GeV. The predictions from the MC signal samples are weighted to account for this difference, by a factor of 0.8–1.0, depending on the p_{T} of the system recoiling against the ISR jets, and the deviation of this weight from 1 is taken as a systematic uncertainty. Further details are given in Appendix B.

Upper limits on the cross section for top-squark pair production are calculated separately for each SR, incorporating the uncertainties of the acceptance and efficiency discussed above, using the LHC-style CL$_{\mathrm{s}}$ criterion [63–65]. For each point in the signal model parameter space, the observed limit is taken from the signal region with the best expected limit. The results from the

BDT analysis are displayed in Fig. 10. The corresponding results from the cut-based analysis, and maps of the most sensitive signal regions for each of the top-squark decay modes, are presented in Appendix A.3. The cross section limits from the BDT analysis improve upon those from the cut-based analysis by up to approximately 40%, depending on the model parameters.

Our results probe top squarks with masses between approximately 150 and 650 GeV, for neutralinos with masses up to approximately 250 GeV, depending on the details of the model. For the $\tilde{t} \to t\tilde{\chi}_1^0$ search, the results are not sensitive to the model points with $m_{\tilde{t}} - m_{\tilde{\chi}_1^0} = M_{\text{top}}$ because the $\tilde{\chi}_1^0$ is produced at rest in the top-quark rest frame. However the results are sensitive to scenarios with $m_{\tilde{t}} - m_{\tilde{\chi}_1^0} < M_{\text{top}}$ in which the top quark in the decay $\tilde{t} \to t\tilde{\chi}_1^0$ is off-shell, including regions of parameter space with the top squark lighter than the top quark.

The acceptance depends on the polarization of the top quarks in the $\tilde{t} \to t\tilde{\chi}_1^0$ scenario, and on the polarization of the charginos and W bosons in the $\tilde{t} \to b\tilde{\chi}^+$ scenario. These polarizations depend on the left/right mixing of the top squarks and on the mixing matrices of the neutralino and chargino [36, 37]. The exclusion regions obtained in the nominal $\tilde{t} \to t\tilde{\chi}_1^0$ scenario with unpolarized top quarks are compared to those obtained with pure left-handed and pure right-handed top quarks in Fig. 11 (left). The limits on the top-squark and $\tilde{\chi}_1^0$ masses vary by ± 10–20 GeV depending on the top-quark polarization.

In the $\tilde{t} \to b\tilde{\chi}^+$ scenario, the acceptance depends on the polarization of the chargino, and on whether the $W\tilde{\chi}_1^0 \tilde{\chi}_1^{\pm}$ coupling is left-handed or right-handed. In the nominal interpretations for the $\tilde{t} \to b\tilde{\chi}^+$ models presented in Fig. 10, the signal events are generated with an unpolarized chargino and a left/right-symmetric $W\tilde{\chi}_1^0 \tilde{\chi}_1^{\pm}$ coupling. We have studied the dependence of our results on these assumptions. We find that the scenarios in which the limits deviate the most from the nominal result correspond to right-handed charginos with either a right-handed $W\tilde{\chi}_1^0 \tilde{\chi}_1^{\pm}$ coupling (maximum sensitivity) or a left-handed $W\tilde{\chi}_1^0 \tilde{\chi}_1^{\pm}$ coupling (minimum sensitivity). This is shown for the $\tilde{t} \to b\tilde{\chi}^+$ $x = 0.5$ model in Fig. 11 (right). The corresponding results for the $x = 0.25$ and 0.75 scenarios can be found in Appendix A.3.

Mixed-decay scenarios, i.e., scenarios with non-zero top-squark decay branching fractions into both $\tilde{t} \to t\tilde{\chi}_1^0$ and $\tilde{t} \to b\tilde{\chi}^+$, have not been considered here. However, our results can be used to draw useful conclusions about these possibilities. We must distinguish between two typical SUSY spectra: one in which the chargino and LSP are nearly mass-degenerate, and the other in which the chargino is considerably heavier. In the degenerate case, corresponding to $x \approx 0$, the acceptance is small for top-squark pairs with one or more $\tilde{t} \to b\tilde{\chi}^+$ decays. This is because the visible decay products in the $\tilde{\chi}_1^+ \to \tilde{\chi}_1^0 + X$ process are soft and likely to escape detection. Thus, to a good approximation, in these scenarios the top-squark pair cross section limit can be extracted by scaling the corresponding limit in the 100% $\tilde{t} \to t\tilde{\chi}_1^0$ model by $\mathcal{B}^2$, where $\mathcal{B}$ is the branching fraction for $\tilde{t} \to t\tilde{\chi}_1^0$. Exclusion regions for a few choices of $\mathcal{B}$ are shown in Fig. 12. In the mixed case with a chargino much heavier than the LSP, a conservative approximate cross section limit can be obtained as $\sigma(pp \to \tilde{t}\tilde{t}^*) < \min(\sigma_0/\mathcal{B}^2, \sigma_+/(1-\mathcal{B})^2)$, where σ_0 and σ_+ are the cross section limits for the 100% $\tilde{t} \to t\tilde{\chi}_1^0$ and 100% $\tilde{t} \to b\tilde{\chi}^+$ scenarios, respectively, and $\mathcal{B}$ is the branching fraction defined above. (The limits σ_0 and σ_+ shown in Fig. 10 are available electronically [66].) This approach is conservative as it uses only one out of the three possible decay modes of the top-squark pair. It should also be noted that in the heavier-chargino scenario it is possible for one additional neutralino ($\tilde{\chi}_2^0$) to be nearly degenerate with the chargino. The decay $\tilde{t} \to t\tilde{\chi}_2^0$ followed by, for example, $\tilde{\chi}_2^0 \to Z\tilde{\chi}_1^0$ or $H\tilde{\chi}_1^0$ would then also be possible. This would further complicate the interpretation of the experimental results.
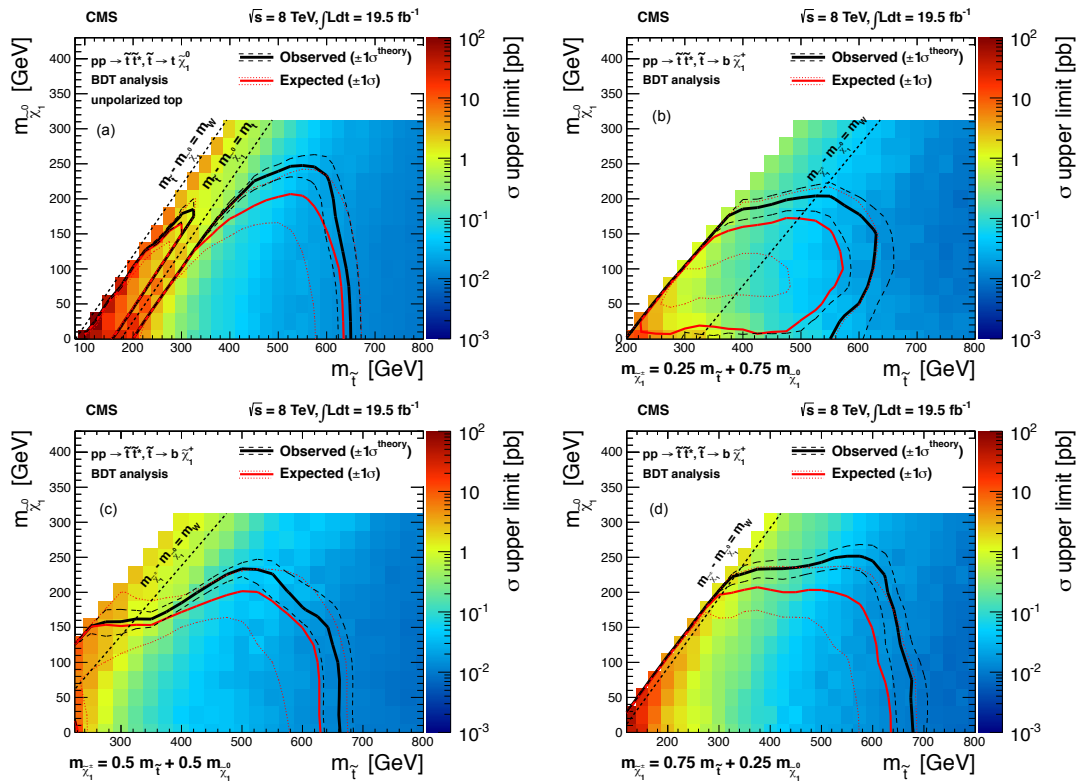
Figure 10: Interpretations using the primary results from the BDT method. (a) $\tilde{t} \to t\tilde{\chi}_1^0$ model; (b) $\tilde{t} \to b\tilde{\chi}^+$ model with $x = 0.25$; (c) $\tilde{t} \to b\tilde{\chi}^+$ model with $x = 0.50$; (d) $\tilde{t} \to b\tilde{\chi}^+$ model with $x = 0.75$; The color scale indicates the observed cross section upper limit. The observed, median expected, and ± 1 standard deviation (σ) expected 95% CL exclusion contours are indicated. The variations in the excluded region due to $\pm 1\sigma$ uncertainty of the theoretical prediction of the cross section for top-squark pair production are also indicated.
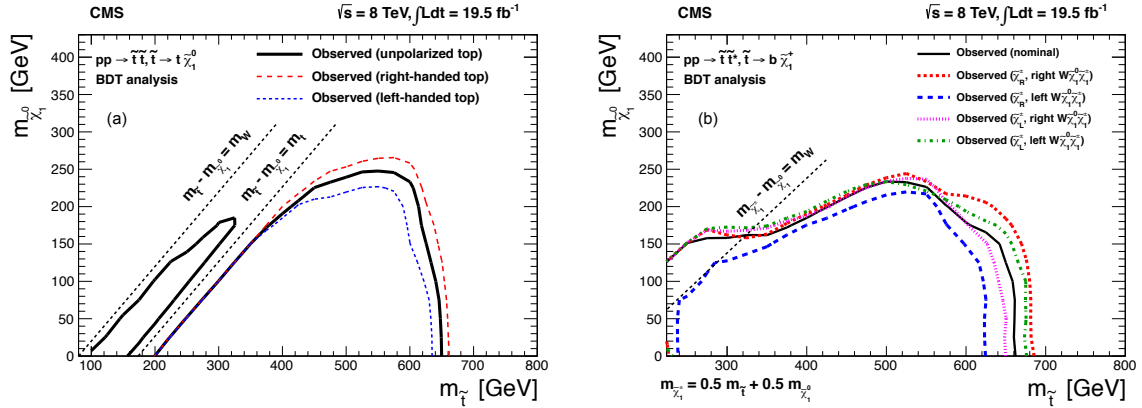
Figure 11: (a) the observed 95% CL excluded regions for the $\widetilde{t} \rightarrow t\widetilde{\chi}^0_1$ model for the case of unpolarized, right-handed, and left-handed top quarks. (b) the observed 95% CL excluded regions for the $\widetilde{t} \rightarrow b\widetilde{\chi}^+$ model with $x = 0.5$ for the nominal scenario, right- vs. left-handed charginos ($\widetilde{\chi}^\pm_R$ and $\widetilde{\chi}^\pm_L$, respectively), and right- vs. left-handed $W\widetilde{\chi}^0_1\widetilde{\chi}^\pm_1$ couplings.
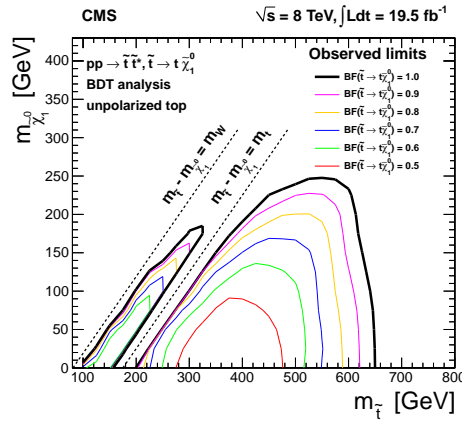
Figure 12: The observed 95% CL excluded regions as a function of the assumed branching fraction for the $\widetilde{t} \rightarrow t\widetilde{\chi}^0_1$ decay mode. The results are based on the assumption that the search has no acceptance for top-squark pair events if one of the top squarks decays in a different mode. See text for details.

10   Summary

We have performed a search for the direct pair production of top squarks in a final state consisting of a single isolated lepton, jets, large missing transverse momentum, and large transverse mass. Signal regions are defined both with requirements on the output of a BDT multivariate discriminator, and with requirements on several kinematic discriminants. The observed yields in the signal regions agree with the predicted backgrounds within the assessed uncertainties. The results are interpreted in the context of models of top-squark pair production and decay. The analysis probes top squarks with masses up to about 650 GeV and significantly restricts the allowed parameter space of natural SUSY scenarios.

Acknowledgements

References

[1] S. Dimopoulos and S. Raby, "Supercolor", *Nucl. Phys. B* **192** (1981) 353, `doi:10.1016/0550-3213(81)90430-2`.

[2] E. Witten, "Dynamical Breaking of Supersymmetry", *Nucl. Phys. B* **188** (1981) 513, `doi:10.1016/0550-3213(81)90006-7`.

[3] M. Dine, W. Fischler, and M. Srednicki, "Supersymmetric Technicolor", *Nucl. Phys. B* **189** (1981) 575, `doi:10.1016/0550-3213(81)90582-4`.

[4] S. Dimopoulos and H. Georgi, "Softly Broken Supersymmetry and SU(5)", *Nucl. Phys. B* **193** (1981) 150, `doi:10.1016/0550-3213(81)90522-8`.

[5] N. Sakai, "Naturalness in Supersymmetric Guts", *Z. Phys. C* **11** (1981) 153, `doi:10.1007/BF01573998`.

[6] R. K. Kaul and P. Majumdar, "Cancellation of quadratically divergent mass corrections in globally supersymmetric spontaneously broken gauge theories", *Nucl. Phys. B* **199** (1982) 36, `doi:10.1016/0550-3213(82)90565-X`.

[7] CMS Collaboration, "The CMS experiment at the CERN LHC", *JINST* **3** (2008) S08004, `doi:10.1088/1748-0221/3/08/S08004`.

[8] R. Barbieri and G. F. Giudice, "Upper bounds on supersymmetric particle masses", *Nucl. Phys. B* **306** (1988) 63, `doi:10.1016/0550-3213(88)90171-X`.

[9] B. de Carlos and J. A. Casas, "One-loop analysis of the electroweak breaking in supersymmetric models and the fine-tuning problem", *Phys. Lett. B* **309** (1993) 320, `doi:10.1016/0370-2693(93)90940-J`, `arXiv:hep-ph/9303291`.

[10] S. Dimopoulos and G. F. Giudice, "Naturalness constraints in supersymmetric theories with non-universal soft terms", *Phys. Lett. B* **357** (1995) 573, `doi:10.1016/0370-2693(95)00961-J`, `arXiv:hep-ph/9507282`.

[11] R. Barbieri, G. Dvali, and L. J. Hall, "Predictions from a U(2) flavour symmetry in supersymmetric theories", *Phys. Lett. B* **377** (1996) 76, `doi:10.1016/0370-2693(96)00318-8`, `arXiv:hep-ph/9512388`.

[12] M. Papucci, J. T. Ruderman, and A. Weiler, "Natural SUSY endures", *JHEP* **09** (2012) 035, `doi:10.1007/JHEP09(2012)035`, `arXiv:1110.6926`.

[13] ATLAS Collaboration, "Observation of a new particle in the search for the Standard Model Higgs boson with the ATLAS detector at the LHC", *Phys. Lett. B* **716** (2012) 1, `doi:10.1016/j.physletb.2012.08.020`, `arXiv:1207.7214`.

[14] CMS Collaboration, "Observation of a new boson at a mass of 125 GeV with the CMS experiment at the LHC", *Phys. Lett. B* **716** (2012) 30, `doi:10.1016/j.physletb.2012.08.021`, `arXiv:1207.7235`.

[15] CMS Collaboration, "Search for a standard-model-like Higgs boson with a mass in the range 145 to 1000 GeV at the LHC", *Eur. Phys. J. C* **73** (2013) 2469, `doi:10.1140/epjc/s10052-013-2469-8`, `arXiv:1304.0213`.

[16] ATLAS Collaboration, "Search for a supersymmetric partner to the top quark in final states with jets and missing transverse momentum at $\sqrt{s} = 7$ TeV with the ATLAS detector", *Phys. Rev. Lett.* **109** (2012) 211802, `doi:10.1103/PhysRevLett.109.211802`, `arXiv:1208.1447`.

[17] ATLAS Collaboration, "Search for direct top squark pair production in final states with one isolated lepton, jets, and missing transverse momentum in $\sqrt{s} = 7$ TeV pp collisions using 4.7 fb^{-1} of ATLAS data", *Phys. Rev. Lett.* **109** (2012) 211803, `doi:10.1103/PhysRevLett.109.211803`, `arXiv:1208.2590`.

[18] ATLAS Collaboration, "Search for light scalar top quark pair production in final states with two leptons with the ATLAS detector in $\sqrt{s} = 7$ TeV proton-proton collisions", *Eur. Phys. J. C* **72** (2012) 2237, `doi:10.1140/epjc/s10052-012-2237-1`, `arXiv:1208.4305`.

[19] ATLAS Collaboration, "Search for light top squark pair production in final states with leptons and b-jets with the ATLAS detector in $\sqrt{s} = 7$ TeV proton-proton collisions", *Phys. Lett. B* **720** (2013) 13, `doi:10.1016/j.physletb.2013.01.049`, `arXiv:1209.2102`.

[20] ATLAS Collaboration, "Search for a heavy top-quark partner in final states with two leptons with the ATLAS detector at the LHC", *JHEP* **11** (2012) 094, `doi:10.1007/JHEP11(2012)094`, `arXiv:1209.4186`.

[21] CDF Collaboration, "Search for the supersymmetric partner of the top quark in $p\bar{p}$ collisions at $\sqrt{s} = 1.96$ TeV", *Phys. Rev. D* **82** (2010) 092001, `doi:10.1103/PhysRevD.82.092001`, `arXiv:1009.0266`.

[22] DØ Collaboration, "Search for pair production of the scalar top quark in the electron+muon final state", *Phys. Lett. B* **696** (2011) 321, `doi:10.1016/j.physletb.2010.12.052`, `arXiv:1009.5950`.

[23] S. Frixione, P. Nason, and C. Oleari, "Matching NLO QCD computations with parton shower simulations: the POWHEG method", *JHEP* **11** (2007) 070, `doi:10.1088/1126-6708/2007/11/070`, `arXiv:0709.2092`.

[24] S. Frixione and B. R. Webber, "Matching NLO QCD computations and parton shower simulations", *JHEP* **06** (2002) 029, `doi:10.1088/1126-6708/2002/06/029`, `arXiv:hep-ph/0204244`.

[25] S. Frixione, P. Nason, and B. R. Webber, "Matching NLO QCD and parton showers in heavy flavor production", *JHEP* **08** (2003) 007, `doi:10.1088/1126-6708/2003/08/007`, `arXiv:hep-ph/0305252`.

[26] J. Alwall et al., "MadGraph 5: going beyond", *JHEP* **06** (2011) 128, `doi:10.1007/JHEP06(2011)128`, `arXiv:1106.0522`.

[27] H.-L. Lai et al., "New parton distributions for collider physics", *Phys. Rev. D* **82** (2010) 074024, `doi:10.1103/PhysRevD.82.074024`, `arXiv:1007.2241`.

[28] J. Pumplin et al., "New generation of parton distributions with uncertainties from global QCD analysis", *JHEP* **07** (2002) 012, `doi:10.1088/1126-6708/2002/07/012`, `arXiv:hep-ph/0201195`.

[29] R. Gavin, Y. Li, F. Petriello, and S. Quackenbush, "W Physics at the LHC with FEWZ 2.1", *Comput. Phys. Commun.* **184** (2013) 208, `doi:10.1016/j.cpc.2012.09.005`, `arXiv:1201.5896`.

[30] N. Kidonakis, "Differential and total cross sections for top pair and single top production", in *XX International Workshop on Deep-Indelastic Scattering and Related Subjects*, p. 831. Bonn, 2012. `arXiv:1205.3453`. `doi:10.3204/DESY-PROC-2012-02/251`.

[31] J. M. Campbell and R. K. Ellis, "$t\bar{t}W^{\pm}$ production and decay at NLO", *JHEP* **07** (2012) 052, `doi:10.1007/JHEP07(2012)052`, `arXiv:1204.5678`.

[32] M. V. Garzelli, A. Kardos, C. G. Papadopoulos, and Z. Trocsanyi, "$t\bar{t}W^{\pm}$ and $t\bar{t}Z$ hadroproduction at NLO accuracy in QCD with Parton Shower and Hadronization Effects", *JHEP* **11** (2012) 056, `doi:10.1007/JHEP11(2012)056`, `arXiv:1208.2665`.

[33] J. M. Campbell and R. K. Ellis, "MCFM for the Tevatron and the LHC", *Nucl. Phys. Proc. Suppl.* **205-206** (2010) 10, `doi:10.1016/j.nuclphysbps.2010.08.011`, `arXiv:1007.3492`.

[34] R. Frederix et al., "Four-lepton production at hadron colliders: aMC@NLO predictions with theoretical uncertainties", *JHEP* **02** (2012) 099, `doi:10.1007/JHEP02(2012)099`, `arXiv:1110.4738`.

[35] T. Sjöstrand, S. Mrenna, and P. Skands, "PYTHIA 6.4 physics and manual", *JHEP* **05** (2006) 026, `doi:10.1088/1126-6708/2006/05/026`, `arXiv:hep-ph/0603175`.

[36] M. Perelstein and A. Weiler, "Polarized tops from stop decays at the LHC", *JHEP* **03** (2009) 141, `doi:10.1088/1126-6708/2009/03/141`, `arXiv:0811.1024`.

[37] I. Low, "Polarized Charginos (and Tops) in Stop Decays", (2013). `arXiv:1304.0491`.

[38] W. Beenakker, R. Höpker, M. Spira, and P. M. Zerwas, "Squark and gluino production at hadron colliders", *Nucl. Phys. B* **492** (1997) 51, `doi:10.1016/S0550-3213(97)00084-9`.

[39] A. Kulesza and L. Motyka, "Threshold resummation for squark-antisquark and gluino-pair production at the LHC", *Phys. Rev. Lett.* **102** (2009) 111802, `doi:10.1103/PhysRevLett.102.111802`.

[40] A. Kulesza and L. Motyka, "Soft gluon resummation for the production of gluino-gluino and squark-antisquark pairs at the LHC", *Phys. Rev. D* **80** (2009) 095004, `doi:10.1103/PhysRevD.80.095004`.

[41] W. Beenakker et al., "Soft-gluon resummation for squark and gluino hadroproduction", *JHEP* **12** (2009) 041, `doi:10.1088/1126-6708/2009/12/041`.

[42] W. Beenakker et al., "Squark and gluino hadroproduction", *Int. J. Mod. Phys. A* **26** (2011) 2637, `doi:10.1142/S0217751X11053560`.

[43] M. Krämer et al., "Supersymmetry production cross sections in pp collisions at $\sqrt{s} = $ 7 TeV", (2012). `arXiv:1206.2892`.

[44] CMS Collaboration, "The fast simulation of the CMS detector at LHC", *J. Phys. Conf. Ser.* **331** (2011) 032049, `doi:10.1088/1742-6596/331/3/032049`.

[45] GEANT4 Collaboration, "GEANT4 — a simulation toolkit", *Nucl. Instrum. Meth. A* **506** (2003) 250, `doi:10.1016/S0168-9002(03)01368-8`.

[46] CMS Collaboration, "Electron Reconstruction and Identification at $\sqrt{s} = 7$ TeV", CMS Physics Analysis Summary CMS-PAS-EGM-10-004, (2010).

[47] CMS Collaboration, "Performance of CMS muon reconstruction in pp collision events at $\sqrt{s} = 7$ TeV", *JINST* **7** (2012) P10002, `doi:10.1088/1748-0221/7/10/P10002`, `arXiv:1206.4071`.

[48] CMS Collaboration, "Commissioning of the Particle-Flow Reconstruction in Minimum-Bias and Jet Events from pp Collisions at 7 TeV", CMS Physics Analysis Summary CMS-PAS-PFT-10-002, (2010).

[49] CMS Collaboration, "Performance of tau-lepton reconstruction and identification in CMS", *JINST* **7** (2012) P01001, `doi:10.1088/1748-0221/7/01/P01001`, `arXiv:1109.6034`.

[50] M. Cacciari, G. P. Salam, and G. Soyez, "The anti-k_t jet clustering algorithm", *JHEP* **04** (2008) 063, `doi:10.1088/1126-6708/2008/04/063`, `arXiv:0802.1189`.

[51] M. Cacciari and G. P. Salam, "Dispelling the N^3 myth for the k_t jet-finder", *Phys. Lett. B* **641** (2006) 57, `doi:10.1016/j.physletb.2006.08.037`.

[52] M. Cacciari, G. P. Salam, and G. Soyez, "FastJet User Manual", *Eur. Phys. J. C* **72** (2012) 1896, `doi:10.1140/epjc/s10052-012-1896-2`, `arXiv:1111.6097`.

[53] M. Cacciari and G. P. Salam, "Pileup subtraction using jet areas", *Phys. Lett. B* **659** (2008) 119, `doi:10.1016/j.physletb.2007.09.077`.

[54] CMS Collaboration, "Identification of b-quark jets with the CMS experiment", *JINST* **8** (2013) P04013, `doi:10.1088/1748-0221/8/04/P04013`, `arXiv:1211.4462`.

[55] Y. Bai, H.-C. Cheng, J. Gallicchio, and J. Gu, "Stop the top background of the stop search", *JHEP* **07** (2012) 110, `doi:10.1007/JHEP07(2012)110`, `arXiv:1203.4813`.

[56] C. G. Lester and D. J. Summers, "Measuring masses of semi-invisibly decaying particles pair produced at hadron colliders", *Phys. Lett. B* **463** (1999) 99, `doi:10.1016/S0370-2693(99)00945-4`, `arXiv:hep-ph/9906349`.

[57] A. Barr, C. Lester, and P. Stephens, "A variable for measuring masses at hadron colliders when missing energy is expected; M_{T2}: the truth behind the glamour", *J. Phys. G* **29** (2003) 2343, `doi:10.1088/0954-3899/29/10/304`, `arXiv:hep-ph/0304226`.

[58] M. Burns, K. Kong, K. T. Matchev, and M. Park, "Using subsystem M_{T2} for complete mass determinations in decay chains with missing energy at hadron colliders", *JHEP* **03** (2009) 143, `doi:10.1088/1126-6708/2009/03/143`, `arXiv:0810.5576`.

[59] CMS Collaboration, "Determination of jet energy calibration and transverse momentum resolution in CMS", *JINST* **6** (2011) P11002, `doi:10.1088/1748-0221/6/11/P11002`, `arXiv:1107.4277`.

[60] Particle Data Group, J. Beringer et al., "Review of Particle Physics", *Phys. Rev. D* **86** (2012) 010001, `doi:10.1103/PhysRevD.86.010001`.

[61] H. Voss, A. Höcker, J. Stelzer, and F. Tegenfeldt, "TMVA: Toolkit for Multivariate Data Analysis with ROOT", in *XIth International Workshop on Advanced Computing and Analysis Techniques in Physics Research (ACAT)*, p. 040. 2007. `arXiv:physics/0703039`.

[62] CMS Collaboration, "CMS luminosity based on pixel cluster counting — Summer 2012 update", CMS Physics Analysis Summary CMS-PAS-LUM-12-001, (2012).

[63] A. L. Read, "Presentation of search results: the CL_S technique", *J. Phys. G* **28** (2002) 2693, `doi:10.1088/0954-3899/28/10/313`.

[64] T. Junk, "Confidence level computation for combining searches with small statistics", *Nucl. Instrum. Meth. A* **434** (1999) 435, `doi:10.1016/S0168-9002(99)00498-2`, `arXiv:hep-ex/9902006`.

[65] ATLAS and CMS Collaborations, LHC Higgs Combination Group, "Procedure for the LHC Higgs boson search combination in Summer 2011", Technical Report ATL-PHYS-PUB 2011-11, CMS NOTE 2011/005, (2011).

[66] CMS Collaboration, "CMS Twiki: PhysicsResultsSUS13011", 2013. Temporary link for supplementary material. To be moved to a permanent location.

A Additional tables and figures

A.1 Further information about systematic uncertainties

The systematic uncertainties for the $\widetilde{t} \to t\widetilde{\chi}_1^0$ cut-based, $\widetilde{t} \to b\widetilde{\chi}^+$ BDT, and $\widetilde{t} \to b\widetilde{\chi}^+$ cut-based analyses are shown in Tables 7, 8, and 9, respectively. The corresponding information for $\widetilde{t} \to t\widetilde{\chi}_1^0$ BDT analysis is given in the body of the paper (see Table 2).

Table 7: The bottom row of this table shows the relative uncertainty (in percent) of the total background predictions for the $\widetilde{t} \to t\widetilde{\chi}_1^0$ cut-based signal regions. The breakdown of this total uncertainty in terms of its individual components is also shown.

Sample	$E_T^{miss} > 150\,\text{GeV}$	$E_T^{miss} > 200\,\text{GeV}$	$E_T^{miss} > 250\,\text{GeV}$	$E_T^{miss} > 300\,\text{GeV}$
Low ΔM Selection				
M_T peak data and MC (stat.)	1.4	2.4	4.0	6.3
$t\bar{t} \to \ell\ell$ N_{jets} modeling	1.6	1.5	1.6	1.5
$t\bar{t} \to \ell\ell$ (CR-ℓt and CR-2ℓ tests)	5.2	7.6	13.1	19.6
2nd lepton veto	1.3	1.2	1.3	1.2
$t\bar{t} \to \ell\ell$ (stat.)	1.9	3.2	5.2	8.0
W+jets cross section	1.1	1.1	1.8	2.2
W+jets (stat.)	2.1	3.2	4.1	5.6
W+jets SF uncertainty	9.4	9.0	7.5	7.0
$1 - \ell$ top (stat.)	0.6	0.9	1.1	1.5
$1 - \ell$ top tail-to-peak ratio	16.0	20.7	18.3	18.5
Rare processes cross sections	2.0	2.6	3.8	5.9
Total	19.8	24.6	25.5	30.9
High ΔM Selection				
M_T peak data and MC (stat.)	3.9	4.8	6.0	8.5
$t\bar{t} \to \ell\ell$ N_{jets} modeling	0.8	0.9	1.0	0.9
$t\bar{t} \to \ell\ell$ (CR-ℓt and CR-2ℓ tests)	4.1	6.1	11.7	14.9
2nd lepton veto	0.7	0.7	0.8	0.7
$t\bar{t} \to \ell\ell$ (stat.)	4.2	5.9	8.4	10.2
W+jets cross section	0.6	0.5	1.3	1.8
W+jets (stat.)	3.8	4.7	5.7	7.7
W+jets SF uncertainty	11.7	10.3	8.8	8.8
$1 - \ell$ top (stat.)	1.8	1.9	2.1	3.4
$1 - \ell$ top tail-to-peak ratio	17.1	21.3	20.9	17.3
Rare processes cross sections	6.1	6.9	7.8	9.2
Total	23.1	27.0	29.3	30.6

Table 8: The bottom row of this table shows the relative uncertainty (in percent) of the total background predictions for the $\widetilde{t} \rightarrow b\widetilde{\chi}^+$ BDT signal regions. The breakdown of this total uncertainty in terms of its individual components is also shown.

$\widetilde{t} \rightarrow b\widetilde{\chi}^+ \; x = 0.75$

Sample	BDT1	BDT2	BDT3	BDT4
M_T peak data and MC (stat.)	3.5	5.3	7.8	1.2
$t\bar{t} \rightarrow \ell\ell \; N_{jets}$ modeling	1.8	1.2	1.1	1.6
$t\bar{t} \rightarrow \ell\ell$ (CR-ℓt and CR-2ℓ tests)	6.0	8.2	11.3	3.6
2nd lepton veto	1.7	1.1	1.0	1.4
$t\bar{t} \rightarrow \ell\ell$ (stat.)	4.3	5.9	9.6	1.4
W+jets cross section	2.7	2.3	2.7	1.4
W+jets (stat.)	4.5	5.3	6.4	2.4
W+jets SF uncertainty	6.9	7.7	7.0	9.9
$1 - \ell$ top (stat.)	1.2	1.2	1.2	0.6
$1 - \ell$ top tail-to-peak ratio	11.3	19.5	17.6	10.7
Rare processes cross sections	1.9	6.2	8.9	1.1
Total	16.8	25.4	27.8	15.5

$\widetilde{t} \rightarrow b\widetilde{\chi}^+ \; x = 0.5$

Sample	BDT1	BDT2–Loose	BDT2–Tight	BDT3	BDT4
M_T peak data and MC (stat.)	3.0	3.3	6.0	5.8	2.4
$t\bar{t} \rightarrow \ell\ell \; N_{jets}$ modeling	1.6	1.3	1.0	1.1	2.1
$t\bar{t} \rightarrow \ell\ell$ (CR-ℓt and CR-2ℓ tests)	5.2	6.4	17.2	11.1	10.3
2nd lepton veto	1.4	1.2	1.0	1.0	1.9
$t\bar{t} \rightarrow \ell\ell$ (stat.)	3.5	4.0	6.6	6.2	2.8
W+jets cross section	2.5	2.6	1.4	3.3	2.8
W+jets (stat.)	2.3	2.2	4.1	3.4	2.3
W+jets SF uncertainty	8.0	8.0	8.1	7.3	5.7
$1 - \ell$ top (stat.)	1.0	1.2	1.5	1.6	0.8
$1 - \ell$ top tail-to-peak ratio	10.3	11.5	18.4	11.7	5.6
Rare processes cross sections	3.3	6.8	8.7	9.4	1.3
Total	15.7	18.0	29.7	22.3	14.4

$\widetilde{t} \rightarrow b\widetilde{\chi}^+ \; x = 0.25$

Sample	BDT1	BDT2	BDT3
M_T peak data and MC (stat.)	4.0	9.0	10.6
$t\bar{t} \rightarrow \ell\ell \; N_{jets}$ modeling	1.5	0.7	0.8
$t\bar{t} \rightarrow \ell\ell$ (CR-ℓt and CR-2ℓ tests)	7.7	11.4	19.1
2nd lepton veto	1.4	0.6	0.8
$t\bar{t} \rightarrow \ell\ell$ (stat.)	5.0	6.5	11.8
W+jets cross section	3.0	1.0	1.5
W+jets (stat.)	2.4	5.3	6.7
W+jets SF uncertainty	7.2	11.3	9.5
$1 - \ell$ top (stat.)	1.3	3.2	4.2
$1 - \ell$ top tail-to-peak ratio	10.8	12.6	13.2
Rare processes cross sections	4.5	6.2	9.6
Total	17.7	24.9	32.3

Table 9: The bottom row of this table shows the relative uncertainty (in percent) of the total background predictions for the $\widetilde{t} \to b\widetilde{\chi}^+$ cut-based signal regions. The breakdown of this total uncertainty in terms of its individual components is also shown.

Sample	$E_T^{miss} > 100\,GeV$	$E_T^{miss} > 150\,GeV$	$E_T^{miss} > 200\,GeV$	$E_T^{miss} > 250\,GeV$
Low ΔM Selection				
M_T peak data and MC (stat.)	0.7	1.3	2.2	3.5
$t\bar{t} \to \ell\ell$ N$_{jets}$ modeling	1.6	1.9	1.9	1.9
$t\bar{t} \to \ell\ell$ (CR-ℓt and CR-2ℓ tests)	2.6	3.2	6.4	12.4
2nd lepton veto	1.3	1.5	1.5	1.5
$t\bar{t} \to \ell\ell$ (stat.)	0.7	1.4	2.4	3.9
W+jets cross section	1.5	2.0	2.5	3.2
W+jets (stat.)	0.8	1.1	1.6	2.2
W+jets SF uncertainty	9.9	6.8	5.7	5.4
$1 - \ell$ top (stat.)	0.3	0.4	0.5	0.7
$1 - \ell$ top tail-to-peak ratio	5.9	11.0	11.7	12.1
Rare processes cross sections	1.1	1.7	2.6	3.7
Total	12.2	14.0	15.6	19.7
High ΔM Selection				
M_T peak data and MC (stat.)	2.9	3.3	4.3	5.5
$t\bar{t} \to \ell\ell$ N$_{jets}$ modeling	1.0	0.9	1.1	0.9
$t\bar{t} \to \ell\ell$ (CR-ℓt and CR-2ℓ tests)	4.8	6.3	10.6	13.4
2nd lepton veto	0.9	0.8	0.9	0.8
$t\bar{t} \to \ell\ell$ (stat.)	2.6	3.9	5.6	7.1
W+jets cross section	2.3	1.5	1.6	1.5
W+jets (stat.)	1.8	2.5	3.2	4.3
W+jets SF uncertainty	11.5	10.2	8.4	8.3
$1 - \ell$ top (stat.)	1.3	1.5	1.5	1.6
$1 - \ell$ top tail-to-peak ratio	5.2	12.5	15.3	16.6
Rare processes cross sections	4.1	7.0	8.7	10.2
Total	15.0	19.7	23.7	27.1

A.2   Additional M_T and BDT output distributions

In this section, M_T and BDT-output distributions in addition to those shown in Figs. 8 and 9 are presented for the $\widetilde{\mathrm{t}} \to \mathrm{t}\widetilde{\chi}_1^0$ (Figs. 13–14) and $\widetilde{\mathrm{t}} \to \mathrm{b}\widetilde{\chi}^+$ (Figs. 15–19) BDT signal regions.
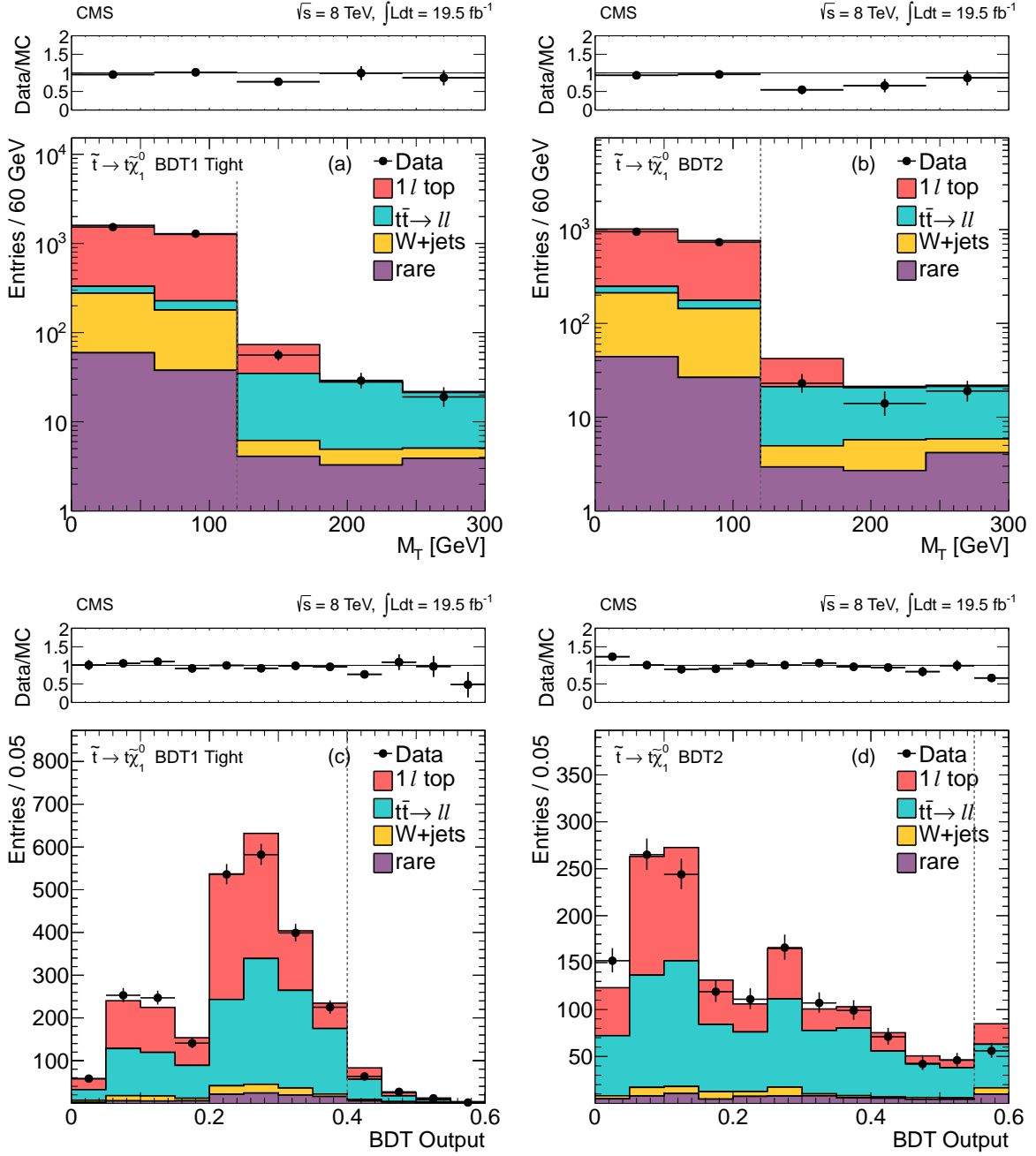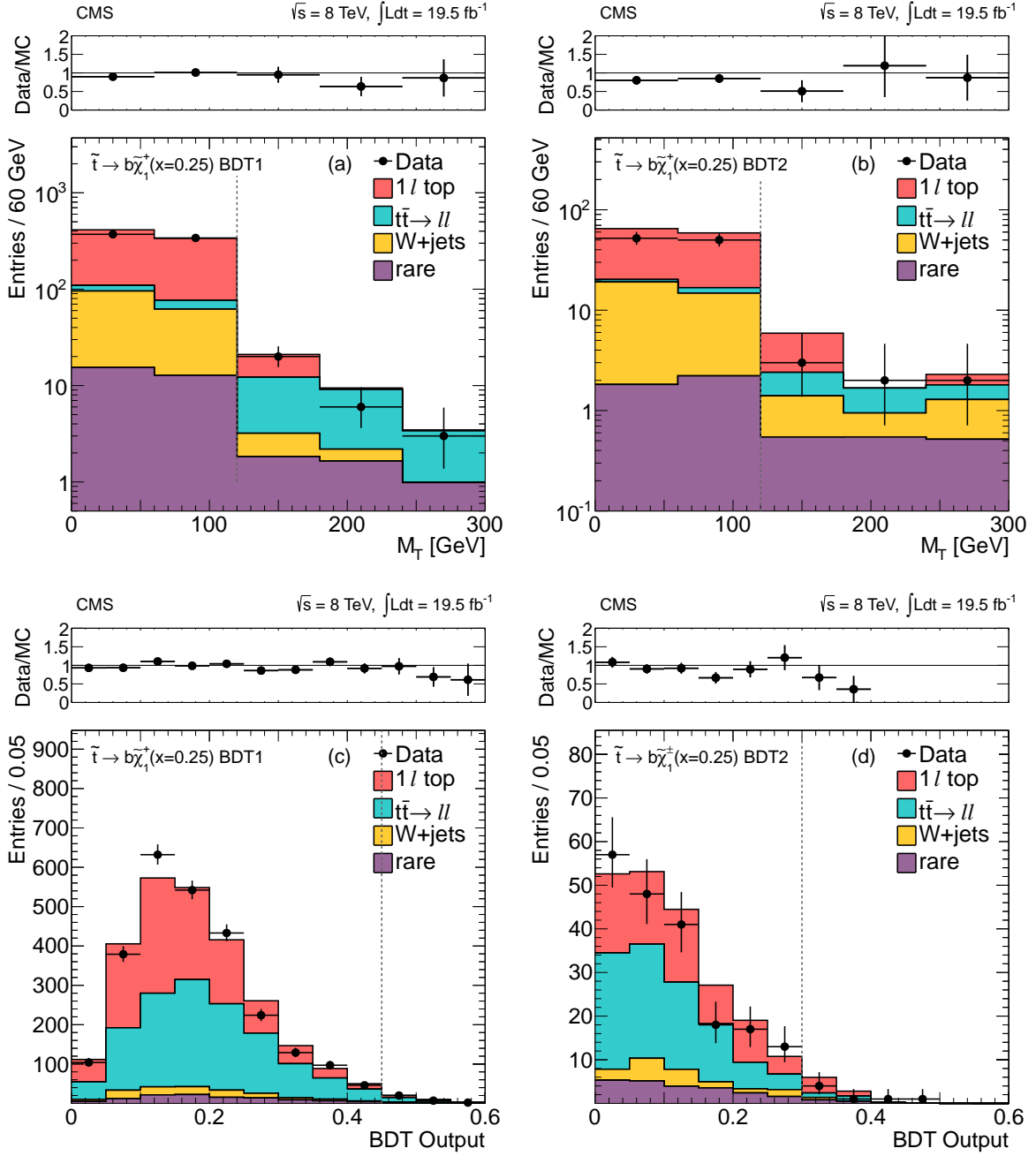
Figure 13: Comparison of data and MC simulation for the distributions of BDT output and M_T corresponding to the $\tilde{t} \to t\tilde{\chi}_1^0$ scenario in training regions 1 and 2. The M_T distributions are shown after the requirement on the BDT output, and the BDT output distributions are shown after the $M_T > 120 \, \text{GeV}$ requirement (these requirements are also indicated by vertical dashed lines on the respective distributions). (a) M_T after the tight cut on the BDT1 output; (b) M_T after the cut on the BDT2 output; (c) BDT1 output after the M_T cut; (d) BDT2 output after the M_T cut. In all distributions the last bin contains the overflow.
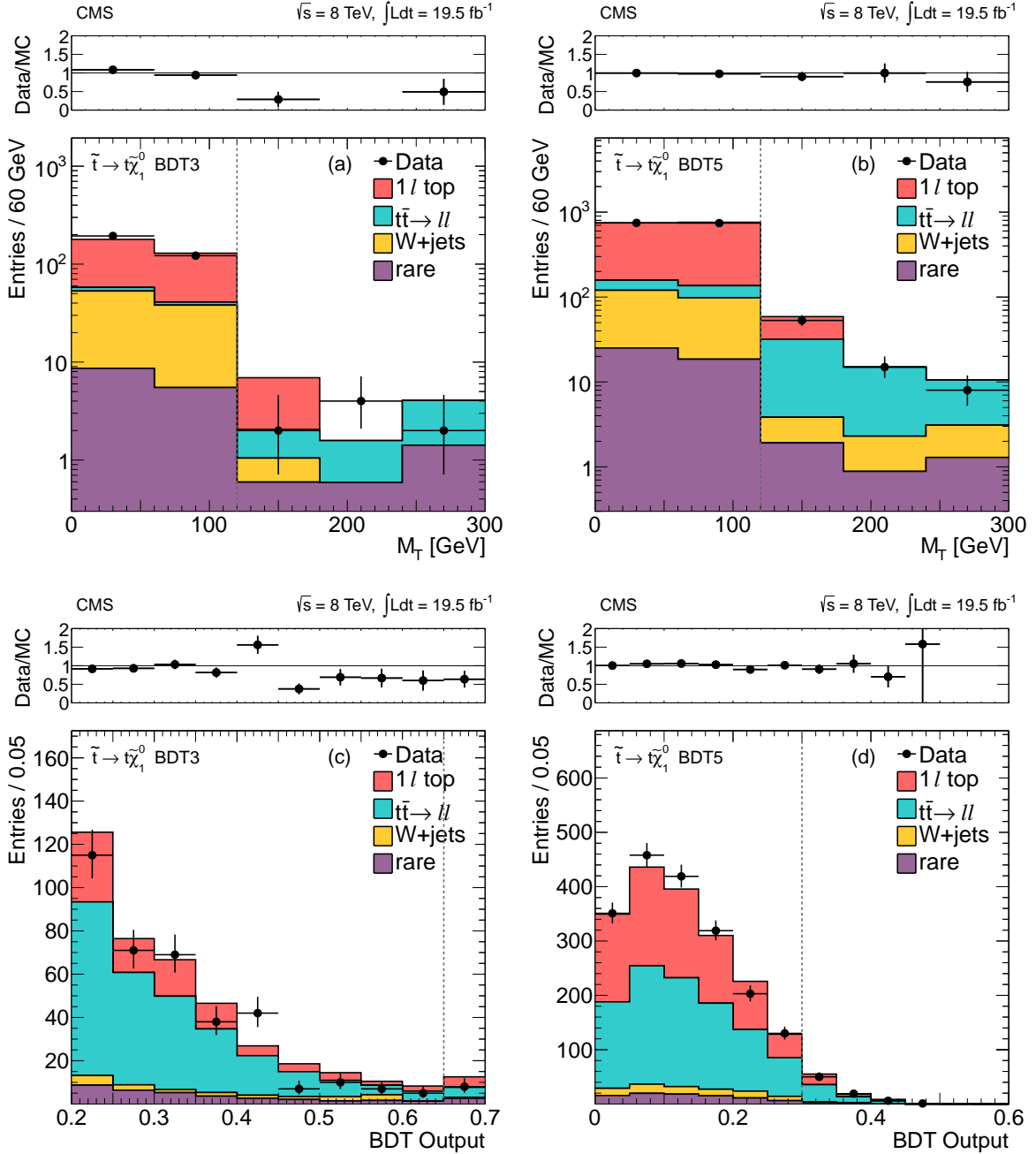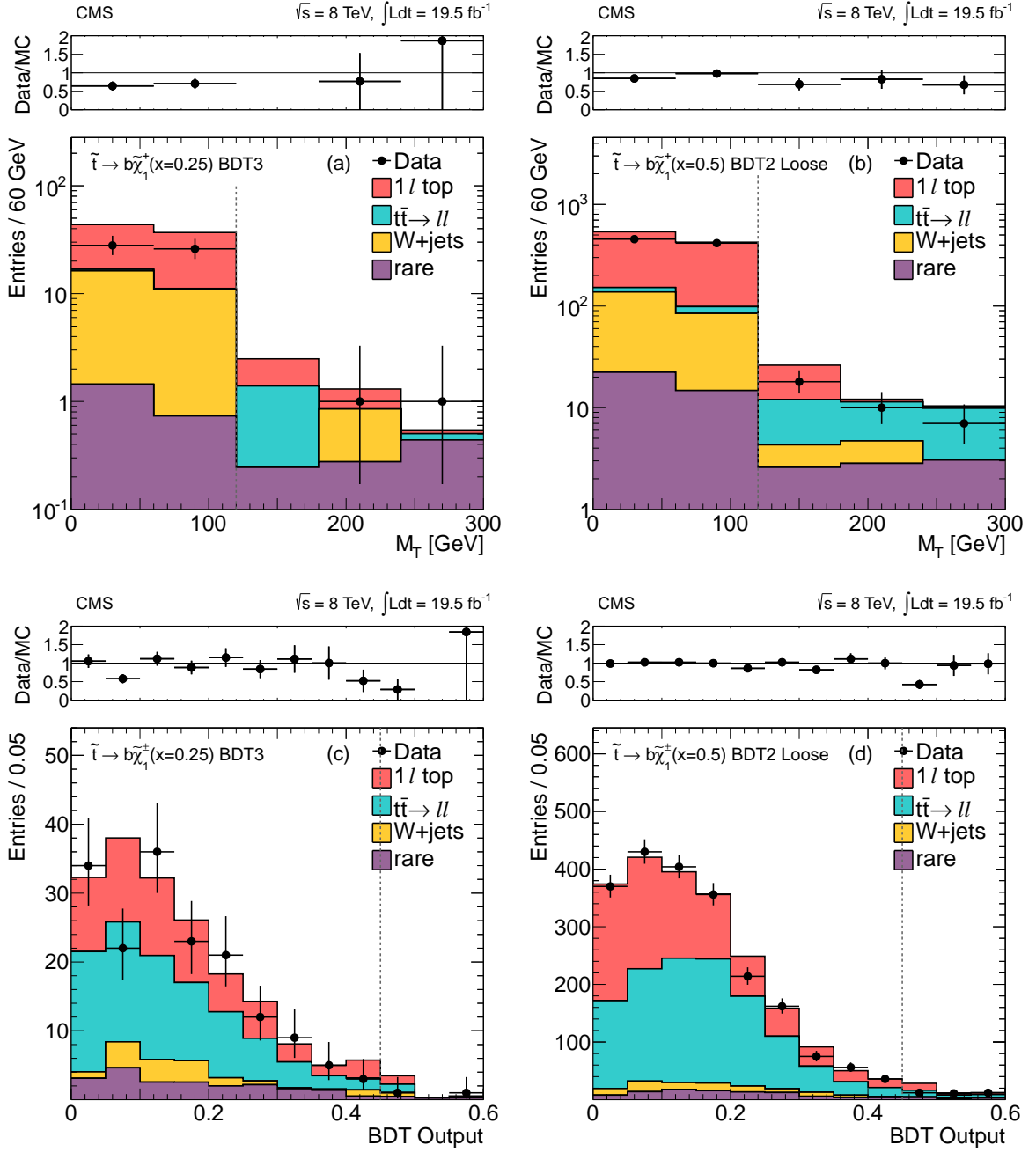
Figure 14: Comparison of data and MC simulation for the distributions of BDT output and M_T corresponding to the $\tilde{t} \to t\tilde{\chi}_1^0$ scenario in training regions 3 and 5. The M_T distributions are shown after the requirement on the BDT output, and the BDT output distributions are shown after the $M_\mathrm{T} > 120\,\mathrm{GeV}$ requirement (these requirements are also indicated by vertical dashed lines on the respective distributions). (a) M_T after the cut on the BDT3 output; (b) M_T after the cut on the BDT5 output; (c) BDT3 output after the M_T cut; (d) BDT5 output after the M_T cut. In all distributions the last bin contains the overflow.
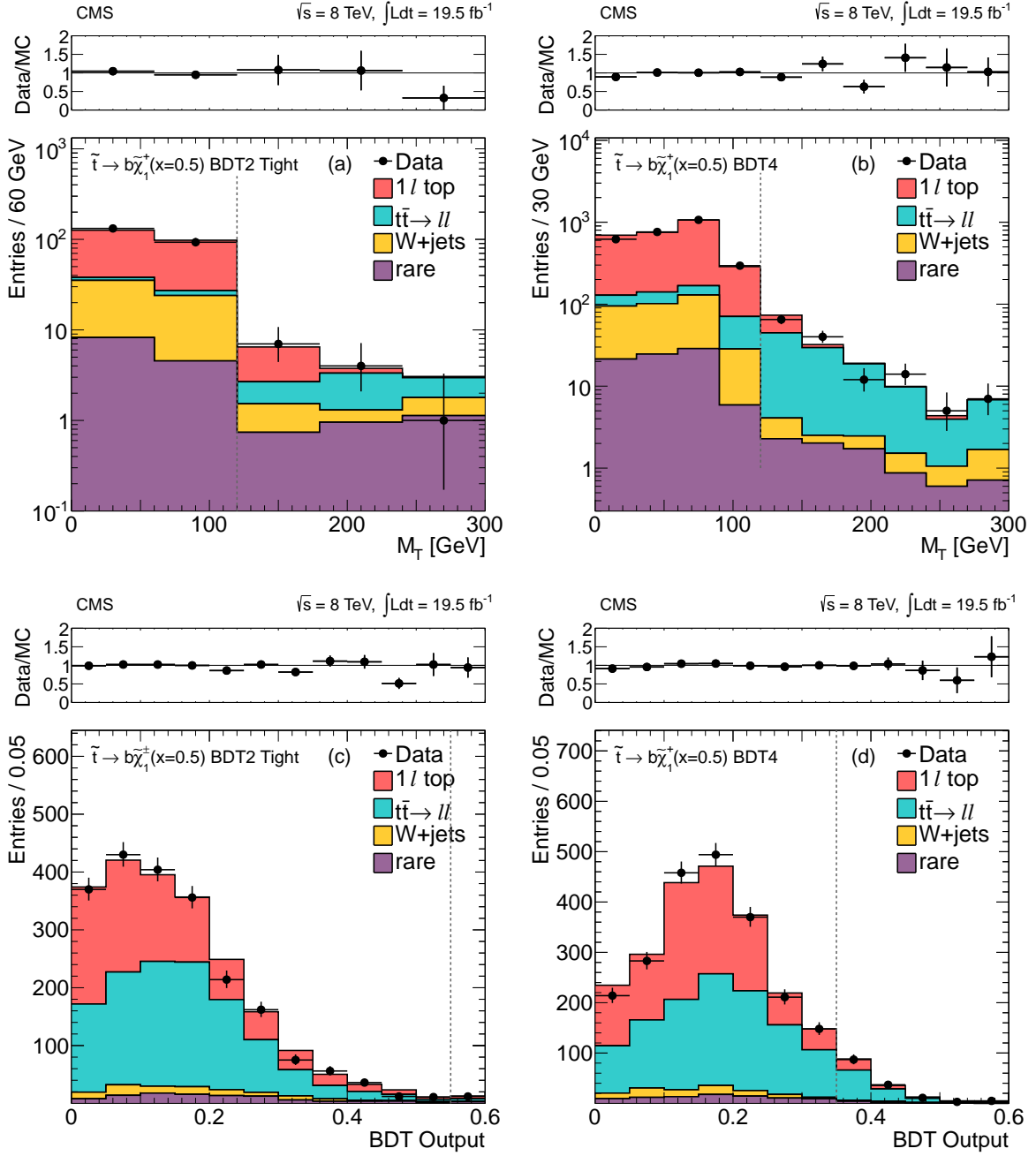
Figure 15: Comparison of data and MC simulation for the distributions of BDT output and M_T corresponding to the $x = 0.25$ $\tilde{t} \to b\tilde{\chi}^+$ scenario in training regions 1 and 2. The M_T distributions are shown after the requirement on the BDT output, and the BDT output distributions are shown after the $M_T > 120$ GeV requirement (these requirements are also indicated by vertical dashed lines on the respective distributions). (a) M_T after the cut on the BDT1 output; (b) M_T after the cut on the BDT2 output; (c) BDT1 output after the M_T cut; (d) BDT2 output after the M_T cut. In all distributions the last bin contains the overflow.
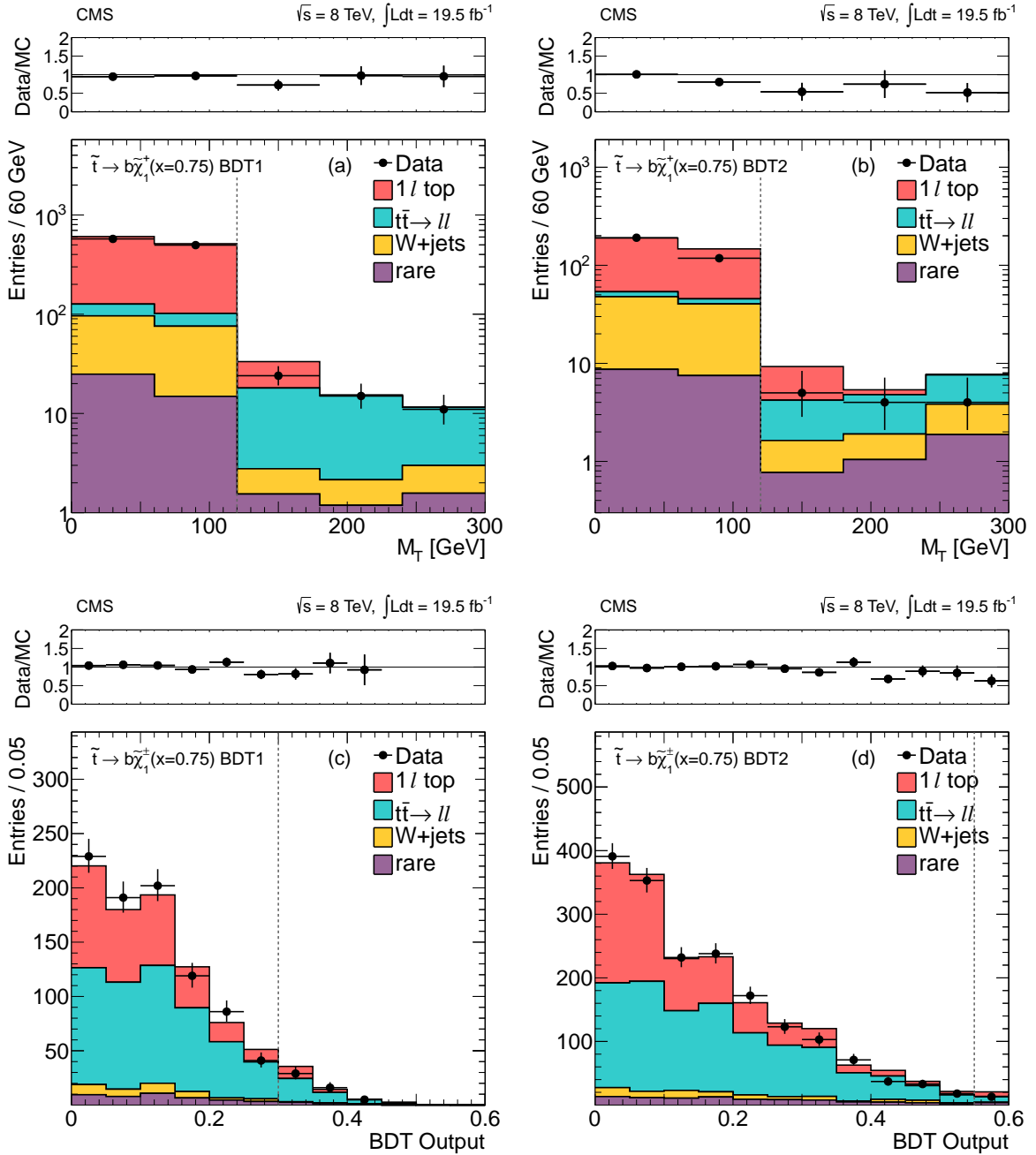
Figure 16: Comparison of data and MC simulation for the distributions of BDT output and M_T corresponding to the $\widetilde{t} \rightarrow b\widetilde{\chi}^+$ scenario in training regions 3 (for $x = 0.25$) and 2 (for $x = 0.5$). The M_T distributions are shown after the requirement on the BDT output, and the BDT output distributions are shown after the $M_T > 120\,\text{GeV}$ requirement (these requirements are also indicated by vertical dashed lines on the respective distributions). (a) M_T after the cut on the BDT3 ($x = 0.25$) output; (b) M_T after the loose cut on the BDT2 ($x = 0.5$) output; (c) BDT3 ($x = 0.25$) output after the M_T cut; (d) BDT2 ($x = 0.5$) output after the M_T cut. In all distributions the last bin contains the overflow.

Figure 17: Comparison of data and MC simulation for the distributions of BDT output and M_T corresponding to the $x = 0.5\,\tilde{t} \to b\tilde{\chi}^+$ scenario in training regions 2 and 4. The M_T distributions are shown after the requirement on the BDT output, and the BDT output distributions are shown after the $M_T > 120\,\mathrm{GeV}$ requirement (these requirements are also indicated by vertical dashed lines on the respective distributions). (a) M_T after the tight cut on the BDT2 output; (b) M_T after the cut on the BDT4 output; (c) BDT2 output after the M_T cut; (d) BDT4 output after the M_T cut. In all distributions the last bin contains the overflow.
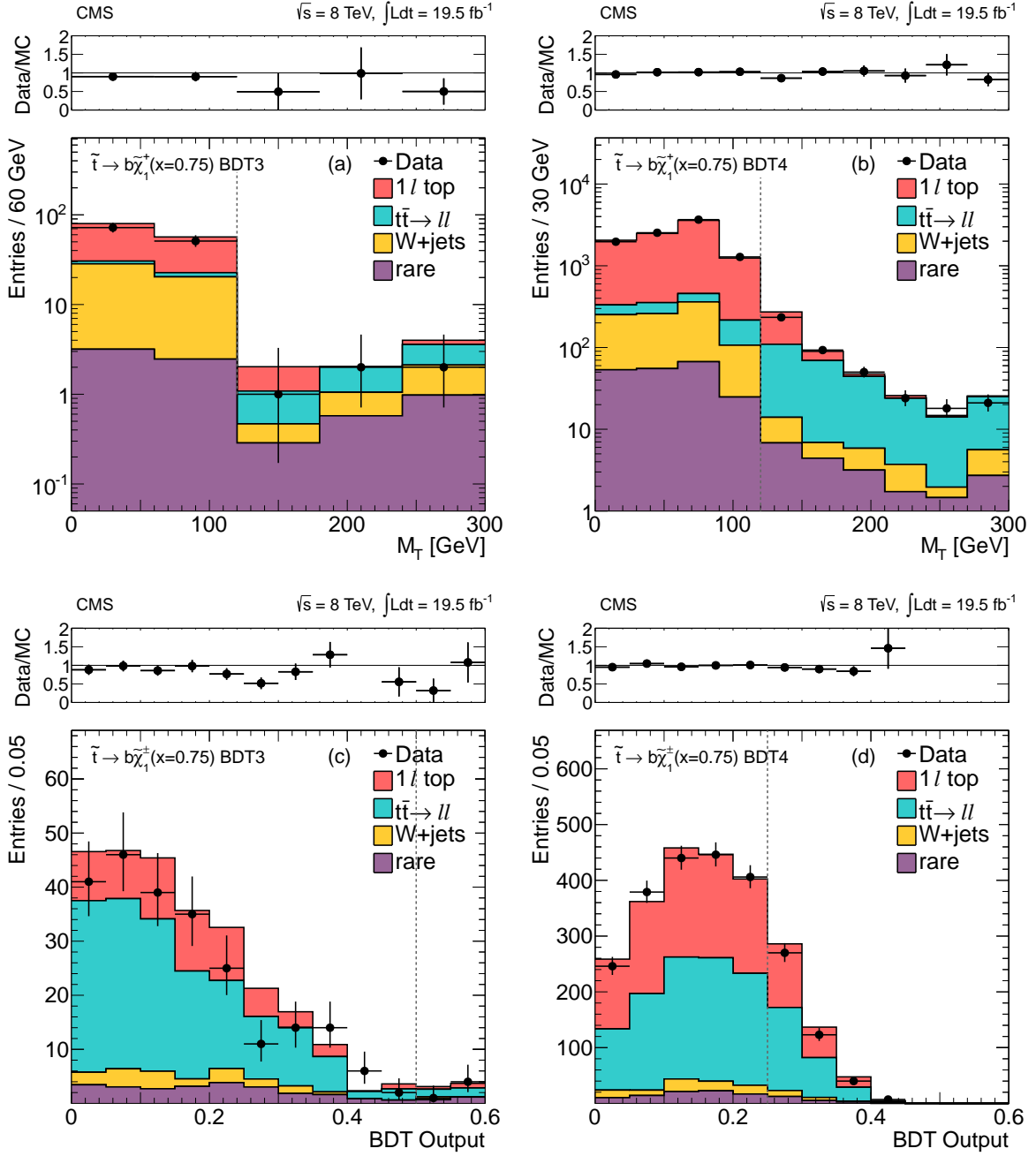
Figure 18: Comparison of data and MC simulation for the distributions of BDT output and M_T corresponding to the $x = 0.75\ \tilde{t} \to b\tilde{\chi}^+$ scenario in training regions 1 and 2. The M_T distributions are shown after the requirement on the BDT output, and the BDT output distributions are shown after the $M_T > 120\,\text{GeV}$ requirement (these requirements are also indicated by vertical dashed lines on the respective distributions). (a) M_T after the cut on the BDT1 output; (b) M_T after the cut on the BDT2 output; (c) BDT1 output after the M_T cut; (d) BDT2 output after the M_T cut. In all distributions the last bin contains the overflow.

Figure 19: Comparison of data and MC simulation for the distributions of BDT output and M_T corresponding to the $x = 0.75$ $\tilde{t} \to b\tilde{\chi}^+$ scenario in training regions 3 and 4. The M_T distributions are shown after the requirement on the BDT output, and the BDT output distributions are shown after the $M_T > 120 \, \text{GeV}$ requirement (these requirements are also indicated by vertical dashed lines on the respective distributions). (a) M_T after the cut on the BDT3 output; (b) M_T after the cut on the BDT4 output; (c) BDT3 output after the M_T cut; (d) BDT4 output after the M_T cut. In all distributions the last bin contains the overflow.

A.3 Further information about model interpretations

The interpretations for the $\tilde{t} \to t\tilde{\chi}_1^0$ and $\tilde{t} \to b\tilde{\chi}^+$ scenarios, using the cut-based analysis, are presented in Fig. 20. Maps of the most sensitive signal regions for the cut-based and BDT searches are shown in Figs. 21 and 22. The variations in the $\tilde{t} \to b\tilde{\chi}^+$ $x = 0.25$ and 0.75 limits due to assumptions about particle polarizations are presented in Fig. 23.
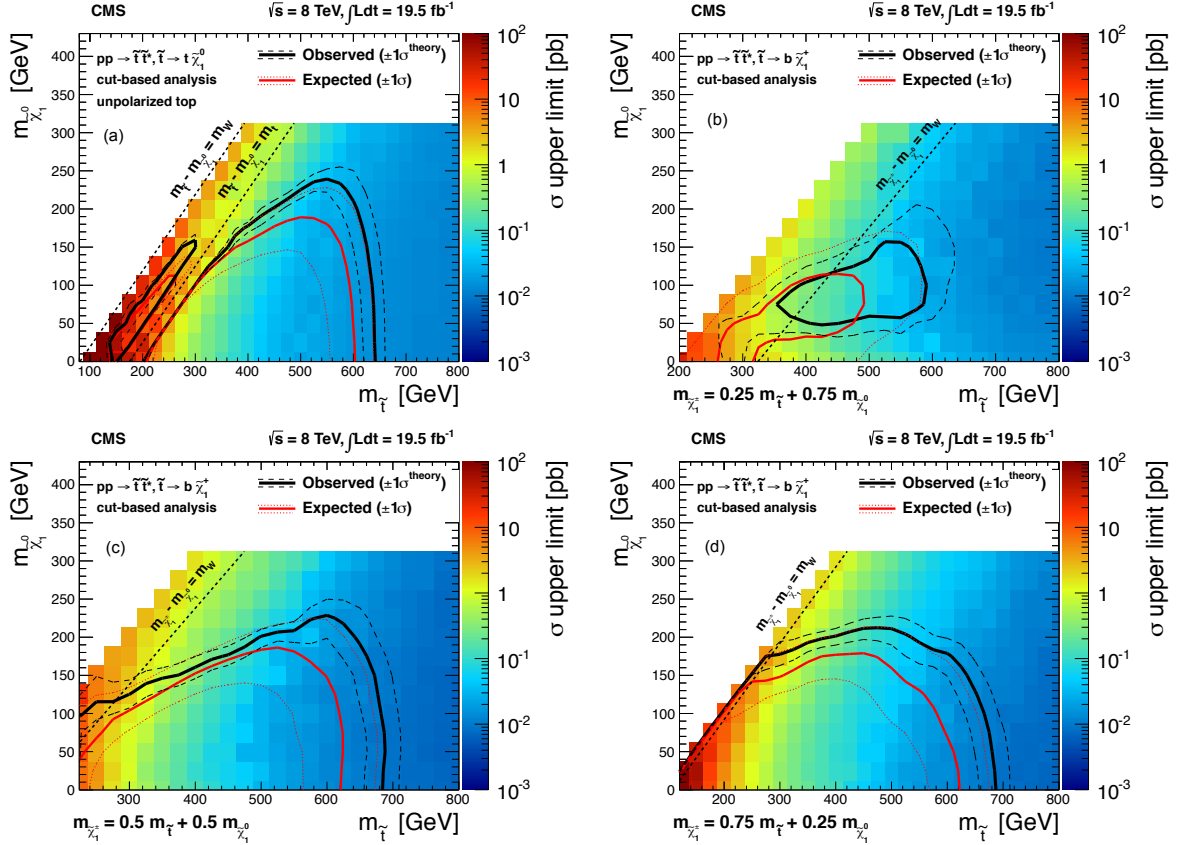

Figure 20: Interpretations based on the results of the cut-based analysis. (a) $\tilde{t} \to t\tilde{\chi}_1^0$ model; (b) $\tilde{t} \to b\tilde{\chi}^+$ model with $x = 0.25$; (c) $\tilde{t} \to b\tilde{\chi}^+$ model with $x = 0.50$; (d) $\tilde{t} \to b\tilde{\chi}^+$ model with $x = 0.75$; The color scale indicates the observed cross section upper limit. The observed (solid black), median expected (solid red), and $\pm 1\sigma$ expected (dotted red) 95% CL exclusion contours are indicated. The variations in the excluded region due to $\pm 1\sigma$ uncertainty of the theoretical prediction of the cross section for top-squark pair production are also indicated.

B Monte Carlo modeling of initial-state radiation

The experimental acceptance for signal events depends on initial-state radiation (ISR). As the simulation is not necessarily expected to model ISR well, we validate the simulation by comparing MADGRAPH MC predictions with data. The predicted p_T spectrum of the system recoiling against the ISR jets is compared with data in Z + jets, $t\bar{t}$, and WZ final states. These processes can be measured with good statistical precision in data and cover a variety of masses and initial states.

Z + jets events are selected by requiring exactly two opposite-sign, same-flavor leptons (ee or $\mu\mu$) with an invariant mass between 81 and 101 GeV. These events, as well as the $t\bar{t}$ and WZ samples discussed below, are collected with dilepton triggers. Events with at least one
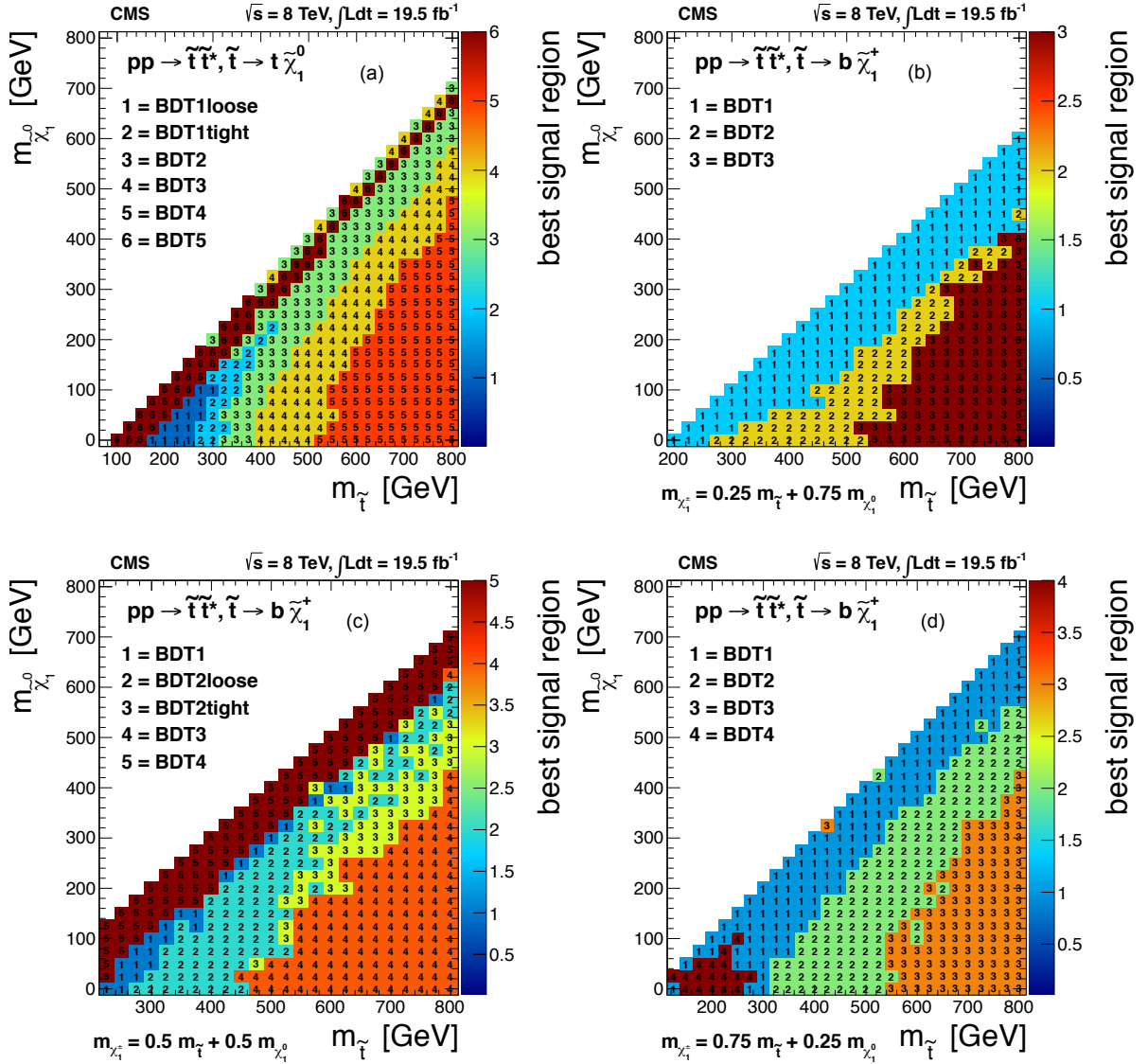
Figure 21: The most sensitive signal region in the $m_{\widetilde{\chi}_1^0}$ vs. $m_{\widetilde{t}}$ parameter space in the BDT analysis, for the (a) $\widetilde{t} \to t\widetilde{\chi}_1^0$ model, and the $\widetilde{t} \to b\widetilde{\chi}^+$ model with chargino mass parameter (b) $x = 0.25$, (c) 0.5, and (d) 0.75. The number indicates the BDT training region.
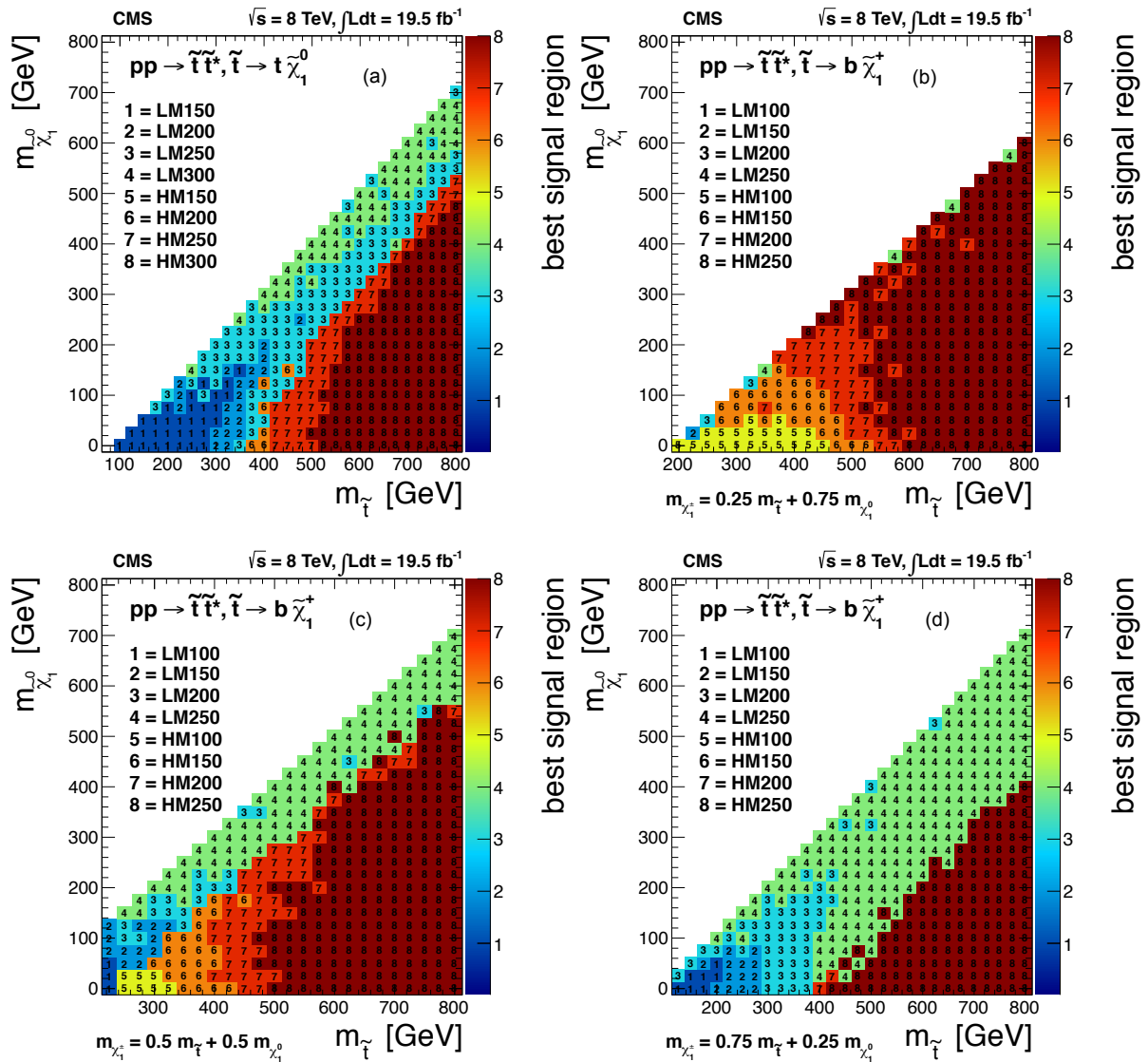
Figure 22: The most sensitive signal region in the $m_{\widetilde{\chi}_1^0}$ vs. $m_{\widetilde{t}}$ parameter space in the cut-based analysis, for the (a) $\widetilde{t} \to t\widetilde{\chi}_1^0$ model, and the $\widetilde{t} \to b\widetilde{\chi}^+$ model with chargino mass parameter (b) $x = 0.25$, (c) 0.5, and (d) 0.75. LM and HM refer to low ΔM and high ΔM, respectively, and the number indicates the E_T^{miss} requirement.
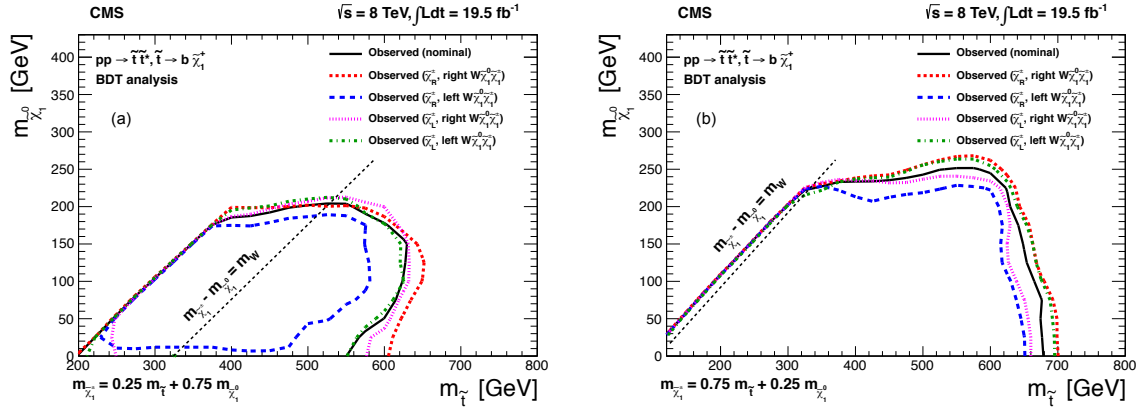
Figure 23: The observed 95% CL excluded regions for the $\tilde{t} \to b\tilde{\chi}^+$ model with (a) $x = 0.25$ and (b) 0.75 for the nominal scenario, right- vs. left-handed charginos ($\tilde{\chi}_R^\pm$ and $\tilde{\chi}_R^\pm$, respectively), and right- vs. left-handed $W\tilde{\chi}_1^0$ $\tilde{\chi}_1^\pm$ couplings.

b-tagged jet or with additional lepton candidates are vetoed to remove contributions from $t\bar{t}$ and diboson (WZ/ZZ) production, respectively. In Z + jets events, the Z boson is expected to be balanced in transverse momentum with the ISR jet system. The p_T of the Z boson is thus computed in two ways: as the p_T of the dilepton system, and, for events with at least one reconstructed jet, as the p_T of the vector sum of the reconstructed jets, termed the "jet system" p_T. The predicted MC spectrum for each quantity is compared with data, as shown in Fig. 24. The MC prediction is normalized to the total data yield so that the shapes can be readily compared. This procedure changes the normalization of the simulation by 4%, consient with the luminosty uncertainty. Agreement is observed at lower p_T, while at higher p_T the MC predictions lie above the data. The predictions from simulation exceed the data by about 10% for $p_T = 150\,\text{GeV}$ and 20% for $p_T = 250\,\text{GeV}$. Both quantities show the same trend, validating the jet recoil method of measuring this quantity. The dilepton p_T and jet system p_T are also checked for events with exactly one, two, or three jets, as well as at least four jets, and in each case the results are consistent with the inclusive results shown in Fig. 24. The impact of the jet energy scale uncertainty, which only affects the jet system p_T, is found to be much smaller than the observed discrepancies.

Dilepton $t\bar{t}$ events are selected by requiring an opposite-sign eμ pair and exactly two b-tagged jets. Events containing a third lepton candidate are vetoed. These requirements select dilepton $t\bar{t}$ events with high purity (about 97% in simulation) and unambiguously identify all the visible $t\bar{t}$ decay products. Because of the presence of neutrinos in the $t\bar{t}$ decays, the p_T of the $t\bar{t}$ cannot be directly measured but can be inferred from the ISR jet recoil system. Additional jets beyond the two b-tagged jets in these events are thus considered to be ISR jets for the purposes of this study, and the "jet system" is formed by the vector sum of ISR jets. The p_T of the jet system defined this way is found in simulation to accurately reproduce the p_T of the generated $t\bar{t}$ system. The predicted jet system p_T spectrum is compared with data in Fig. 25. Agreement is found at lower p_T. At higher p_T, the simulation is consistent with the data to within the uncertainties, but it also exhibits a trend to overpredict the data, as in the case of Z + jets events. The jet system p_T is also checked for events with exactly one, two, or three jets, as well as at least four jets, and in each case the results are consistent with the inclusive results shown in Fig. 25. Again, the effect of the jet energy scale uncertainty is examined and found to be small.

Finally, $WZ \to \ell\nu\ell\ell$ events are selected by requiring exactly three leptons, with two opposite-sign same-flavor leptons (ee or $\mu\mu$) consistent with the Z boson mass and a third lepton (e

or μ) with $M_T > 50\,\mathrm{GeV}$. Events with at least one b-tagged jet are vetoed. The expected purity of this selection from simulation is about 83%, with about 7% of events coming from ZZ production. As with $t\bar{t}$ events, the neutrino in the final state prevents a direct measurement of the WZ system p_T, but the jet recoil system can be used and is defined in the same way as for the $Z + \text{jets}$ sample. In data, this selection yields on the order of 1000 events, so the statistical uncertainty at high values of jet system p_T is large. As for the $t\bar{t}$ MC simulated events, the WZ simulation is found to be consistent with the data to within the uncertainties, but also shows a trend to overpredict the data at large p_T that is consistent with the level observed for the $Z + \text{jets}$ events.

Given the MC overprediction observed in the high-statistics $Z + \text{jets}$ events, and the consistency of the other final states with this result, weights are derived to correct the MC prediction as a function of the p_T of the system recoiling against ISR jets. These weights are applied to the MADGRAPH signal samples used in this analysis, and the full values of the corrections are taken as a systematic uncertainty. The values of the weights range from 0–20% depending on the p_T of the system recoiling against ISR jets. The shaded bands shown on the ratio plots in Figs. 24–25 are centered on the weighted MC prediction, with the width of the band showing the associated uncertainty.
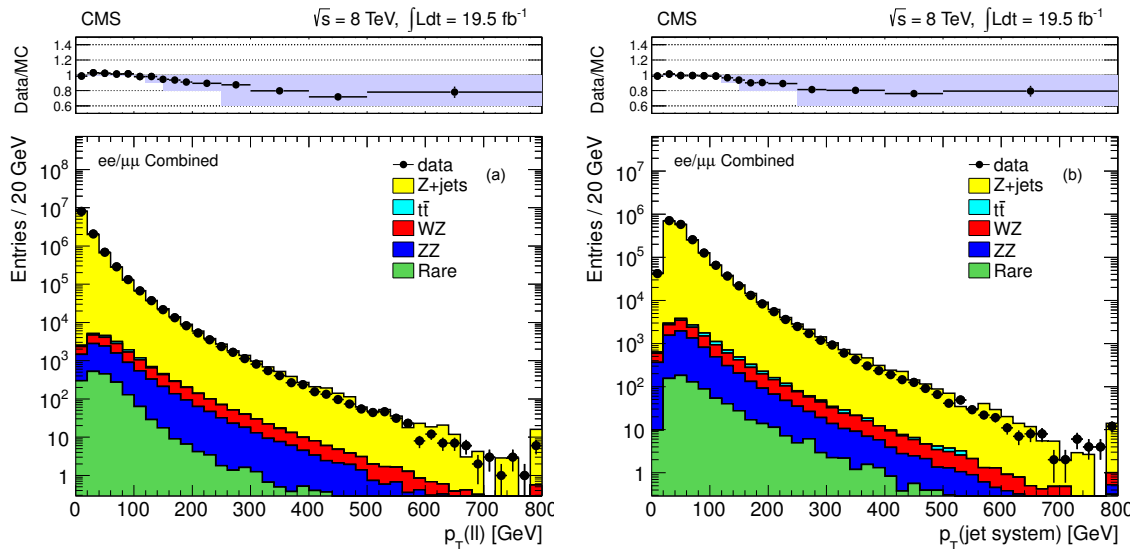

Figure 24: Comparison of data to MC predictions for the (a) dilepton p_T and (b) jet recoil system p_T in $Z + \text{jets}$ events. The MC prediction is normalized to the total data yield. The data/MC ratio is also shown. The shaded band is centered on the weight values. The width of the band indicates the associated systematic uncertainty. In both distributions the last bin contains the overflow.
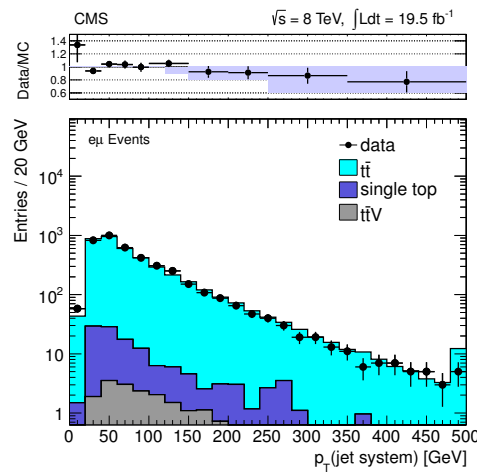
Figure 25: Comparison of data to MC prediction for the jet recoil system p_T in $t\bar{t}$ events. The MC prediction is normalized to the total data yield. The ratio of data/MC is also shown. The shaded band shows the weights derived for MC simulation and the variation to assess systematic uncertainties. The last bin contains the overflow.

C   The CMS Collaboration

Yerevan Physics Institute, Yerevan, Armenia
S. Chatrchyan, V. Khachatryan, A.M. Sirunyan, A. Tumasyan

Institut für Hochenergiephysik der OeAW, Wien, Austria
W. Adam, T. Bergauer, M. Dragicevic, J. Erö, C. Fabjan[1], M. Friedl, R. Frühwirth[1], V.M. Ghete, N. Hörmann, J. Hrubec, M. Jeitler[1], W. Kiesenhofer, V. Knünz, M. Krammer[1], I. Krätschmer, D. Liko, I. Mikulec, D. Rabady[2], B. Rahbaran, C. Rohringer, H. Rohringer, R. Schöfbeck, J. Strauss, A. Taurok, W. Treberer-Treberspurg, W. Waltenberger, C.-E. Wulz[1]

National Centre for Particle and High Energy Physics, Minsk, Belarus
V. Mossolov, N. Shumeiko, J. Suarez Gonzalez

Universiteit Antwerpen, Antwerpen, Belgium
S. Alderweireldt, M. Bansal, S. Bansal, T. Cornelis, E.A. De Wolf, X. Janssen, A. Knutsson, S. Luyckx, L. Mucibello, S. Ochesanu, B. Roland, R. Rougny, Z. Staykova, H. Van Haevermaet, P. Van Mechelen, N. Van Remortel, A. Van Spilbeeck

Vrije Universiteit Brussel, Brussel, Belgium
F. Blekman, S. Blyweert, J. D'Hondt, A. Kalogeropoulos, J. Keaveney, S. Lowette, M. Maes, A. Olbrechts, S. Tavernier, W. Van Doninck, P. Van Mulders, G.P. Van Onsem, I. Villella

Université Libre de Bruxelles, Bruxelles, Belgium
C. Caillol, B. Clerbaux, G. De Lentdecker, L. Favart, A.P.R. Gay, T. Hreus, A. Léonard, P.E. Marage, A. Mohammadi, L. Perniè, T. Reis, T. Seva, L. Thomas, C. Vander Velde, P. Vanlaer, J. Wang

Ghent University, Ghent, Belgium
V. Adler, K. Beernaert, L. Benucci, A. Cimmino, S. Costantini, S. Dildick, G. Garcia, B. Klein, J. Lellouch, A. Marinov, J. Mccartin, A.A. Ocampo Rios, D. Ryckbosch, M. Sigamani, N. Strobbe, F. Thyssen, M. Tytgat, S. Walsh, E. Yazgan, N. Zaganidis

Université Catholique de Louvain, Louvain-la-Neuve, Belgium
S. Basegmez, C. Beluffi[3], G. Bruno, R. Castello, A. Caudron, L. Ceard, G.G. Da Silveira, C. Delaere, T. du Pree, D. Favart, L. Forthomme, A. Giammanco[4], J. Hollar, P. Jez, V. Lemaitre, J. Liao, O. Militaru, C. Nuttens, D. Pagano, A. Pin, K. Piotrzkowski, A. Popov[5], M. Selvaggi, M. Vidal Marono, J.M. Vizan Garcia

Université de Mons, Mons, Belgium
N. Beliy, T. Caebergs, E. Daubie, G.H. Hammad

Centro Brasileiro de Pesquisas Fisicas, Rio de Janeiro, Brazil
G.A. Alves, M. Correa Martins Junior, T. Martins, M.E. Pol, M.H.G. Souza

Universidade do Estado do Rio de Janeiro, Rio de Janeiro, Brazil
W.L. Aldá Júnior, W. Carvalho, J. Chinellato[6], A. Custódio, E.M. Da Costa, D. De Jesus Damiao, C. De Oliveira Martins, S. Fonseca De Souza, H. Malbouisson, M. Malek, D. Matos Figueiredo, L. Mundim, H. Nogima, W.L. Prado Da Silva, A. Santoro, A. Sznajder, E.J. Tonelli Manganote[6], A. Vilela Pereira

Universidade Estadual Paulista [a], Universidade Federal do ABC [b], São Paulo, Brazil
C.A. Bernardes[b], F.A. Dias[a,7], T.R. Fernandez Perez Tomei[a], E.M. Gregores[b], C. Lagana[a], P.G. Mercadante[b], S.F. Novaes[a], Sandra S. Padula[a]

Institute for Nuclear Research and Nuclear Energy, Sofia, Bulgaria
V. Genchev[2], P. Iaydjiev[2], S. Piperov, M. Rodozov, G. Sultanov, M. Vutova

University of Sofia, Sofia, Bulgaria
A. Dimitrov, R. Hadjiiska, V. Kozhuharov, L. Litov, B. Pavlov, P. Petkov

Institute of High Energy Physics, Beijing, China
J.G. Bian, G.M. Chen, H.S. Chen, C.H. Jiang, D. Liang, S. Liang, X. Meng, J. Tao, X. Wang, Z. Wang

State Key Laboratory of Nuclear Physics and Technology, Peking University, Beijing, China
C. Asawatangtrakuldee, Y. Ban, Y. Guo, W. Li, S. Liu, Y. Mao, S.J. Qian, H. Teng, D. Wang, L. Zhang, W. Zou

Universidad de Los Andes, Bogota, Colombia
C. Avila, C.A. Carrillo Montoya, L.F. Chaparro Sierra, J.P. Gomez, B. Gomez Moreno, J.C. Sanabria

Technical University of Split, Split, Croatia
N. Godinovic, D. Lelas, R. Plestina[8], D. Polic, I. Puljak

University of Split, Split, Croatia
Z. Antunovic, M. Kovac

Institute Rudjer Boskovic, Zagreb, Croatia
V. Brigljevic, K. Kadija, J. Luetic, D. Mekterovic, S. Morovic, L. Tikvica

University of Cyprus, Nicosia, Cyprus
A. Attikis, G. Mavromanolakis, J. Mousa, C. Nicolaou, F. Ptochos, P.A. Razis

Charles University, Prague, Czech Republic
M. Finger, M. Finger Jr.

Academy of Scientific Research and Technology of the Arab Republic of Egypt, Egyptian Network of High Energy Physics, Cairo, Egypt
A.A. Abdelalim[9], Y. Assran[10], S. Elgammal[9], A. Ellithi Kamel[11], M.A. Mahmoud[12], A. Radi[13,14]

National Institute of Chemical Physics and Biophysics, Tallinn, Estonia
M. Kadastik, M. Müntel, M. Murumaa, M. Raidal, L. Rebane, A. Tiko

Department of Physics, University of Helsinki, Helsinki, Finland
P. Eerola, G. Fedi, M. Voutilainen

Helsinki Institute of Physics, Helsinki, Finland
J. Härkönen, V. Karimäki, R. Kinnunen, M.J. Kortelainen, T. Lampén, K. Lassila-Perini, S. Lehti, T. Lindén, P. Luukka, T. Mäenpää, T. Peltola, E. Tuominen, J. Tuominiemi, E. Tuovinen, L. Wendland

Lappeenranta University of Technology, Lappeenranta, Finland
T. Tuuva

DSM/IRFU, CEA/Saclay, Gif-sur-Yvette, France
M. Besancon, F. Couderc, M. Dejardin, D. Denegri, B. Fabbro, J.L. Faure, F. Ferri, S. Ganjour, A. Givernaud, P. Gras, G. Hamel de Monchenault, P. Jarry, E. Locci, J. Malcles, L. Millischer, A. Nayak, J. Rander, A. Rosowsky, M. Titov

Laboratoire Leprince-Ringuet, Ecole Polytechnique, IN2P3-CNRS, Palaiseau, France
S. Baffioni, F. Beaudette, L. Benhabib, M. Bluj[15], P. Busson, C. Charlot, N. Daci, T. Dahms,
M. Dalchenko, L. Dobrzynski, A. Florent, R. Granier de Cassagnac, M. Haguenauer, P. Miné,
C. Mironov, I.N. Naranjo, M. Nguyen, C. Ochando, P. Paganini, D. Sabes, R. Salerno, Y. Sirois,
C. Veelken, A. Zabi

**Institut Pluridisciplinaire Hubert Curien, Université de Strasbourg, Université de Haute
Alsace Mulhouse, CNRS/IN2P3, Strasbourg, France**
J.-L. Agram[16], J. Andrea, D. Bloch, J.-M. Brom, E.C. Chabert, C. Collard, E. Conte[16],
F. Drouhin[16], J.-C. Fontaine[16], D. Gelé, U. Goerlach, C. Goetzmann, P. Juillot, A.-C. Le Bihan,
P. Van Hove

**Centre de Calcul de l'Institut National de Physique Nucleaire et de Physique des Particules,
CNRS/IN2P3, Villeurbanne, France**
S. Gadrat

**Université de Lyon, Université Claude Bernard Lyon 1, CNRS-IN2P3, Institut de Physique
Nucléaire de Lyon, Villeurbanne, France**
S. Beauceron, N. Beaupere, G. Boudoul, S. Brochet, J. Chasserat, R. Chierici, D. Contardo,
P. Depasse, H. El Mamouni, J. Fan, J. Fay, S. Gascon, M. Gouzevitch, B. Ille, T. Kurca,
M. Lethuillier, L. Mirabito, S. Perries, L. Sgandurra, V. Sordini, M. Vander Donckt, P. Verdier,
S. Viret, H. Xiao

**Institute of High Energy Physics and Informatization, Tbilisi State University, Tbilisi,
Georgia**
Z. Tsamalaidze[17]

RWTH Aachen University, I. Physikalisches Institut, Aachen, Germany
C. Autermann, S. Beranek, M. Bontenackels, B. Calpas, M. Edelhoff, L. Feld, N. Heracleous,
O. Hindrichs, K. Klein, A. Ostapchuk, A. Perieanu, F. Raupach, J. Sammet, S. Schael,
D. Sprenger, H. Weber, B. Wittmer, V. Zhukov[5]

RWTH Aachen University, III. Physikalisches Institut A, Aachen, Germany
M. Ata, J. Caudron, E. Dietz-Laursonn, D. Duchardt, M. Erdmann, R. Fischer, A. Güth,
T. Hebbeker, C. Heidemann, K. Hoepfner, D. Klingebiel, S. Knutzen, P. Kreuzer,
M. Merschmeyer, A. Meyer, M. Olschewski, K. Padeken, P. Papacz, H. Pieta, H. Reithler,
S.A. Schmitz, L. Sonnenschein, J. Steggemann, D. Teyssier, S. Thüer, M. Weber

RWTH Aachen University, III. Physikalisches Institut B, Aachen, Germany
V. Cherepanov, Y. Erdogan, G. Flügge, H. Geenen, M. Geisler, W. Haj Ahmad, F. Hoehle,
B. Kargoll, T. Kress, Y. Kuessel, J. Lingemann[2], A. Nowack, I.M. Nugent, L. Perchalla, O. Pooth,
A. Stahl

Deutsches Elektronen-Synchrotron, Hamburg, Germany
I. Asin, N. Bartosik, J. Behr, W. Behrenhoff, U. Behrens, A.J. Bell, M. Bergholz[18], A. Bethani,
K. Borras, A. Burgmeier, A. Cakir, L. Calligaris, A. Campbell, S. Choudhury, F. Costanza,
C. Diez Pardos, S. Dooling, T. Dorland, G. Eckerlin, D. Eckstein, G. Flucke, A. Geiser,
I. Glushkov, A. Grebenyuk, P. Gunnellini, S. Habib, J. Hauk, G. Hellwig, D. Horton, H. Jung,
M. Kasemann, P. Katsas, C. Kleinwort, H. Kluge, M. Krämer, D. Krücker, E. Kuznetsova,
W. Lange, J. Leonard, K. Lipka, W. Lohmann[18], B. Lutz, R. Mankel, I. Marfin, I.-A. Melzer-
Pellmann, A.B. Meyer, J. Mnich, A. Mussgiller, S. Naumann-Emme, O. Novgorodova,
F. Nowak, J. Olzem, H. Perrey, A. Petrukhin, D. Pitzl, R. Placakyte, A. Raspereza, P.M. Ribeiro

Cipriano, C. Riedl, E. Ron, M.Ö. Sahin, J. Salfeld-Nebgen, R. Schmidt[18], T. Schoerner-Sadenius, N. Sen, M. Stein, R. Walsh, C. Wissing

University of Hamburg, Hamburg, Germany
M. Aldaya Martin, V. Blobel, H. Enderle, J. Erfle, E. Garutti, U. Gebbert, M. Görner, M. Gosselink, J. Haller, K. Heine, R.S. Höing, G. Kaussen, H. Kirschenmann, R. Klanner, R. Kogler, J. Lange, I. Marchesini, T. Peiffer, N. Pietsch, D. Rathjens, C. Sander, H. Schettler, P. Schleper, E. Schlieckau, A. Schmidt, M. Schröder, T. Schum, M. Seidel, J. Sibille[19], V. Sola, H. Stadie, G. Steinbrück, J. Thomsen, D. Troendle, E. Usai, L. Vanelderen

Institut für Experimentelle Kernphysik, Karlsruhe, Germany
C. Barth, C. Baus, J. Berger, C. Böser, E. Butz, T. Chwalek, W. De Boer, A. Descroix, A. Dierlamm, M. Feindt, M. Guthoff[2], F. Hartmann[2], T. Hauth[2], H. Held, K.H. Hoffmann, U. Husemann, I. Katkov[5], J.R. Komaragiri, A. Kornmayer[2], P. Lobelle Pardo, D. Martschei, M.U. Mozer, Th. Müller, M. Niegel, A. Nürnberg, O. Oberst, J. Ott, G. Quast, K. Rabbertz, F. Ratnikov, S. Röcker, F.-P. Schilling, G. Schott, H.J. Simonis, F.M. Stober, R. Ulrich, J. Wagner-Kuhr, S. Wayand, T. Weiler, M. Zeise

Institute of Nuclear and Particle Physics (INPP), NCSR Demokritos, Aghia Paraskevi, Greece
G. Anagnostou, G. Daskalakis, T. Geralis, S. Kesisoglou, A. Kyriakis, D. Loukas, A. Markou, C. Markou, E. Ntomari, I. Topsis-giotis

University of Athens, Athens, Greece
L. Gouskos, A. Panagiotou, N. Saoulidou, E. Stiliaris

University of Ioánnina, Ioánnina, Greece
X. Aslanoglou, I. Evangelou, G. Flouris, C. Foudas, P. Kokkas, N. Manthos, I. Papadopoulos, E. Paradas

KFKI Research Institute for Particle and Nuclear Physics, Budapest, Hungary
G. Bencze, C. Hajdu, P. Hidas, D. Horvath[20], F. Sikler, V. Veszpremi, G. Vesztergombi[21], A.J. Zsigmond

Institute of Nuclear Research ATOMKI, Debrecen, Hungary
N. Beni, S. Czellar, J. Molnar, J. Palinkas, Z. Szillasi

University of Debrecen, Debrecen, Hungary
J. Karancsi, P. Raics, Z.L. Trocsanyi, B. Ujvari

National Institute of Science Education and Research, Bhubaneswar, India
S.K. Swain[22]

Panjab University, Chandigarh, India
S.B. Beri, V. Bhatnagar, N. Dhingra, R. Gupta, M. Kaur, M.Z. Mehta, M. Mittal, N. Nishu, A. Sharma, J.B. Singh

University of Delhi, Delhi, India
Ashok Kumar, Arun Kumar, S. Ahuja, A. Bhardwaj, B.C. Choudhary, A. Kumar, S. Malhotra, M. Naimuddin, K. Ranjan, P. Saxena, V. Sharma, R.K. Shivpuri

Saha Institute of Nuclear Physics, Kolkata, India
S. Banerjee, S. Bhattacharya, K. Chatterjee, S. Dutta, B. Gomber, Sa. Jain, Sh. Jain, R. Khurana, A. Modak, S. Mukherjee, D. Roy, S. Sarkar, M. Sharan, A.P. Singh

Bhabha Atomic Research Centre, Mumbai, India
A. Abdulsalam, D. Dutta, S. Kailas, V. Kumar, A.K. Mohanty[2], L.M. Pant, P. Shukla, A. Topkar

Tata Institute of Fundamental Research - EHEP, Mumbai, India
T. Aziz, R.M. Chatterjee, S. Ganguly, S. Ghosh, M. Guchait[23], A. Gurtu[24], G. Kole, S. Kumar, M. Maity[25], G. Majumder, K. Mazumdar, G.B. Mohanty, B. Parida, K. Sudhakar, N. Wickramage[26]

Tata Institute of Fundamental Research - HECR, Mumbai, India
S. Banerjee, S. Dugad

Institute for Research in Fundamental Sciences (IPM), Tehran, Iran
H. Arfaei, H. Bakhshiansohi, S.M. Etesami[27], A. Fahim[28], A. Jafari, M. Khakzad, M. Mohammadi Najafabadi, S. Paktinat Mehdiabadi, B. Safarzadeh[29], M. Zeinali

University College Dublin, Dublin, Ireland
M. Grunewald

INFN Sezione di Bari [a]**, Università di Bari** [b]**, Politecnico di Bari** [c]**, Bari, Italy**
M. Abbrescia[a,b], L. Barbone[a,b], C. Calabria[a,b], S.S. Chhibra[a,b], A. Colaleo[a], D. Creanza[a,c], N. De Filippis[a,c], M. De Palma[a,b], L. Fiore[a], G. Iaselli[a,c], G. Maggi[a,c], M. Maggi[a], B. Marangelli[a,b], S. My[a,c], S. Nuzzo[a,b], N. Pacifico[a], A. Pompili[a,b], G. Pugliese[a,c], G. Selvaggi[a,b], L. Silvestris[a], G. Singh[a,b], R. Venditti[a,b], P. Verwilligen[a], G. Zito[a]

INFN Sezione di Bologna [a]**, Università di Bologna** [b]**, Bologna, Italy**
G. Abbiendi[a], A.C. Benvenuti[a], D. Bonacorsi[a,b], S. Braibant-Giacomelli[a,b], L. Brigliadori[a,b], R. Campanini[a,b], P. Capiluppi[a,b], A. Castro[a,b], F.R. Cavallo[a], G. Codispoti[a,b], M. Cuffiani[a,b], G.M. Dallavalle[a], F. Fabbri[a], A. Fanfani[a,b], D. Fasanella[a,b], P. Giacomelli[a], C. Grandi[a], L. Guiducci[a,b], S. Marcellini[a], G. Masetti[a], M. Meneghelli[a,b], A. Montanari[a], F.L. Navarria[a,b], F. Odorici[a], A. Perrotta[a], F. Primavera[a,b], A.M. Rossi[a,b], T. Rovelli[a,b], G.P. Siroli[a,b], N. Tosi[a,b], R. Travaglini[a,b]

INFN Sezione di Catania [a]**, Università di Catania** [b]**, Catania, Italy**
S. Albergo[a,b], G. Cappello[a,b], M. Chiorboli[a,b], S. Costa[a,b], F. Giordano[a,2], R. Potenza[a,b], A. Tricomi[a,b], C. Tuve[a,b]

INFN Sezione di Firenze [a]**, Università di Firenze** [b]**, Firenze, Italy**
G. Barbagli[a], V. Ciulli[a,b], C. Civinini[a], R. D'Alessandro[a,b], E. Focardi[a,b], S. Frosali[a,b], E. Gallo[a], S. Gonzi[a,b], V. Gori[a,b], P. Lenzi[a,b], M. Meschini[a], S. Paoletti[a], G. Sguazzoni[a], A. Tropiano[a,b]

INFN Laboratori Nazionali di Frascati, Frascati, Italy
L. Benussi, S. Bianco, F. Fabbri, D. Piccolo

INFN Sezione di Genova [a]**, Università di Genova** [b]**, Genova, Italy**
P. Fabbricatore[a], R. Ferretti[a,b], F. Ferro[a], M. Lo Vetere[a,b], R. Musenich[a], E. Robutti[a], S. Tosi[a,b]

INFN Sezione di Milano-Bicocca [a]**, Università di Milano-Bicocca** [b]**, Milano, Italy**
A. Benaglia[a], M.E. Dinardo[a,b], S. Fiorendi[a,b], S. Gennai[a], A. Ghezzi[a,b], P. Govoni[a,b], M.T. Lucchini[a,b,2], S. Malvezzi[a], R.A. Manzoni[a,b,2], A. Martelli[a,b,2], D. Menasce[a], L. Moroni[a], M. Paganoni[a,b], D. Pedrini[a], S. Ragazzi[a,b], N. Redaelli[a], T. Tabarelli de Fatis[a,b]

INFN Sezione di Napoli [a]**, Università di Napoli 'Federico II'** [b]**, Università della Basilicata (Potenza)** [c]**, Università G. Marconi (Roma)** [d]**, Napoli, Italy**
S. Buontempo[a], N. Cavallo[a,c], A. De Cosa[a,b], F. Fabozzi[a,c], A.O.M. Iorio[a,b], L. Lista[a], S. Meola[a,d,2], M. Merola[a], P. Paolucci[a,2]

INFN Sezione di Padova [a]**, Università di Padova** [b]**, Università di Trento (Trento)** [c]**, Padova, Italy**
P. Azzi[a], N. Bacchetta[a], D. Bisello[a,b], A. Branca[a,b], R. Carlin[a,b], P. Checchia[a], T. Dorigo[a], M. Galanti[a,b,2], F. Gasparini[a,b], U. Gasparini[a,b], P. Giubilato[a,b], A. Gozzelino[a], K. Kanishchev[a,c], S. Lacaprara[a], I. Lazzizzera[a,c], M. Margoni[a,b], A.T. Meneguzzo[a,b], M. Michelotto[a], F. Montecassiano[a], M. Passaseo[a], J. Pazzini[a,b], M. Pegoraro[a], N. Pozzobon[a,b], P. Ronchese[a,b], F. Simonetto[a,b], E. Torassa[a], M. Tosi[a,b], P. Zotto[a,b], A. Zucchetta[a,b], G. Zumerle[a,b]

INFN Sezione di Pavia [a]**, Università di Pavia** [b]**, Pavia, Italy**
M. Gabusi[a,b], S.P. Ratti[a,b], C. Riccardi[a,b], P. Vitulo[a,b]

INFN Sezione di Perugia [a]**, Università di Perugia** [b]**, Perugia, Italy**
M. Biasini[a,b], G.M. Bilei[a], L. Fanò[a,b], P. Lariccia[a,b], G. Mantovani[a,b], M. Menichelli[a], A. Nappi[a,b†], F. Romeo[a,b], A. Saha[a], A. Santocchia[a,b], A. Spiezia[a,b]

INFN Sezione di Pisa [a]**, Università di Pisa** [b]**, Scuola Normale Superiore di Pisa** [c]**, Pisa, Italy**
K. Androsov[a,30], P. Azzurri[a], G. Bagliesi[a], T. Boccali[a], G. Broccolo[a,c], R. Castaldi[a], M.A. Ciocci[a,30], R.T. D'Agnolo[a,c,2], R. Dell'Orso[a], F. Fiori[a,c], L. Foà[a,c], A. Giassi[a], M.T. Grippo[a,30], A. Kraan[a], F. Ligabue[a,c], T. Lomtadze[a], L. Martini[a,30], A. Messineo[a,b], C.S. Moon[a,31], F. Palla[a], A. Rizzi[a,b], A. Savoy-Navarro[a,32], A.T. Serban[a], P. Spagnolo[a], P. Squillacioti[a,30], R. Tenchini[a], G. Tonelli[a,b], A. Venturi[a], P.G. Verdini[a], C. Vernieri[a,c]

INFN Sezione di Roma [a]**, Università di Roma** [b]**, Roma, Italy**
L. Barone[a,b], F. Cavallari[a], D. Del Re[a,b], M. Diemoz[a], M. Grassi[a,b], E. Longo[a,b], F. Margaroli[a,b], P. Meridiani[a], F. Micheli[a,b], S. Nourbakhsh[a,b], G. Organtini[a,b], R. Paramatti[a], S. Rahatlou[a,b], C. Rovelli[a], L. Soffi[a,b]

INFN Sezione di Torino [a]**, Università di Torino** [b]**, Università del Piemonte Orientale (Novara)** [c]**, Torino, Italy**
N. Amapane[a,b], R. Arcidiacono[a,c], S. Argiro[a,b], M. Arneodo[a,c], R. Bellan[a,b], C. Biino[a], N. Cartiglia[a], S. Casasso[a,b], M. Costa[a,b], A. Degano[a,b], N. Demaria[a], C. Mariotti[a], S. Maselli[a], E. Migliore[a,b], V. Monaco[a,b], M. Musich[a], M.M. Obertino[a,c], N. Pastrone[a], M. Pelliccioni[a,2], A. Potenza[a,b], A. Romero[a,b], M. Ruspa[a,c], R. Sacchi[a,b], A. Solano[a,b], A. Staiano[a], U. Tamponi[a]

INFN Sezione di Trieste [a]**, Università di Trieste** [b]**, Trieste, Italy**
S. Belforte[a], V. Candelise[a,b], M. Casarsa[a], F. Cossutti[a,2], G. Della Ricca[a,b], B. Gobbo[a], C. La Licata[a,b], M. Marone[a,b], D. Montanino[a,b], A. Penzo[a], A. Schizzi[a,b], A. Zanetti[a]

Kangwon National University, Chunchon, Korea
S. Chang, T.Y. Kim, S.K. Nam

Kyungpook National University, Daegu, Korea
D.H. Kim, G.N. Kim, J.E. Kim, D.J. Kong, S. Lee, Y.D. Oh, H. Park, D.C. Son

Chonnam National University, Institute for Universe and Elementary Particles, Kwangju, Korea
J.Y. Kim, Zero J. Kim, S. Song

Korea University, Seoul, Korea
S. Choi, D. Gyun, B. Hong, M. Jo, H. Kim, T.J. Kim, K.S. Lee, S.K. Park, Y. Roh

University of Seoul, Seoul, Korea
M. Choi, J.H. Kim, C. Park, I.C. Park, S. Park, G. Ryu

Sungkyunkwan University, Suwon, Korea
Y. Choi, Y.K. Choi, J. Goh, M.S. Kim, E. Kwon, B. Lee, J. Lee, S. Lee, H. Seo, I. Yu

Vilnius University, Vilnius, Lithuania
I. Grigelionis, A. Juodagalvis

Centro de Investigacion y de Estudios Avanzados del IPN, Mexico City, Mexico
H. Castilla-Valdez, E. De La Cruz-Burelo, I. Heredia-de La Cruz[33], R. Lopez-Fernandez, J. Martínez-Ortega, A. Sanchez-Hernandez, L.M. Villasenor-Cendejas

Universidad Iberoamericana, Mexico City, Mexico
S. Carrillo Moreno, F. Vazquez Valencia

Benemerita Universidad Autonoma de Puebla, Puebla, Mexico
H.A. Salazar Ibarguen

Universidad Autónoma de San Luis Potosí, San Luis Potosí, Mexico
E. Casimiro Linares, A. Morelos Pineda, M.A. Reyes-Santos

University of Auckland, Auckland, New Zealand
D. Krofcheck

University of Canterbury, Christchurch, New Zealand
P.H. Butler, R. Doesburg, S. Reucroft, H. Silverwood

National Centre for Physics, Quaid-I-Azam University, Islamabad, Pakistan
M. Ahmad, M.I. Asghar, J. Butt, H.R. Hoorani, S. Khalid, W.A. Khan, T. Khurshid, S. Qazi, M.A. Shah, M. Shoaib

National Centre for Nuclear Research, Swierk, Poland
H. Bialkowska, B. Boimska, T. Frueboes, M. Górski, M. Kazana, K. Nawrocki, K. Romanowska-Rybinska, M. Szleper, G. Wrochna, P. Zalewski

Institute of Experimental Physics, Faculty of Physics, University of Warsaw, Warsaw, Poland
G. Brona, K. Bunkowski, M. Cwiok, W. Dominik, K. Doroba, A. Kalinowski, M. Konecki, J. Krolikowski, M. Misiura, W. Wolszczak

Laboratório de Instrumentação e Física Experimental de Partículas, Lisboa, Portugal
N. Almeida, P. Bargassa, C. Beirão Da Cruz E Silva, P. Faccioli, P.G. Ferreira Parracho, M. Gallinaro, F. Nguyen, J. Rodrigues Antunes, J. Seixas[2], J. Varela, P. Vischia

Joint Institute for Nuclear Research, Dubna, Russia
S. Afanasiev, P. Bunin, M. Gavrilenko, I. Golutvin, I. Gorbunov, A. Kamenev, V. Karjavin, V. Konoplyanikov, A. Lanev, A. Malakhov, V. Matveev, P. Moisenz, V. Palichik, V. Perelygin, S. Shmatov, N. Skatchkov, V. Smirnov, A. Zarubin

Petersburg Nuclear Physics Institute, Gatchina (St. Petersburg), Russia
S. Evstyukhin, V. Golovtsov, Y. Ivanov, V. Kim, P. Levchenko, V. Murzin, V. Oreshkin, I. Smirnov, V. Sulimov, L. Uvarov, S. Vavilov, A. Vorobyev, An. Vorobyev

Institute for Nuclear Research, Moscow, Russia
Yu. Andreev, A. Dermenev, S. Gninenko, N. Golubev, M. Kirsanov, N. Krasnikov, A. Pashenkov, D. Tlisov, A. Toropin

Institute for Theoretical and Experimental Physics, Moscow, Russia
V. Epshteyn, M. Erofeeva, V. Gavrilov, N. Lychkovskaya, V. Popov, G. Safronov, S. Semenov, A. Spiridonov, V. Stolin, E. Vlasov, A. Zhokin

P.N. Lebedev Physical Institute, Moscow, Russia
V. Andreev, M. Azarkin, I. Dremin, M. Kirakosyan, A. Leonidov, G. Mesyats, S.V. Rusakov, A. Vinogradov

Skobeltsyn Institute of Nuclear Physics, Lomonosov Moscow State University, Moscow, Russia
A. Belyaev, E. Boos, M. Dubinin[7], L. Dudko, A. Ershov, A. Gribushin, V. Klyukhin, O. Kodolova, I. Lokhtin, A. Markina, S. Obraztsov, S. Petrushanko, V. Savrin, A. Snigirev

State Research Center of Russian Federation, Institute for High Energy Physics, Protvino, Russia
I. Azhgirey, I. Bayshev, S. Bitioukov, V. Kachanov, A. Kalinin, D. Konstantinov, V. Krychkine, V. Petrov, R. Ryutin, A. Sobol, L. Tourtchanovitch, S. Troshin, N. Tyurin, A. Uzunian, A. Volkov

University of Belgrade, Faculty of Physics and Vinca Institute of Nuclear Sciences, Belgrade, Serbia
P. Adzic[34], M. Djordjevic, M. Ekmedzic, J. Milosevic

Centro de Investigaciones Energéticas Medioambientales y Tecnológicas (CIEMAT), Madrid, Spain
M. Aguilar-Benitez, J. Alcaraz Maestre, C. Battilana, E. Calvo, M. Cerrada, M. Chamizo Llatas[2], N. Colino, B. De La Cruz, A. Delgado Peris, D. Domínguez Vázquez, C. Fernandez Bedoya, J.P. Fernández Ramos, A. Ferrando, J. Flix, M.C. Fouz, P. Garcia-Abia, O. Gonzalez Lopez, S. Goy Lopez, J.M. Hernandez, M.I. Josa, G. Merino, E. Navarro De Martino, J. Puerta Pelayo, A. Quintario Olmeda, I. Redondo, L. Romero, J. Santaolalla, M.S. Soares, C. Willmott

Universidad Autónoma de Madrid, Madrid, Spain
C. Albajar, J.F. de Trocóniz

Universidad de Oviedo, Oviedo, Spain
H. Brun, J. Cuevas, J. Fernandez Menendez, S. Folgueras, I. Gonzalez Caballero, L. Lloret Iglesias, J. Piedra Gomez

Instituto de Física de Cantabria (IFCA), CSIC-Universidad de Cantabria, Santander, Spain
J.A. Brochero Cifuentes, I.J. Cabrillo, A. Calderon, S.H. Chuang, J. Duarte Campderros, M. Fernandez, G. Gomez, J. Gonzalez Sanchez, A. Graziano, C. Jorda, A. Lopez Virto, J. Marco, R. Marco, C. Martinez Rivero, F. Matorras, F.J. Munoz Sanchez, T. Rodrigo, A.Y. Rodríguez-Marrero, A. Ruiz-Jimeno, L. Scodellaro, I. Vila, R. Vilar Cortabitarte

CERN, European Organization for Nuclear Research, Geneva, Switzerland
D. Abbaneo, E. Auffray, G. Auzinger, M. Bachtis, P. Baillon, A.H. Ball, D. Barney, J. Bendavid, J.F. Benitez, C. Bernet[8], G. Bianchi, P. Bloch, A. Bocci, A. Bonato, O. Bondu, C. Botta, H. Breuker, T. Camporesi, G. Cerminara, T. Christiansen, J.A. Coarasa Perez, S. Colafranceschi[35], M. D'Alfonso, D. d'Enterria, A. Dabrowski, A. David, F. De Guio, A. De Roeck, S. De Visscher, S. Di Guida, M. Dobson, N. Dupont-Sagorin, A. Elliott-Peisert, J. Eugster, G. Franzoni, W. Funk, G. Georgiou, M. Giffels, D. Gigi, K. Gill, D. Giordano, M. Girone, M. Giunta, F. Glege, R. Gomez-Reino Garrido, S. Gowdy, R. Guida, J. Hammer, M. Hansen, P. Harris, C. Hartl, A. Hinzmann, V. Innocente, P. Janot, E. Karavakis, K. Kousouris, K. Krajczar, P. Lecoq, Y.-J. Lee, C. Lourenço, N. Magini, L. Malgeri, M. Mannelli, L. Masetti, F. Meijers, S. Mersi, E. Meschi, R. Moser, M. Mulders, P. Musella, E. Nesvold, L. Orsini, E. Palencia Cortezon, E. Perez, L. Perrozzi, A. Petrilli, A. Pfeiffer, M. Pierini, M. Pimiä, D. Piparo, M. Plagge, L. Quertenmont, A. Racz, W. Reece, G. Rolandi[36], M. Rovere, H. Sakulin, F. Santanastasio, C. Schäfer, C. Schwick,

S. Sekmen, A. Sharma, P. Siegrist, P. Silva, M. Simon, P. Sphicas[37], D. Spiga, B. Stieger, M. Stoye, A. Tsirou, G.I. Veres[21], J.R. Vlimant, H.K. Wöhri, S.D. Worm[38], W.D. Zeuner

Paul Scherrer Institut, Villigen, Switzerland
W. Bertl, K. Deiters, W. Erdmann, K. Gabathuler, R. Horisberger, Q. Ingram, H.C. Kaestli, S. König, D. Kotlinski, U. Langenegger, D. Renker, T. Rohe

Institute for Particle Physics, ETH Zurich, Zurich, Switzerland
F. Bachmair, L. Bäni, L. Bianchini, P. Bortignon, M.A. Buchmann, B. Casal, N. Chanon, A. Deisher, G. Dissertori, M. Dittmar, M. Donegà, M. Dünser, P. Eller, K. Freudenreich, C. Grab, D. Hits, P. Lecomte, W. Lustermann, B. Mangano, A.C. Marini, P. Martinez Ruiz del Arbol, D. Meister, N. Mohr, F. Moortgat, C. Nägeli[39], P. Nef, F. Nessi-Tedaldi, F. Pandolfi, L. Pape, F. Pauss, M. Peruzzi, M. Quittnat, F.J. Ronga, M. Rossini, L. Sala, A.K. Sanchez, A. Starodumov[40], M. Takahashi, L. Tauscher[†], A. Thea, K. Theofilatos, D. Treille, C. Urscheler, R. Wallny, H.A. Weber

Universität Zürich, Zurich, Switzerland
C. Amsler[41], V. Chiochia, C. Favaro, M. Ivova Rikova, B. Kilminster, B. Millan Mejias, P. Robmann, H. Snoek, S. Taroni, M. Verzetti, Y. Yang

National Central University, Chung-Li, Taiwan
M. Cardaci, K.H. Chen, C. Ferro, C.M. Kuo, S.W. Li, W. Lin, Y.J. Lu, R. Volpe, S.S. Yu

National Taiwan University (NTU), Taipei, Taiwan
P. Bartalini, P. Chang, Y.H. Chang, Y.W. Chang, Y. Chao, K.F. Chen, C. Dietz, U. Grundler, W.-S. Hou, Y. Hsiung, K.Y. Kao, Y.J. Lei, R.-S. Lu, D. Majumder, E. Petrakou, X. Shi, J.G. Shiu, Y.M. Tzeng, M. Wang

Chulalongkorn University, Bangkok, Thailand
B. Asavapibhop, N. Suwonjandee

Cukurova University, Adana, Turkey
A. Adiguzel, M.N. Bakirci[42], S. Cerci[43], C. Dozen, I. Dumanoglu, E. Eskut, S. Girgis, G. Gokbulut, E. Gurpinar, I. Hos, E.E. Kangal, A. Kayis Topaksu, G. Onengut[44], K. Ozdemir, S. Ozturk[42], A. Polatoz, K. Sogut[45], D. Sunar Cerci[43], B. Tali[43], H. Topakli[42], M. Vergili

Middle East Technical University, Physics Department, Ankara, Turkey
I.V. Akin, T. Aliev, B. Bilin, S. Bilmis, M. Deniz, H. Gamsizkan, A.M. Guler, G. Karapinar[46], K. Ocalan, A. Ozpineci, M. Serin, R. Sever, U.E. Surat, M. Yalvac, M. Zeyrek

Bogazici University, Istanbul, Turkey
E. Gülmez, B. Isildak[47], M. Kaya[48], O. Kaya[48], S. Ozkorucuklu[49], N. Sonmez[50]

Istanbul Technical University, Istanbul, Turkey
H. Bahtiyar[51], E. Barlas, K. Cankocak, Y.O. Günaydin[52], F.I. Vardarlı, M. Yücel

National Scientific Center, Kharkov Institute of Physics and Technology, Kharkov, Ukraine
L. Levchuk, P. Sorokin

University of Bristol, Bristol, United Kingdom
J.J. Brooke, E. Clement, D. Cussans, H. Flacher, R. Frazier, J. Goldstein, M. Grimes, G.P. Heath, H.F. Heath, L. Kreczko, C. Lucas, Z. Meng, S. Metson, D.M. Newbold[38], K. Nirunpong, S. Paramesvaran, A. Poll, S. Senkin, V.J. Smith, T. Williams

Rutherford Appleton Laboratory, Didcot, United Kingdom
K.W. Bell, A. Belyaev[53], C. Brew, R.M. Brown, D.J.A. Cockerill, J.A. Coughlan, K. Harder,

S. Harper, J. Ilic, E. Olaiya, D. Petyt, B.C. Radburn-Smith, C.H. Shepherd-Themistocleous, I.R. Tomalin, W.J. Womersley

Imperial College, London, United Kingdom
R. Bainbridge, O. Buchmuller, D. Burton, D. Colling, N. Cripps, M. Cutajar, P. Dauncey, G. Davies, M. Della Negra, W. Ferguson, J. Fulcher, D. Futyan, A. Gilbert, A. Guneratne Bryer, G. Hall, Z. Hatherell, J. Hays, G. Iles, M. Jarvis, G. Karapostoli, M. Kenzie, R. Lane, R. Lucas[38], L. Lyons, A.-M. Magnan, J. Marrouche, B. Mathias, R. Nandi, J. Nash, A. Nikitenko[40], J. Pela, M. Pesaresi, K. Petridis, M. Pioppi[54], D.M. Raymond, S. Rogerson, A. Rose, C. Seez, P. Sharp[†], A. Sparrow, A. Tapper, M. Vazquez Acosta, T. Virdee, S. Wakefield, N. Wardle

Brunel University, Uxbridge, United Kingdom
M. Chadwick, J.E. Cole, P.R. Hobson, A. Khan, P. Kyberd, D. Leggat, D. Leslie, W. Martin, I.D. Reid, P. Symonds, L. Teodorescu, M. Turner

Baylor University, Waco, USA
J. Dittmann, K. Hatakeyama, A. Kasmi, H. Liu, T. Scarborough

The University of Alabama, Tuscaloosa, USA
O. Charaf, S.I. Cooper, C. Henderson, P. Rumerio

Boston University, Boston, USA
A. Avetisyan, T. Bose, C. Fantasia, A. Heister, P. Lawson, D. Lazic, J. Rohlf, D. Sperka, J. St. John, L. Sulak

Brown University, Providence, USA
J. Alimena, S. Bhattacharya, G. Christopher, D. Cutts, Z. Demiragli, A. Ferapontov, A. Garabedian, U. Heintz, S. Jabeen, G. Kukartsev, E. Laird, G. Landsberg, M. Luk, M. Narain, M. Segala, T. Sinthuprasith, T. Speer

University of California, Davis, Davis, USA
R. Breedon, G. Breto, M. Calderon De La Barca Sanchez, S. Chauhan, M. Chertok, J. Conway, R. Conway, P.T. Cox, R. Erbacher, M. Gardner, R. Houtz, W. Ko, A. Kopecky, R. Lander, T. Miceli, D. Pellett, J. Pilot, F. Ricci-Tam, B. Rutherford, M. Searle, J. Smith, M. Squires, M. Tripathi, S. Wilbur, R. Yohay

University of California, Los Angeles, USA
V. Andreev, D. Cline, R. Cousins, S. Erhan, P. Everaerts, C. Farrell, M. Felcini, J. Hauser, M. Ignatenko, C. Jarvis, G. Rakness, P. Schlein[†], E. Takasugi, P. Traczyk, V. Valuev, M. Weber

University of California, Riverside, Riverside, USA
J. Babb, R. Clare, J. Ellison, J.W. Gary, G. Hanson, J. Heilman, P. Jandir, H. Liu, O.R. Long, A. Luthra, M. Malberti, H. Nguyen, A. Shrinivas, J. Sturdy, S. Sumowidagdo, R. Wilken, S. Wimpenny

University of California, San Diego, La Jolla, USA
W. Andrews, J.G. Branson, G.B. Cerati, S. Cittolin, D. Evans, A. Holzner, R. Kelley, M. Lebourgeois, J. Letts, I. Macneill, S. Padhi, C. Palmer, G. Petrucciani, M. Pieri, M. Sani, V. Sharma, S. Simon, E. Sudano, M. Tadel, Y. Tu, A. Vartak, S. Wasserbaech[55], F. Würthwein, A. Yagil, J. Yoo

University of California, Santa Barbara, Santa Barbara, USA
D. Barge, C. Campagnari, T. Danielson, K. Flowers, P. Geffert, C. George, F. Golf, J. Incandela, C. Justus, D. Kovalskyi, V. Krutelyov, R. Magaña Villalba, N. Mccoll, V. Pavlunin, J. Richman, R. Rossin, D. Stuart, W. To, C. West

California Institute of Technology, Pasadena, USA
A. Apresyan, A. Bornheim, J. Bunn, Y. Chen, E. Di Marco, J. Duarte, D. Kcira, Y. Ma, A. Mott, H.B. Newman, C. Pena, C. Rogan, M. Spiropulu, V. Timciuc, J. Veverka, R. Wilkinson, S. Xie, R.Y. Zhu

Carnegie Mellon University, Pittsburgh, USA
V. Azzolini, A. Calamba, R. Carroll, T. Ferguson, Y. Iiyama, D.W. Jang, Y.F. Liu, M. Paulini, J. Russ, H. Vogel, I. Vorobiev

University of Colorado at Boulder, Boulder, USA
J.P. Cumalat, B.R. Drell, W.T. Ford, A. Gaz, E. Luiggi Lopez, U. Nauenberg, J.G. Smith, K. Stenson, K.A. Ulmer, S.R. Wagner

Cornell University, Ithaca, USA
J. Alexander, A. Chatterjee, N. Eggert, L.K. Gibbons, W. Hopkins, A. Khukhunaishvili, B. Kreis, N. Mirman, G. Nicolas Kaufman, J.R. Patterson, A. Ryd, E. Salvati, W. Sun, W.D. Teo, J. Thom, J. Thompson, J. Tucker, Y. Weng, L. Winstrom, P. Wittich

Fairfield University, Fairfield, USA
D. Winn

Fermi National Accelerator Laboratory, Batavia, USA
S. Abdullin, M. Albrow, J. Anderson, G. Apollinari, L.A.T. Bauerdick, A. Beretvas, J. Berryhill, P.C. Bhat, K. Burkett, J.N. Butler, V. Chetluru, H.W.K. Cheung, F. Chlebana, S. Cihangir, V.D. Elvira, I. Fisk, J. Freeman, Y. Gao, E. Gottschalk, L. Gray, D. Green, O. Gutsche, D. Hare, R.M. Harris, J. Hirschauer, B. Hooberman, S. Jindariani, M. Johnson, U. Joshi, K. Kaadze, B. Klima, S. Kunori, S. Kwan, J. Linacre, D. Lincoln, R. Lipton, J. Lykken, K. Maeshima, J.M. Marraffino, V.I. Martinez Outschoorn, S. Maruyama, D. Mason, P. McBride, K. Mishra, S. Mrenna, Y. Musienko[56], C. Newman-Holmes, V. O'Dell, O. Prokofyev, N. Ratnikova, E. Sexton-Kennedy, S. Sharma, W.J. Spalding, L. Spiegel, L. Taylor, S. Tkaczyk, N.V. Tran, L. Uplegger, E.W. Vaandering, R. Vidal, J. Whitmore, W. Wu, F. Yang, J.C. Yun

University of Florida, Gainesville, USA
D. Acosta, P. Avery, D. Bourilkov, M. Chen, T. Cheng, S. Das, M. De Gruttola, G.P. Di Giovanni, D. Dobur, A. Drozdetskiy, R.D. Field, M. Fisher, Y. Fu, I.K. Furic, J. Hugon, B. Kim, J. Konigsberg, A. Korytov, A. Kropivnitskaya, T. Kypreos, J.F. Low, K. Matchev, P. Milenovic[57], G. Mitselmakher, L. Muniz, R. Remington, A. Rinkevicius, N. Skhirtladze, M. Snowball, J. Yelton, M. Zakaria

Florida International University, Miami, USA
V. Gaultney, S. Hewamanage, S. Linn, P. Markowitz, G. Martinez, J.L. Rodriguez

Florida State University, Tallahassee, USA
T. Adams, A. Askew, J. Bochenek, J. Chen, B. Diamond, J. Haas, S. Hagopian, V. Hagopian, K.F. Johnson, H. Prosper, V. Veeraraghavan, M. Weinberg

Florida Institute of Technology, Melbourne, USA
M.M. Baarmand, B. Dorney, M. Hohlmann, H. Kalakhety, F. Yumiceva

University of Illinois at Chicago (UIC), Chicago, USA
M.R. Adams, L. Apanasevich, V.E. Bazterra, R.R. Betts, I. Bucinskaite, J. Callner, R. Cavanaugh, O. Evdokimov, L. Gauthier, C.E. Gerber, D.J. Hofman, S. Khalatyan, P. Kurt, F. Lacroix, D.H. Moon, C. O'Brien, C. Silkworth, D. Strom, P. Turner, N. Varelas

The University of Iowa, Iowa City, USA
U. Akgun, E.A. Albayrak[51], B. Bilki[58], W. Clarida, K. Dilsiz, F. Duru, S. Griffiths, J.-P. Merlo, H. Mermerkaya[59], A. Mestvirishvili, A. Moeller, J. Nachtman, C.R. Newsom, H. Ogul, Y. Onel, F. Ozok[51], S. Sen, P. Tan, E. Tiras, J. Wetzel, T. Yetkin[60], K. Yi

Johns Hopkins University, Baltimore, USA
B.A. Barnett, B. Blumenfeld, S. Bolognesi, G. Giurgiu, A.V. Gritsan, G. Hu, P. Maksimovic, C. Martin, M. Swartz, A. Whitbeck

The University of Kansas, Lawrence, USA
P. Baringer, A. Bean, G. Benelli, R.P. Kenny III, M. Murray, D. Noonan, S. Sanders, R. Stringer, J.S. Wood

Kansas State University, Manhattan, USA
A.F. Barfuss, I. Chakaberia, A. Ivanov, S. Khalil, M. Makouski, Y. Maravin, L.K. Saini, S. Shrestha, I. Svintradze

Lawrence Livermore National Laboratory, Livermore, USA
J. Gronberg, D. Lange, F. Rebassoo, D. Wright

University of Maryland, College Park, USA
A. Baden, B. Calvert, S.C. Eno, J.A. Gomez, N.J. Hadley, R.G. Kellogg, T. Kolberg, Y. Lu, M. Marionneau, A.C. Mignerey, K. Pedro, A. Peterman, A. Skuja, J. Temple, M.B. Tonjes, S.C. Tonwar

Massachusetts Institute of Technology, Cambridge, USA
A. Apyan, G. Bauer, W. Busza, I.A. Cali, M. Chan, L. Di Matteo, V. Dutta, G. Gomez Ceballos, M. Goncharov, D. Gulhan, Y. Kim, M. Klute, Y.S. Lai, A. Levin, P.D. Luckey, T. Ma, S. Nahn, C. Paus, D. Ralph, C. Roland, G. Roland, G.S.F. Stephans, F. Stöckli, K. Sumorok, D. Velicanu, R. Wolf, B. Wyslouch, M. Yang, Y. Yilmaz, A.S. Yoon, M. Zanetti, V. Zhukova

University of Minnesota, Minneapolis, USA
B. Dahmes, A. De Benedetti, A. Gude, J. Haupt, S.C. Kao, K. Klapoetke, Y. Kubota, J. Mans, N. Pastika, R. Rusack, M. Sasseville, A. Singovsky, N. Tambe, J. Turkewitz

University of Mississippi, Oxford, USA
J.G. Acosta, L.M. Cremaldi, R. Kroeger, S. Oliveros, L. Perera, R. Rahmat, D.A. Sanders, D. Summers

University of Nebraska-Lincoln, Lincoln, USA
E. Avdeeva, K. Bloom, S. Bose, D.R. Claes, A. Dominguez, M. Eads, R. Gonzalez Suarez, J. Keller, I. Kravchenko, J. Lazo-Flores, S. Malik, F. Meier, G.R. Snow

State University of New York at Buffalo, Buffalo, USA
J. Dolen, A. Godshalk, I. Iashvili, S. Jain, A. Kharchilava, A. Kumar, S. Rappoccio, Z. Wan

Northeastern University, Boston, USA
G. Alverson, E. Barberis, D. Baumgartel, M. Chasco, J. Haley, A. Massironi, D. Nash, T. Orimoto, D. Trocino, D. Wood, J. Zhang

Northwestern University, Evanston, USA
A. Anastassov, K.A. Hahn, A. Kubik, L. Lusito, N. Mucia, N. Odell, B. Pollack, A. Pozdnyakov, M. Schmitt, S. Stoynev, K. Sung, M. Velasco, S. Won

University of Notre Dame, Notre Dame, USA
D. Berry, A. Brinkerhoff, K.M. Chan, M. Hildreth, C. Jessop, D.J. Karmgard, J. Kolb, K. Lannon,

W. Luo, S. Lynch, N. Marinelli, D.M. Morse, T. Pearson, M. Planer, R. Ruchti, J. Slaunwhite, N. Valls, M. Wayne, M. Wolf

The Ohio State University, Columbus, USA
L. Antonelli, B. Bylsma, L.S. Durkin, C. Hill, R. Hughes, K. Kotov, T.Y. Ling, D. Puigh, M. Rodenburg, G. Smith, C. Vuosalo, B.L. Winer, H. Wolfe

Princeton University, Princeton, USA
E. Berry, P. Elmer, V. Halyo, P. Hebda, J. Hegeman, A. Hunt, P. Jindal, S.A. Koay, P. Lujan, D. Marlow, T. Medvedeva, M. Mooney, J. Olsen, P. Piroué, X. Quan, A. Raval, H. Saka, D. Stickland, C. Tully, J.S. Werner, S.C. Zenz, A. Zuranski

University of Puerto Rico, Mayaguez, USA
E. Brownson, A. Lopez, H. Mendez, J.E. Ramirez Vargas

Purdue University, West Lafayette, USA
E. Alagoz, D. Benedetti, G. Bolla, D. Bortoletto, M. De Mattia, A. Everett, Z. Hu, M. Jones, K. Jung, O. Koybasi, M. Kress, N. Leonardo, D. Lopes Pegna, V. Maroussov, P. Merkel, D.H. Miller, N. Neumeister, I. Shipsey, D. Silvers, A. Svyatkovskiy, F. Wang, W. Xie, L. Xu, H.D. Yoo, J. Zablocki, Y. Zheng

Purdue University Calumet, Hammond, USA
N. Parashar

Rice University, Houston, USA
A. Adair, B. Akgun, K.M. Ecklund, F.J.M. Geurts, W. Li, B. Michlin, B.P. Padley, R. Redjimi, J. Roberts, J. Zabel

University of Rochester, Rochester, USA
B. Betchart, A. Bodek, R. Covarelli, P. de Barbaro, R. Demina, Y. Eshaq, T. Ferbel, A. Garcia-Bellido, P. Goldenzweig, J. Han, A. Harel, D.C. Miner, G. Petrillo, D. Vishnevskiy, M. Zielinski

The Rockefeller University, New York, USA
A. Bhatti, R. Ciesielski, L. Demortier, K. Goulianos, G. Lungu, S. Malik, C. Mesropian

Rutgers, The State University of New Jersey, Piscataway, USA
S. Arora, A. Barker, J.P. Chou, C. Contreras-Campana, E. Contreras-Campana, D. Duggan, D. Ferencek, Y. Gershtein, R. Gray, E. Halkiadakis, D. Hidas, A. Lath, S. Panwalkar, M. Park, R. Patel, V. Rekovic, J. Robles, S. Salur, S. Schnetzer, C. Seitz, S. Somalwar, R. Stone, S. Thomas, P. Thomassen, M. Walker

University of Tennessee, Knoxville, USA
G. Cerizza, M. Hollingsworth, K. Rose, S. Spanier, Z.C. Yang, A. York

Texas A&M University, College Station, USA
O. Bouhali[61], R. Eusebi, W. Flanagan, J. Gilmore, T. Kamon[62], V. Khotilovich, R. Montalvo, I. Osipenkov, Y. Pakhotin, A. Perloff, J. Roe, A. Safonov, T. Sakuma, I. Suarez, A. Tatarinov, D. Toback

Texas Tech University, Lubbock, USA
N. Akchurin, C. Cowden, J. Damgov, C. Dragoiu, P.R. Dudero, K. Kovitanggoon, S.W. Lee, T. Libeiro, I. Volobouev

Vanderbilt University, Nashville, USA
E. Appelt, A.G. Delannoy, S. Greene, A. Gurrola, W. Johns, C. Maguire, Y. Mao, A. Melo, M. Sharma, P. Sheldon, B. Snook, S. Tuo, J. Velkovska

University of Virginia, Charlottesville, USA
M.W. Arenton, S. Boutle, B. Cox, B. Francis, J. Goodell, R. Hirosky, A. Ledovskoy, C. Lin, C. Neu, J. Wood

Wayne State University, Detroit, USA
S. Gollapinni, R. Harr, P.E. Karchin, C. Kottachchi Kankanamge Don, P. Lamichhane, A. Sakharov

University of Wisconsin, Madison, USA
D.A. Belknap, L. Borrello, D. Carlsmith, M. Cepeda, S. Dasu, S. Duric, E. Friis, M. Grothe, R. Hall-Wilton, M. Herndon, A. Hervé, P. Klabbers, J. Klukas, A. Lanaro, R. Loveless, A. Mohapatra, I. Ojalvo, T. Perry, G.A. Pierro, G. Polese, I. Ross, T. Sarangi, A. Savin, W.H. Smith, J. Swanson

†: Deceased
1: Also at Vienna University of Technology, Vienna, Austria
2: Also at CERN, European Organization for Nuclear Research, Geneva, Switzerland
3: Also at Institut Pluridisciplinaire Hubert Curien, Université de Strasbourg, Université de Haute Alsace Mulhouse, CNRS/IN2P3, Strasbourg, France
4: Also at National Institute of Chemical Physics and Biophysics, Tallinn, Estonia
5: Also at Skobeltsyn Institute of Nuclear Physics, Lomonosov Moscow State University, Moscow, Russia
6: Also at Universidade Estadual de Campinas, Campinas, Brazil
7: Also at California Institute of Technology, Pasadena, USA
8: Also at Laboratoire Leprince-Ringuet, Ecole Polytechnique, IN2P3-CNRS, Palaiseau, France
9: Also at Zewail City of Science and Technology, Zewail, Egypt
10: Also at Suez Canal University, Suez, Egypt
11: Also at Cairo University, Cairo, Egypt
12: Also at Fayoum University, El-Fayoum, Egypt
13: Also at British University in Egypt, Cairo, Egypt
14: Now at Ain Shams University, Cairo, Egypt
15: Also at National Centre for Nuclear Research, Swierk, Poland
16: Also at Université de Haute Alsace, Mulhouse, France
17: Also at Joint Institute for Nuclear Research, Dubna, Russia
18: Also at Brandenburg University of Technology, Cottbus, Germany
19: Also at The University of Kansas, Lawrence, USA
20: Also at Institute of Nuclear Research ATOMKI, Debrecen, Hungary
21: Also at Eötvös Loránd University, Budapest, Hungary
22: Also at Tata Institute of Fundamental Research - EHEP, Mumbai, India
23: Also at Tata Institute of Fundamental Research - HECR, Mumbai, India
24: Now at King Abdulaziz University, Jeddah, Saudi Arabia
25: Also at University of Visva-Bharati, Santiniketan, India
26: Also at University of Ruhuna, Matara, Sri Lanka
27: Also at Isfahan University of Technology, Isfahan, Iran
28: Also at Sharif University of Technology, Tehran, Iran
29: Also at Plasma Physics Research Center, Science and Research Branch, Islamic Azad University, Tehran, Iran
30: Also at Università degli Studi di Siena, Siena, Italy
31: Also at Centre National de la Recherche Scientifique (CNRS) - IN2P3, Paris, France
32: Also at Purdue University, West Lafayette, USA
33: Also at Universidad Michoacana de San Nicolas de Hidalgo, Morelia, Mexico